ISSN (ISSN-L) 2735-6817
ISSN (ONLINE) 2735-6817
ISSN (PRINT) 2735-7155
Volumen 2 • Número 2
Agosto 2022

UNIVERSIDAD TECNOLÓGICA METROPOLITANA
del Estado de Chile
UTEM

Revista de **Modelamiento Matemático de Sistemas Biológicos**

Grupo MatBio-UTEM
Departamento de Matemática
Facultad de Ciencias Naturales, Matemática y Medio Ambiente

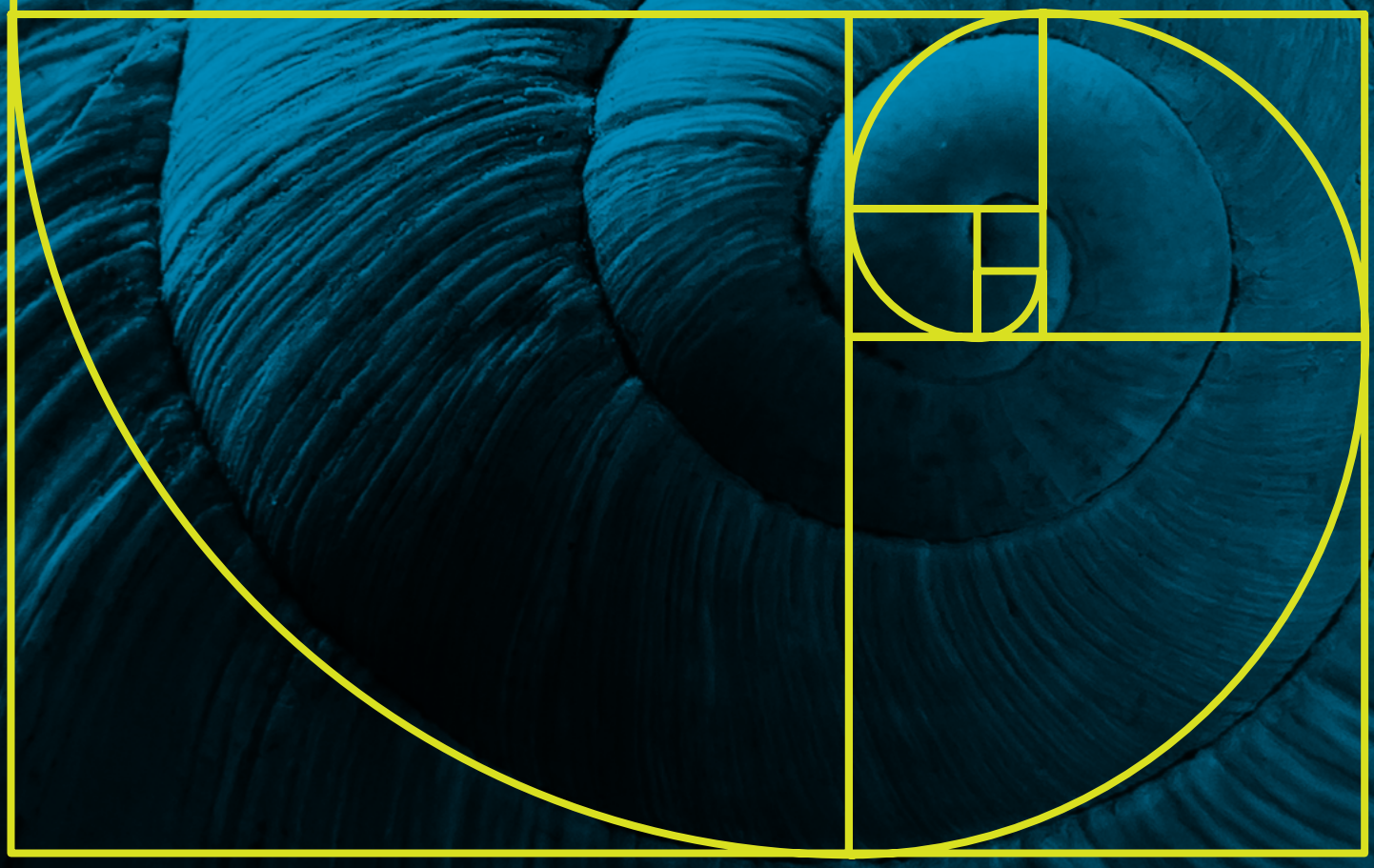

UNIVERSIDAD TECNOLÓGICA METROPOLITANA
del Estado de Chile

ISSN: 2735-6817
Volumen 2 • Número 2
Agosto 2022

Revista de **Modelamiento Matemático de Sistemas Biológicos**

Grupo MatBio-UTEM
Departamento de Matemática
Facultad de Ciencias Naturales, Matemática y Medio Ambiente

revistammsb.utem.cl

EDICIONES UNIVERSIDAD
TECNOLÓGICA METROPOLITANA

Facultad de Ciencias Naturales, Matemáticas
y Medio Ambiente
Departamento de Matemática
Grupo MatBio-UTEM

Revista Modelamiento Matemático de Sistemas Biológicos
Journal of Mathematical Modelling of Biological Systems

ISSN (ISSN-L) 2735-6817
ISSN (ONLINE) 2735-6817
ISSN (PRINT) 2735-7155
Volumen 2, Nº 2, agosto 2022

INFORMACIONES

Revista Modelamiento Matemático de Sistemas Biológicos
Grupo MatBio-UTEM
Departamento de Matemáticas Facultad de Ciencias Naturales, Matemática y Medio Ambiente

Correspondencia: Las Palmeras 3360, Ñuñoa, Santiago, Chile.
Código Postal 7800003. Teléfono: (56-2) 27877221

Correo electrónico: revista.mmsb@utem.cl

Políticas Editoriales

1. Carácter: la revista Modelamiento Matemático de Sistemas Biológicos (MMSB) es una publicación en línea, de acceso abierto, universal, gratuita y sin restricciones de circulación de sus contenidos. MMSB busca ser reconocida por su calidad de contenidos y rigurosidad en los procesos de edición y publicación.

2. Misión. Rev. model. mat. sist. biol. busca difundir trabajos originales e inéditos que incrementen el conocimiento y comprensión de sistemas biológicos a través del modelamiento matemático como herramienta principal de análisis. Las áreas temáticas incluidas en la revista son:

- Dinámica de Poblaciones
- Sustentabilidad
- Biodiversidad
- Epidemiología
- Enfermedades no infecciosas
- Biotecnología
- Biomateriales
- Neurociencia
- Genética
- Fisiología
- Biología celular
- Entre otros temas de origen biológico que puedan ser modelados y estudiados matemáticamente

3. **Visión.** Rev. model. mat. sist. biol. promueve el acceso al conocimiento de manera democrática y sin fines de lucro, libre circulación y acceso inmediato de sus artículos, siempre que se cite adecuadamente la fuente.

La revista busca valorizar la investigación científica producida en América Latina y el Caribe, aunque no de manera restrictiva geográficamente, ofreciendo una plataforma de divulgación científica para los trabajos de investigadores de la región, sin perjuicio de que se trata de una publicación disponible para los investigadores de todo el mundo.

4. **Fecha y número de publicaciones anuales:** Rev. model. mat. sist. biol. publicará tres números regulares por cada volumen, en los meses de: abril, agosto y diciembre de cada año.

La Rev. model. mat. sist. biol. se reserva el derecho de publicar volúmenes especiales que pueden ser dedicados a una temática específica o vinculados a un evento científico.

5. Alcance idiomático: Español-Inglés.

6. **Política de derechos de autor, publicación y acceso a los contenidos:** Rev. model. mat. sist. biol., Universidad Tecnológica Metropolitana como editora se reserva las atribuciones de comunicación y difusión según las practicas del derecho de autor chilenas, y declara una política de acceso abierto (OA), bajo el principio de disponibilidad inmediata y gratuita, bajo la licencia Creative Commons Reconocimiento 4.0 Internacional License (CC BY 4.0) (https://creativecommons.org/licenses/by/4.0/), siempre que le sea reconocida la autoría de la creación original, a menos que se indique lo contrario.

La revista adhiere a los principios de Investigación Abierta (Open Science) y a los Principios FAIR (Findable, Accessible, Interoperable, and Reusable), para la gestión de datos científicos.

7.- Cargos por envío y/o publicación artículos

La revista no tiene cargos por procesamiento de artículos (APC).

La revista no tiene cargos por envío de artículos.

8. **Para los autores:** se autoriza establecer copia en repositorios institucionales o personales, de preprint o posprint, siempre y cuando se cite la fuente o sitio institucional donde han sido publicados originalmente. Véase Políticas de apertura de la revista en: Sherpa Romeo AURA - Amelica

9. **Para los lectores:** se autoriza la reproducción total o parcial de los textos aquí publicados siempre y cuando se cite debidamente la autoría y fuente completa, así como la dirección electrónica de la publicación.

10. **La responsabilidad de sus autores/as y de las opiniones expresadas** no necesariamente reflejan la postura de la editorial, la revista o de la Universidad Tecnológica Metropolitana (UTEM).

Las opiniones y hechos consignados en cada artículo son de exclusiva responsabilidad de sus autores/as, así como de la idoneidad ética como investigadores.

Además, al enviar un trabajo a evaluar para publicación, hacen explícito que el manuscrito es de su autoría y que se respetan los derechos de propiedad intelectual de terceros. También es su responsabilidad asegurarse de tener las autorizaciones para usar, reproducir e imprimir el material que no sea de su propiedad/autoría (cuadros, gráficas, mapas, diagramas, fotografías, etcétera).

Cuando un autor(a) identifica en su artículo un error importánte, deberá informar de inmediato a los editores y proporcionar toda la información necesaria para hacer las correcciones pertinentes y/o elaborar una retractación o corrección en caso de que terceros detecten errores.

11. **La responsabilidad de los editores**

Decisión de publicación: garantizarán la selección de las personas evaluadoras más calificadas y especialistas científicamente para emitir una apreciación crítica y experta del trabajo, con los menores sesgos posibles.

Integridad ética: evalúan los artículos enviados para su publicación sobre la base del mérito científico de los contenidos, sin discriminación ni opinión de género o política de las personas autoras, y en consideración a las políticas de género en la publicación en base a las recomendaciones de la ANID - Chile 2021.

Confidencialidad: se comprometen a la confidencialidad de los manuscritos, su autoría y evaluación, de forma que el anonimato preserve la integridad intelectual de todo el proceso. Respeto de los tiempos: son responsables máximos del cumplimiento de los límites de tiempo para las revisiones y la publicación de los trabajos aceptados, para asegurar una rápida difusión de sus resultados.

12. **Código ético.** La Rev. model. mat. sist. biol. adhiere al Código del Commitee on Publication Ethics (COPE) para discutir y o sancionar toda materia relativa a los aspectos de la ética de la publicación. Véase: COPE Principios de Transparencia y Mejores Prácticas en Publicaciones Académicas, disponible en: https://doi.org/10.24318/cope.2019.1.13

13. **Conflicto de interés:** La Revista requiere que los autores, revisores, declaren cualquier conflicto de intereses en conexión con el artículo remitido. Si los hay, es imperativo que los identifiquen, e informen en detalle cuál fue su relación con el trabajo presentado.

14. **Detección o prevención del plagio.** MMSB emplea el sistema de detección de plagio de la Universidad (UTEM) (véase https://www.urkund.com/es/), con motivo de salvaguardar la pertinencia u originalidad de los contenidos que se publicarán.

Si posteriormente a la publicación de un artículo el Consejo editorial detecta o es informado de plagio, mala conducta en la investigación, la Revista puede retirar el artículo e informa retractación, adicionalmente puede emprender en contra de las personas autoras las acciones legales que correspondan.

15.- **Preservación de los contenidos.** En Repositorio Institucional SIBUTEM

Indexación en bases de datos, directorios: Latindex, Sistema Regional de Información Revistas Científicas de América Latina, el Caribe, España y Portugal; ROAD: Directory of Open Access Scholarly Resources; AURA Amelica Unesco; Sherpa Romeo.

Repositorios: Repositorio académico UTEM; Google Académico.

Editorial Policies

1. Character. The Journal of Mathematical Modeling of Biological Systems (MMSM) is an official publication of the Metropolitan Technological University, published through Ediciones UTEM.

2. Mission. MMSB seeks to disseminate original and unpublished works that increase the knowledge and understanding of biological systems through mathematical modeling as the main tool of analysis. The subject areas included in the journal are:

- Population Dynamics
- Sustainability
- Biodiversity
- Epidemiology
- Non-infectious diseases
- Biotechnology
- Biomaterials
- Neuroscience
- Genetics
- Physiology
- Cell biolog
- Among other topics of biological origin that can be modeled and studied mathematically.

3. Vision. MMSM promotes access to knowledge in a democratic and non-profit manner, therefore the journal does not charge authors for publication or access charges for readers, nor does it restrict the free circulation of its articles (however, the source must always be correctly referenced).

In addition, it seeks to value the scientific research produced in Latin America and the Caribbean, offering a showcase for the work of young researchers in the region, without prejudice to the fact that it is a publication available to researchers from all over the world and of all ages.

4. MMSB will publish an annual volume, with three issues per volume, with a publication date in April, August and December of each year.

MMSB will also publish special volumes that can be dedicated to a specific topic or linked to a scientific event.

5. Language scope: Spanish-English.

6. Publication policy and access to content. MMSB has an open access policy, under the principle of free availability, to research products for the general public.

7. For authors. it is authorized to establish a copy in institutional or personal repositories, preprint or postprint, as long as the source or institutional site where they were originally published is cited.

8. For readers. the total or partial reproduction of the texts published here is authorized as long as the authorship and full source are duly cited, as well as the electronic address of the publication.

9. The opinions expressed by the authors do not necessarily reflect the position of the publisher, the journal or the Universidad Tecnológica Metropolitana (UTEM).

10. Code of Ethics. the Journal adheres to the Code of the Committee on Publication Ethics (COPE) to discuss and or sanction all matters related to ethical aspects of the publication. See: COPE Principles of Transparency and Best Practices in Academic Publications, available at: https://doi.org/10.24318/cope.2019.1.13

11. Code of Ethics. Detection or prevention of plagiarism. MMSB uses the University's plagiarism detection system (UTEM) (see https://www.urkund.com/es/), in order to safeguard the relevance or originality of the content to be published.

Tabla de contenidos

2	Raul Abreu de Assis	BRASIL	Universidade do Estado de Mato Grosso	When shape matters: using a simple mathematical model to estimate critical area sizes in conservation
	Mazílio Coronel Mala-vazi	BRASIL	Universidade do Estado de Mato Grosso	
	Rubens Pazim	BRASIL	Universidade do Estado de Mato Grosso	
	Gustavo Canale	BRASIL	Universidade do Estado de Mato Grosso	
	Moiseis Cecconello	BRASIL	Universidade do Estado de Mato Grosso	
	Odair José Teixeira da Fonseca	BRASIL	Universidade Federal de Rondônia	
3	Rodrigo Gutiérrez	CHILE	Universidad Católica del Maule	Temporal dynamics of alcohol consumption patterns: The peer pressure and binge drinkers' role
	J.G. Vergaño-Salazar	COLOMBIA	Universidad del Quindío	
	Claudio Rojas-Jara	CHILE	Universidad Católica del Maule	
	Nicole Martínez-Jeraldo	CHILE	Universidad Católica del Maule	
4	Martina Cossa	ITALIA	Università di Torino	Prey gathering may act as a counte-rattack measure against predators
	Ester Cravero	ITALIA	Università di Torino	
	Masaki Pugliese	ITALIA	Università di Torino	
	Ezio Venturino	ITALIA	Università di Torino	

An algorithm for the identification of indicator taxonomic units and their use in analyses of ecosystem state

Un algoritmo para la identificación de unidades taxonómicas indicadoras y su uso en análisis del estado del ecosistemas

de la Vega Hernán[1], Falco Liliana[1,2], Saravia Leonardo[3,4], Sandler Rosana[2], Duhour Andrés[1,5], Velazco Víctor N[1,2] and Coviella Carlos[1,2]

[1] *Departamento de Ciencias Básicas, Universidad Nacional de Luján, Argentina*
[2] *Programa de Investigaciones en Ecología Terrestre, Instituto de Ecología y Desarrollo Sustentable (INEDES) UNLu – CONICET*
[3] *Instituto de Ciencias, Universidad Nacional de General Sarmiento, Argentina*
[4] *CADIC, CONICET.*
[5] *Grupo de Sustentabilidad Agropecuaria, Instituto de Ecología y Desarrollo Sustentable (INEDES) UNLu - CONICET*

Reception date of the manuscript: 25/05/2022
Acceptance date of the manuscript: 09/06/2022
Publication date: 31/08/2022

Abstract—Biological community structure can be used as an ecological state descriptor, and the sensitivity of some taxonomic groups or biological entities to environmental conditions allows for their use as ecological state indicators. This work describes an algorithm developed for the identification of such taxonomic units when comparing environments or ecosystems under different anthropic impacts. Based solely on presence or absence information in a database, the algorithm identifies indicator taxonomic units for each environment, estimates the belonging of any additional samples to a given environment, approximates the ecological niche of any taxonomic unit based on two or more selected environmental factors, and analyzes the frequency of any taxonomic unit in a selected combination of the environmental factors chosen. By using the approximation to the ecological niche of the taxonomic units present, given a new sample, the physicochemical parameters of the environment it was taken can be estimated by the units present in the sample. These analyses can be performed simultaneously for two or more taxonomic units. This work provides a description of how the mathematical method was developed. Based on this methodology, a freely downloadable R package for easy use was developed, (Ecoindicators, DOI: https://github.com/lsaravia/EcoIndicators). One of the advantages of this method, and the R-package mentioned is that it can be used for any ecosystem for which there is a suitable biological dataset associated with environmental factors. In addition, both this mathematical procedure and the package referred to, can be tailored by other researchers to fit their own needs.

Keywords—Anthropic Impact, Ecological Indices, Mathematical Ecology, Sustainability

Resumen— La estructura de una comunidad biológica puede usarse como un descriptor del estado ecológico, y la sensibilidad de algunos grupos taxonómicos o entidades biológicas a las condiciones ambientales, permite que sean usados como indicadores de dicho estado. Este trabajo describe el desarrollo de un algoritmo para la identificación de tales unidades taxonómicas al comparar ambientes o ecosistemas bajo diferentes impactos antrópicos. Basado únicamente en información de presencia o ausencia en una base de datos, el algoritmo identifica unidades taxonómicas indicadoras de cada ambiente, estima la pertenencia de cualquier muestra adicional a un ambiente dado, aproxima el nicho ecológico de cualquier unidad taxonómica con base en dos o más factores ambientales seleccionados y analiza la frecuencia de cualquier unidad taxonómica en la combinación de los factores ambientales elegidos. Utilizando la aproximación al nicho ecológico de las unidades taxonómicas presentes en la base de datos, dada una nueva muestra, se pueden estimar ciertos parámetros fisicoquímicos del ambiente de donde provino tal muestra a partir de las especies presentes en la misma. Estos análisis se pueden realizar simultáneamente para dos o más unidades taxonómicas. Este trabajo proporciona una descripción de cómo se desarrolló este procedimiento matemático. Con base en la metodología aquí descripta, se desarrolló un paquete R de fácil descarga y uso gratuito (Ecoindicators, DOI: https://github.com/lsaravia/EcoIndicators). Una de las ventajas de este método, y del paquete R mencionado, es que puede usarse para cualquier ecosistema para el que exista un conjunto de datos biológicos adecuados asociados con factores ambientales. Además, tanto este procedimiento matemático como el paquete al que se hace referencia, pueden ser adaptados por otros investigadores para que se ajusten a sus propias necesidades.

Palabras clave—Impacto Antrópico, Índices Ecológicos, Ecología Matemática, Sustentabilidad

INTRODUCTION

The development of biological indices of environmental status as a tool to assess anthropic impact is increasingly used in many systems (Melo-Merino, 2020). These biological status indices are well developed for aquatic environments but their development for terrestrial environments is still incipient (Guerra et al., 2021). The European Water Framework Directive, for example, required that all surface waters in Europe have biological indices of water quality by 2015 (European-Parliament, 2000). However, the development of reliable ecological quality indices requires not only the identification of those biological units considered to be indicators, but also the development of objective methodologies for the construction of such indices. A current characteristic of the development of these indices is the general lack of standardized tools and methodologies for the objective selection of variables and for their construction (Velásquez et al., 2007). The purpose of this work is to advance in the design of such unbiased tools and the methodologies that can be used for the construction of ecological system state indices. Thus, we designed an algorithm to classify the most relevant characteristics of ecosystems and estimate the values of parameters considered of interest, using the presence and absence of certain taxonomic units. Such units considered here as the biological entities of different taxonomic hierarchy used in this work, from samples of the same system. The work started from a database of soil samples that contain measurements of physical and chemical parameters as well as the presence and absence in each sample of different taxonomic units as defined above. The samples were obtained over two years of sampling in sites of different intensity of anthropic use of the same soil. The identification of the different biological units that make up the edaphic biota, as well as their interactions and dynamics, are difficult to assess due largely to the methods necessary for their extraction and the small size of the individuals that compose it. However, the information gradually collected over decades, is reaching the point where it is becoming possible to focus the work on the development of comparative studies on the structure and functioning of the edaphic biota. These studies will then make possible the analysis of the stability of the interaction networks for evaluating the state of different ecological systems (Fortin et al., 2021) or of the same system under different intensities of anthropic impact (Potapov et al., 2019). As a first step, certain taxonomic units were selected, called here "indicators" that were then used (observing their presence or absence) to estimate from which environment a soil sample came. As a second step, the presence or absence of such units was used to estimate values of some physical and chemical parameters of interest. To carry out this task in an automated way with different databases, an algorithm was developed that allows to complete all these stages in a single step. The first problem addressed was to determine, when receiving new soil samples, to which environment they correspond. The focus of interest in this part, was to make this classification taking into account those units present or absent, regardless of the values of the chemical and physical parameters of the samples. With that aim, it was first sought to distinguish "indicator units" that, through their presence or absence, increase or decrease the probability that a sample belongs to a specific environment. With this information, and observing only those presences or absences in new soil samples, the algorithm estimates which environment they come from and assigns a probability to that estimation. In the following section this procedure is detailed and in the final section a test is carried out with a database corresponding to a soil of the rolling pampas (Buenos Aires, Argentina). A second objective consisted in relating the presence of taxonomic units (indicator units) in the samples with the levels of certain physical and chemical parameters of interest. This problem was tackled by describing the intersection of the ecological niches sensu Hutchinson (1957) of the groups present with respect to those parameters.

To this end, it was necessary to choose a simple calculation to obtain an approximation of the niches. A "grid" of the ranges of the physical and chemical parameters of the database was built and then a "convex capsule" from a representative part of the existing cloud of biological data was adjusted. This whole process is described in the last section. It is also intended for the entire procedure to be written in a free language known to researchers in the area, with the intention that it can be tested by other professionals and improved by other developers.

Methodology: construction of the algorithm step by step.

The database has the structure (Figure 1) in which the columns are completed with measurements of physical and chemical parameters and of the gross abundances for each taxonomic unit present in each of the samples obtained from a same type of soil with different intensities of anthropic impact.

PROCEDURE FOR ESTIMATING A SAMPLE BELONGING TO A GIVEN ENVIRONMENT

From the samples obtained from an experimental design and reaching the laboratory, the assignment probability that relates a sample to a particular environment is calculated. This step, to calculate the probability of assignment, begins by considering the presence / absence (Figure 2) of the taxonomic units present in the sample.

As indicated above, the algorithm considers the presence or absence of each taxonomic unit, therefore, the columns of the taxonomic units obtained from the database are transformed into a matrix of zeros and ones. In this first version, the number of samples from each environment is required to be the same. So, the first matrix obtained is:

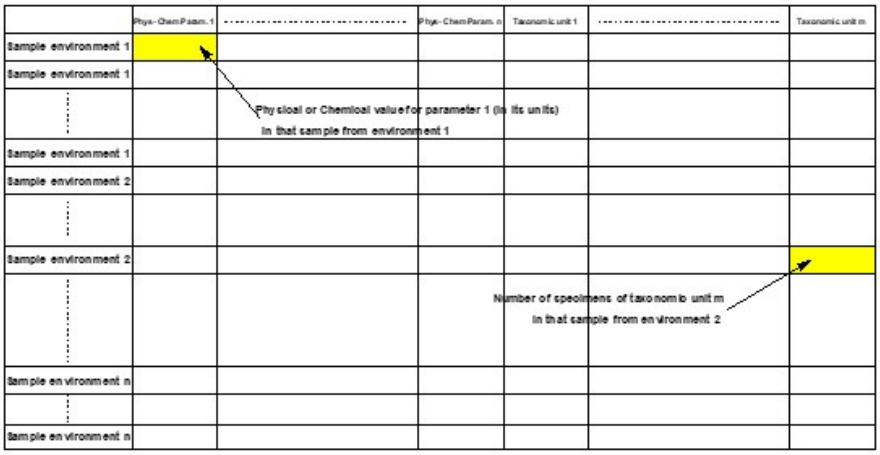

Figure 1: Database structure. The samples come from the same soil subjected to three different intensities of anthropic use (environment). Each line contains the physicochemical data and the taxonomic units found in each sample.

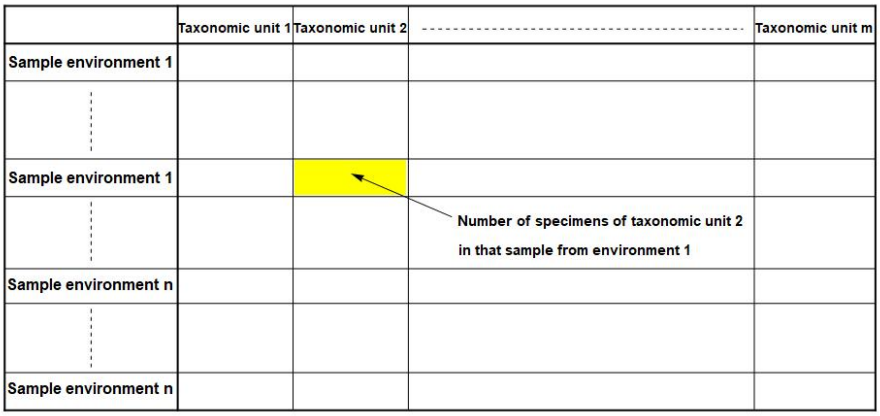

Figure 2: Trimmed table, containing only information about the taxonomic units present or absent. Each row is a sample with the values corresponding to the number of individuals of each taxonomic unit found in that sample.

$$E = \begin{pmatrix} e_1^{1,1} & \cdots & \cdots & \cdots & e_m^{1,1} \\ \vdots & & & & \vdots \\ e_1^{1,k} & \cdots & \cdots & \cdots & e_m^{1,k} \\ e_1^{2,1} & \cdots & \cdots & \cdots & e_m^{2,1} \\ \vdots & & & & \vdots \\ e_1^{2,k} & \cdots & \cdots & \cdots & e_m^{2,k} \\ \vdots & & \vdots & & \vdots \\ \vdots & \cdots & e_j^{l,i} & \cdots & \vdots \\ \vdots & & \vdots & & \vdots \\ e_1^{n,1} & \cdots & \cdots & \cdots & e_m^{n,1} \\ \vdots & & & & \vdots \\ e_1^{n,k} & \cdots & \cdots & \cdots & e_m^{n,k} \end{pmatrix}$$

Where the term $e_j^{l,i}$ indicates if there were appearances of the species j in i the sample l. More precisely:

$$e_j^{l,i} = \begin{cases} 1, & \text{if there were appearances of the species } j \text{ in the sample } i \text{ of the environment } l \\ 0, & \text{if there were no appearances} \end{cases}$$

Selection of indicator unit

The idea that is being tested here is to measure the difference between the expected and observed values. As the number of samples k corresponding to each of the environments n is the same, if the appearance of each taxonomic unit j were independent of the environments, it would be expected that the proportion of appearances of each taxonomic unit in each environment was uniform. To specify the latter, let's take a taxonomic unit j and add its occurrences in the environment l, then add all its occurrences in the database, take the quotient between the two and call that number O_j^l that is:

$$O_j^l = \frac{\sum_{i=1}^{k} e_j^{l,i}}{\sum_{l=1}^{n}\sum_{i=1}^{k} e_j^{l,i}}$$

were O_j^l gives the proportion of appearances observed, with

respect to the total of appearances of the unit j, in the environment l.

If the unit j were independent of the different environments, would be expected then that it your occurrence O_j^l be approximately $\frac{1}{n}$ the same for each environment $l = 1,\ldots,n$ this is ($O_j^1 \cong O_j^2 \cong \ldots \cong O_j^n \cong \frac{1}{n}$).

We call E_j^l this expected value and we have that $E_j^l = \frac{1}{n}$ for $l = 1 \ldots n$ and $j = 1 \ldots m$. We test the hypothesis

$O_j^1 = O_j^2 = \ldots = O_j^n = \frac{1}{n}$ with a standard Hypothesis Test using the Chi-square distribution χ^2 by:

$$\chi^2 = \sum_{l=1}^{n} \frac{\left(O_j^l - E_j^l\right)^2}{E_j^l} = \sum_{l=1}^{n} \frac{\left(O_j^l - \frac{1}{n}\right)^2}{\frac{1}{n}}$$

If the value exceeds the threshold given by $\alpha = 0{,}05$, the hypothesis is rejected and it is considered that the occurrences of that taxonomic unit vary between environments.

Units whose distribution is not uniform with respect to the environments are called Indicator Units, and are those in which their occurrences are not independent of the environments being considered. A number r of indicator units is thus obtained $E_{j_1}, E_{j_2}, \ldots, E_{j_r}$. It is through their appearances or absences the procedure seeks to determine the belonging of a new sample to a certain environment.

To visualize this, the algorithm generates a graph with the distributions of each unit in each environment and indicates the number of total occurrences of each one in the database (see Figure 6). This last datum is considered in the calculation above so as not to use units that appeared only a few times to be of significance in the analysis.

Environment estimation

Once the Indicator Units have been obtained, we seek to determine which particular environment it belongs to. Specifically, the negation of the Null Hypothesis test (with $alpha = 0{,}05$): "the observed proportion of that unit in that environment is $\frac{1}{n}$ïs used to construct the D matrix based on the differences between the expected value E_j^l and the observed occurrence rate O_j^l, so that each $d_{j_1}^1$ is equal to $O_{j_s}^l - \frac{1}{n}$

$$D = \begin{pmatrix} d_{j_1}^1 & \cdots & \cdots & \cdots & d_{j_m}^1 \\ \vdots & & \vdots & & \vdots \\ \vdots & \cdots & d_{j_s}^l & \cdots & \vdots \\ \vdots & & \vdots & & \vdots \\ d_{j_1}^n & \cdots & \cdots & \cdots & d_{j_m}^n \end{pmatrix}$$

where

$$d_{j_s}^l = \begin{cases} O_{j_s}^l - \frac{1}{n}, & \text{if the test found a difference significant between the proportion of observed partitions of the indicator species } j_s \text{ in the environment } l \text{ with respect to what expected } (\frac{1}{n}) \\ 0, & \text{if the test found no significant differences} \end{cases}$$

The rationale is that these coefficients $d_{j_s}^l$, before the appearance of a unit in a sample j_s, add or subtract probabilities (or neither of those two things) that this new sample belongs to a certain environment. For instance, suppose there are three different environments and the algorithm has selected two indicator units. Furthermore, assume that the proportions of occurrences of each indicator unit in each environment with respect to its total occurrences (the values $O_{j_s}^l$), were:

	Indicator unit 1	Indicator unit 2
Environment 1	0.35	0.10
Environment 2	0.60	0.62
Environment 3	0.05	0.28

Suppose additionally that the tests carried out on each unit in each environment to see if the observed proportions deviate from those expected (which in this case would be $\frac{1}{3} \cong 0{,}33$) gives a negative value for Indicator Unit 1 in Environment 1 and for Indicator Unit 2 in Environment 1. Environment 3, then the array of values $d_{j_s}^l$ would be (rounding the values):

	Indicator unit 1	Indicator unit 2
Environment 1	0	-0.23
Environment 2	0.27	0.29
Environment 3	-0.28	0

where that 0 of Indicator Unit 1 in Environment 1 indicates that the test did not find a significant difference between what was observed and what was expected, and that 0,27 f Indicator Unit 1 in Environment 2 indicates that the test did find a significant difference. The algorithm then takes that difference $d_1^2 = O_1^2 - E_1^2 = O_1^2 - \frac{1}{3} = 0{,}60 - \frac{1}{3} \cong 0{,}27$, and repeats the procedure with the other values of the matrix. A concrete example of the construction of this matrix is given in Figure 7 of last section.

As stated before, the idea is that these numbers add or subtract probabilities that a sample belongs to a certain environment. For example, if Indicator Unit 1 appears in a new sample, Environment 2 will add 0.27 points to the probability of that sample belonging to that environment while Environment 3 would subtract 0.28 points.

The way the procedure uses that information is as follows. Suppose that a number q of new samples are received, all from the same environment, an environment that the procedure seeks to identify. To continue with the previous example (with three Environments and two Indicating Units) suppose

that we receive four samples in which the following quantities of each Indicating Unit are recorded in each Environment:

	Indicator unit 1	Indicator unit 2
Sample 1	0	5
Sample 2	3	20
Sample 3	0	30
Sample 4	8	10

The matrix is again translated so that it only contains presences and absences

	Indicator unit 1	Indicator unit 2
Sample 1	0	1
Sample 2	1	1
Sample 3	0	1
Sample 4	1	1

Preserving the subscripts that have been used for the indicator units, this matrix would then have the form:

$$M = \begin{pmatrix} M^1_{j_1} & \cdots & \cdots & \cdots & M^1_{j_m} \\ \vdots & & \vdots & & \vdots \\ \vdots & \cdots & M^h_{j_s} & \cdots & \vdots \\ \vdots & & \vdots & & \vdots \\ M^q_{j_1} & \cdots & \cdots & \cdots & M^q_{j_m} \end{pmatrix}$$

where

$$M^h_{j_s} = \begin{cases} 1, & \text{if indicator unit } j_s \text{ appears in sample } h \\ 0, & \text{if no appeareances of that unit were registered} \end{cases}$$

A vector of occurrences of the samples is then built that contains, in each coordinate, several of the samples received where there were occurrences of each unit:

$$A = \left(\sum_{h=1}^{q} M^h_{j_1}, \ldots\ldots, \sum_{h=1}^{q} M^h_{j_m} \right)$$

In the example provided it would be

$$A = (0+1+0+1, 1+1+1+1) = (2,4)$$

Then the values of the matrix D should be added, (which increase or decrease the chances of belonging to a certain environment) according to the number of samples in which there were appearances of each Unit. It is then calculated $R = A.D^t$ that it is the product between the matrix (the vector) A nd the transpose of the matrix D. In the example:

$$R = (2,4) \cdot \begin{pmatrix} 0 & 0{,}27 & -0{,}28 \\ -0{,}23 & 0{,}29 & 0 \end{pmatrix} = (-0{,}92, 1{,}7, -0{,}56)$$

Each coordinate of the vector R corresponds to one of the environments, in the example:

$$\begin{array}{ccccc} \textit{Environmen}\ 1 & & \textit{Environmen}\ 2 & & \textit{Environmen}\ 3 \\ (\ -0{,}92 & , & 1{,}7 & , & -0{,}56\ ) \end{array}$$

The largest of these coordinates indicates the environment the procedure is looking for. That is, the procedure considers that the set of samples corresponds to the environment whose coordinate has the highest value in the vector R. In the example it corresponds to Environment 2.

Estimations validation

Even before receiving new samples of the system, it is of great interest to test the operation of the algorithm. One strategy for this is to take the original database and take some random samples from it from the same environment, as if they were new samples, run the algorithm and verify if it is correct in the prediction, errs in the prediction or it is not able to give an answer regarding which environment the samples belong to. Let's go back to the matrix E. The rows in this matrix contain all the samples in the database and in each of the lines there are zeros or ones according to whether or not there are occurrences of each unit in the base. Here, the algorithm separates this matrix into three sub-matrices containing each of the samples from a single environment, as:

$$E^1 = \begin{pmatrix} e^{1,1}_1 & \cdots & e^{1,1}_m \\ \vdots & & \vdots \\ e^{1,k}_1 & \cdots & e^{1,k}_m \end{pmatrix}, \quad E^2 = \begin{pmatrix} e^{2,1}_1 & \cdots & e^{2,1}_m \\ \vdots & & \vdots \\ e^{2,k}_1 & \cdots & e^{2,k}_m \end{pmatrix},$$

$$\ldots\ldots\ldots, E^n = \begin{pmatrix} e^{n,1}_1 & \cdots & e^{n,1}_m \\ \vdots & & \vdots \\ e^{n,k}_1 & \cdots & e^{n,k}_m \end{pmatrix}$$

The algorithm now randomly chooses one of these matrices and a random sample from that matrix, runs the process as if it were a new sample and determines if it was correct in the prediction, erred in the prediction or could not give a prediction. It repeats this process n times and calculates the percentage of hits, misses, and no prediction results. Subsequently, it repeats the process described above, but this time taking two samples from each environment (instead of one). Then it takes three samples from each environment and so on up to thirty samples from each environment or the maximum possible if the database does not contain that many samples per environment. The algorithm then returns three graphs (hits, misses and no prediction) displaying the previous calculations, which gives an idea of the accuracy of the predictions. In the example shown in last section the resulting graphs are shown for the example given here (Figure 8).

ESTIMATION OF PHYSICAL AND CHEMICAL PARAMETERS FROM THE UNITS PRESENT

When trying to link biological, physical and chemical data, several problems immediately appear, some of them quite obvious: The number of variables is usually very large and the necessary computing power exceeds the capacity of the available resources. The choice of the way forward becomes difficult if one wants to simplify the problem.

Niche approximation

For its practical application, the interest is usually focused on relating only a limited number of physical and chemical parameters with only some of the units. Thus, we select a quantity "c" of physical and chemical parameters that here are called "$p_1, p_2, \ldots, p_c$" and a taxonomic unit "e". If in a sample of the database there is an occurrence of the unit "e",

Figure 3: The entire point cloud according to $[max_{p_1}, min_{p_1}] \times [max_{p_2}, min_{p_2}] \times \ldots \times [max_{p_c}, min_{p_c}]$

a vector $(v_1, v_2, \ldots, v_c)$ can be built with the values registered in that sample of the parameters "$p_1, p_2, \ldots, p_c$". Performing this task for all samples in which there is an occurrence of the unit taxonomic "e",we obtain a çloud.ºf points in space $\mathbb{R}^c$.

In the cases $c = 1, 2, 3$ that point cloud can be graphed.

Now let's take the ranges in which each parameter of interest moves, in this way we obtain for each parameter "p_j" a value "max_{p_j}" and a value "min_{p_j}" with which a "hypercubeïs constructed that contains the entire point cloud that represents the presence of the taxonomic unit "e".

The hypercube containing the total point cloud for the taxonomic unit e can be segmented by choosing a number d that will divide each interval $[min_{p_j}, max_{p_j}]$ obtaining smaller hypercubes called d_c in which c is the number of selected physical-chemical parameters and d is the number of times each number of the physical-chemical parameters will be divided in. The choice of these values will be subject to the computing power of the computers and can be selected based on the researcher's criteria.

In the case $c = 3$, of the three-dimensional case shown, there are many algorithms capable of constructing the "convex capsule" of the point cloud as a way to approximate the niche of the species with respect to the three particular parameters chosen.

The point cloud can be observed within different squares (figure 4) of resolution d representing the hypercubes d_c. The number of occurrences of the taxonomic unit e in each hypercube d_c is recorded to obtain a "fit"value from the point cloud.

Parameter estimation

Point clouds for the occurrence of two taxonomic units taking into account the same physicochemical parameters, cooccur in a few hypercubes (figure 5). Then the intervals can be limited under observation of the physicochemical parameters. The algorithm distinguishes the hypercubes where there were appearances of the taxonomic units by collecting and ordering the information. Hypercubes are labeled by d_c

Here we tried two different approaches:

In the first one, for each taxonomic unit, the occurrence number for each hypercube is obtained. An "occurrence" matrix is created that shows the number of occurrences of each unit in each cube. In this matrix, the rows m are the database

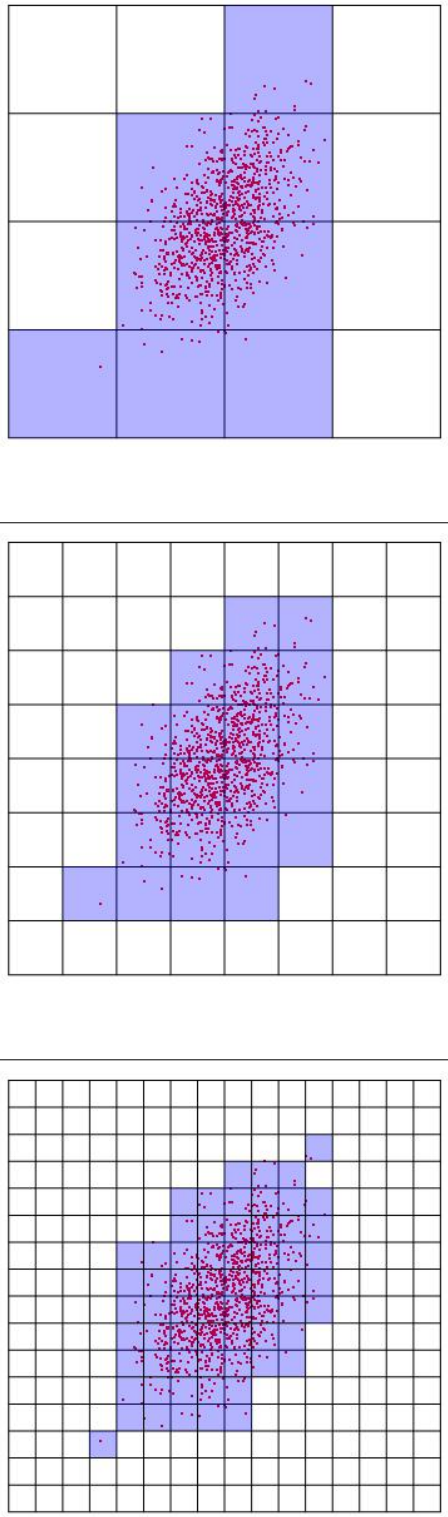

Figure 4: Different resolutions of the point cloud according to the size of the cells or grid resolution.

samples and the columns are the hypercubes d_c, so each value $a_{i,j}$ indicates the number of samples in which the unit i appears in the j cube.

This matrix is tedious to calculate and requires time. For this reason, the algorithm exports the matrix obtained as a csv file and later reads the values directly from that file. The algorithm, on the one hand, returns which taxonomic units appear in a sample and in which hypercube dc they are found.

On the other hand, given a number of taxonomic units then

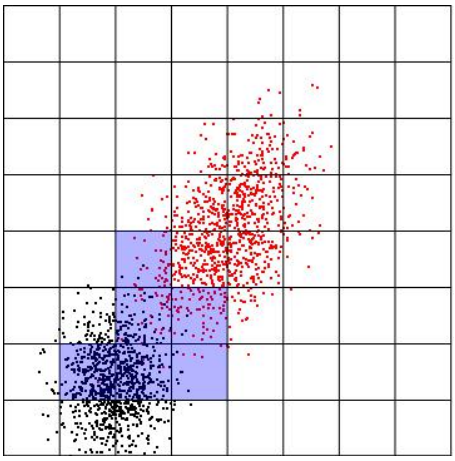

Figure 5: Superposition of the cloud of points corresponding to two taxonomic units and a grid that represents hypercubes d_c. The shaded area corresponds to the hypercubes in which the joint appearance of both taxonomic units occurs.

it returns the samples, from the database, in which all those taxonomic units appear at the same time and in which cubes they appear. Also, given a number of taxonomic units, it returns how many times all those units appear together in each cube. Each of the described steps are used to create a function that returns the hypercubes where the taxonomic units occur and the probability of being in a certain cube (knowing that all those units appeared in that sample).

As a second approach, m vectors are created (one for each species) of d^c coordinates (one for each cube). Each one of these vectors, contains either a 1 if that particular species appears at least once in a given cube, or a 0 if it never appeared in that cube. These vectors are easier to calculate than the matrix "appearance" described above, because it contains less information. These approach saves processing time and computer resources, but some other calculations cannot be performed this way.

If we then choose a certain number of species and want to visualize in which cubes they appear together, we only need to obtain the product, coordinate by coordinate, of the vectors of each species, and look in which coordinate each species appear a 1.

INDICATOR UNITS WITHIN THE GRID

Indicator units are characterized by appearing more in certain environments than in others (Dufrêne and Legendre, 1997). Proceeding as in the previous section, those physicochemical parameters of interest are chosen and the corresponding grid is made, with which more information can be obtained on how the difference between the expected and observed proportion of the units in each environment occurs. If we observe one indicator unit within the grid, the difference between the expected and the observed proportions in each cube can be calculated, which allows to visualize cubes (or "zones", sets of cubes) where the difference is greater. To do this:

A function is created that indicates the number of times and the percentage in which each cube appears in each environment.

The number of times and the percentage in which each cube appears in the entire database is calculated (without discriminating between environments).

With the above data, a matrix is built that has in each row the number of times each cube appears in each environment and in total.

Given a unit, the number and percentage of occurrences in each cube discriminated by environment are recorded (the number and percentage of occurrences in each cube having already been calculated without discriminating by environment).

With the previous data, a matrix is constructed that in each row shows the number of occurrences of the unit in each cube, discriminated by environment and in total.

The next step is to build a matrix called "Projections" that shows an estimate of how many times the unit should appear in each cube in each environment, assuming that its appearances were independent of the environment. Specifically, if we call:

- $c_{i,j}$ to the number of times the cube appears i in the environment j
- a_i to the number of appearances of the unit in the cube i in total (without discriminating by environment)
- c_i to the number of times the cube appears i in total (without discriminating by environment)

then the Projection matrix has in place the (i, j) value

$$\frac{c_{i,j} \, . \, a_i}{c_i}$$

as an estimate of the number of times the unit should appear in the cube i in the environment j

The difference between the last two matrices is then calculated, and shows the difference between the observed and the expected appearances of the unit in question in each cube and in each environment. This difference is also calculated as a percentage. These differences are displayed using histograms. This visualization becomes more relevant as long as the number of cubes is not too large.

A CONCRETE EXAMPLE OF HOW THE ALGORITHM WORKS

Example of Environment Estimation.

This section shows a concrete example of the use of the described process and the calculations and results obtained for that case. The database used in this example corresponds to a soil from the Pampean plain (Buenos Aires, Argentina). Each sample in this database collects measurements of fifteen physical and chemical parameters and the presence or absence of forty-three taxonomic units. The database has 216 samples in total corresponding to three different environments (72 samples from each environment). Environment 1 corresponds to a naturalized grassland (NG), Environment 2 to a grazing field that shifted to agriculture two years before the start of the samplings (CG), and Environment 3 is an environment of continuous intensive agriculture for at least 40 years (AG). The procedure begins with the selection of the indicator units, for them the matrices described in the section

"Selection of indicator unit" are calculated. Here (see Figure 6) the graph is shown where the difference between the observed and expected occurrences expressed as percentages is observed. In this case, as there are three environments, the value of the expected proportions (if the units were independent of them) is $\frac{1}{n} = \frac{1}{3}$ and it is represented by a horizontal line.

The procedure goes as in the section "Environment Estimation" and a coefficient matrix D:

	rho	par	vei	eup	Mic	Euk
NG	0,00	−0,33	0,00	−0,22	0,42	−0,33
CG	−0,22	0,66	−0,33	−0,33	−0,28	0,66
AG	0,24	−0,33	0,29	0,55	−0,14	−0,33

rho = rhodacaroidea par = parasitoidea
vei = veigaioidea eup = euphthiracaroidea
Mic = Micdub Euk = Euker

Now suppose that samples of the same type of soil were received but about their environments (or management) we do not know, and this process is used to determine which environment/management they belong to. As described in section "Environment Estimation", we take the coordinates corresponding to the indicator units and they are replaced by 0 if there were no occurrences of the units in that sample and 1 if there were. Then:

	rho	par	vei	eup	Mic	Euk
Sample 1	0	0	0	0	1	0
Sample 2	1	0	1	0	0	0
Sample 3	0	0	1	0	1	0

For instance, sample numbers 27, 35, and 36 of the database give these results and all three belong to the same NG environment.

The values of the samples are added:

	rho	par	vei	eup	Mic	Euk
Sum	1	0	2	0	2	0

The product between this last vector is then carried out with the transpose of the matrix D:

$$\begin{pmatrix} 1 & 0 & 2 & 0 & 2 & 0 \end{pmatrix} \cdot \begin{pmatrix} 0 & -0{,}22 & 0{,}24 \\ -0{,}33 & 0{,}66 & -0{,}33 \\ 0 & -0{,}33 & 0{,}29 \\ -0{,}22 & -0{,}33 & 0{,}55 \\ 0{,}42 & -0{,}28 & -0{,}14 \\ -0{,}33 & 0{,}66 & -0{,}33 \end{pmatrix} =$$

$$= \begin{pmatrix} 0{,}84 & -1{,}44 & 0{,}54 \end{pmatrix}$$

That is:

NG	CG	AG
0,84	−1,44	0,54

As the largest of the numbers corresponds to the NG environment, it is concluded that the samples come from that environment.

In this case, the prediction coincides with the actual origin of the samples. As described in section "Estimations validation", this process was carried out several times with one sample, with two samples, with three samples, and so on. The percentages of hits, misses, and times in which the algorithm cannot decide which environment the set of received samples belongs to are then calculated. The percentages are shown in Figure 7.

Example of Estimation of parameters from the units present.

In this example, the physical-chemical parameters that have been chosen (Sandler, 2019) were P, OM and N. It can be observed that the minimum and maximum values recorded for P are 0.00 and 75.78; those corresponding to OM are 1.51 y 9.2, and those of N are 0.14 and 0.51. Each of these ranges is divided into 3 parts (d=3) and a "grid" formed by 27 cubes is obtained as shown in Figure 8.

From the observation of the appearances of each unit within the grid, the procedure goes as described in section "Parameter estimation".

For example, the simultaneous appearance of the units Onychiuridae, Isotomidae, Eupodoidea and Aporos is detected only in samples that appear in the cube delimited by $0{,}00 \leq P < 25{,}26$, $4{,}08 \leq Mo < 6{,}66$ y $0{,}26 \leq N < 0{,}39$ (Figure 10).

The simultaneous appearance of the units "Hypogastruridae", Çrotoniodea", and "Juveniles" is only detected in samples that appear in the cube delimited by $0{,}00 \leq P < 25{,}26$, $4{,}08 \leq Mo < 6{,}66$ and $0{,}14 \leq N < 0{,}26$ in the cube delimited by $0{,}00 \leq P < 25{,}26$, $4{,}08 \leq Mo < 6{,}66$ and $0{,}26 \leq N < 0{,}39$. Joining both cubes it can then be determined a zone of simultaneous appearances is delimited by $0{,}00 \leq P < 25{,}26$, $4{,}08 \leq Mo < 6{,}66$ and $0{,}14 \leq N < 0{,}39$ (Figure 11).

Example of Indicator units within the grid

Let's now take the parameters P, Mo y N as in the previous subsection and build the same division into cubes. Let us also take the indicator unit Rhodacaroidea and compare its distribution in each cube in each environment with the expected distribution if the appearances of the unit were independent of the different environments.

The three graphs that are in the upper part of Figure 12 show how many times that unit appears in each cube and in each environment (cubes numbered here from 1 to 27). The three graphs in the lower part show how many times it should appear under the hypothesis of independence of environments.

It can be seen in Figure 6 that the unit Rhodacaroidea (with the number 7) appears more frequently than expected (which in the example is 33 percent) in environment 3 (environment AG), less frequently than expected in environment 2 (CG) and with the frequency expected in environment 1 (NG). These differences between what is observed and what is expected can be found in some aspects of Figure 12. It can be seen, for example, that in the cubes that appear with the numbers 1, 4, and 5, there is a marked difference upwards (between expected and observed) in the AG environment and

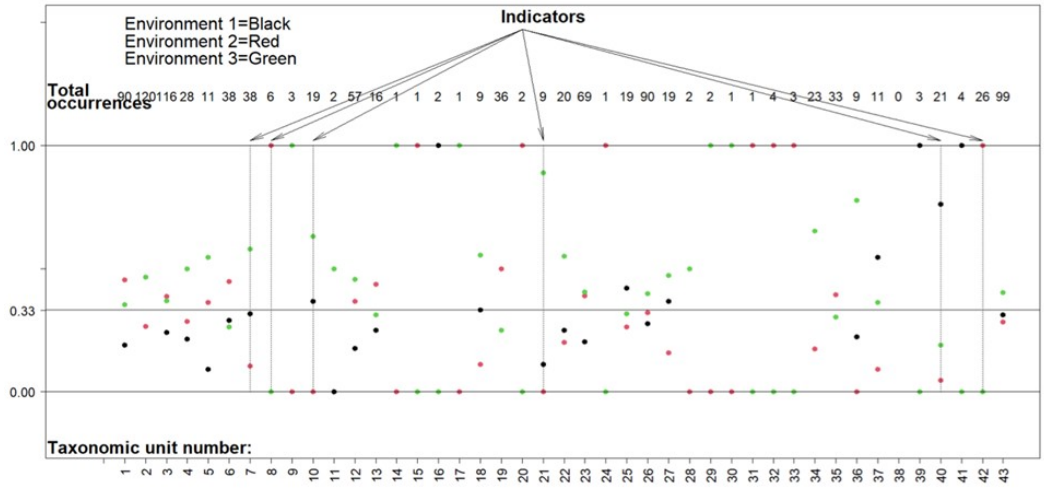

Figure 6: All taxonomic units labeled with numbers are shown. Total number of occurrences of the tagged taxonomic units. The vertical axis represents the rate of occurrence of a taxonomic unit, the limit 0.33 is the expected value E_j^l. Vertical dotted lines are those indicator species. Environments are represented by colors. Environment 1 = black Environment 2 = red Environment 3 = green. The units selected as indicators are Rhodacaroidea; Parasitoidea; Veigaioidea; Euphthiracaroidea; Microscolex dubius; Eukerria stagnalis.

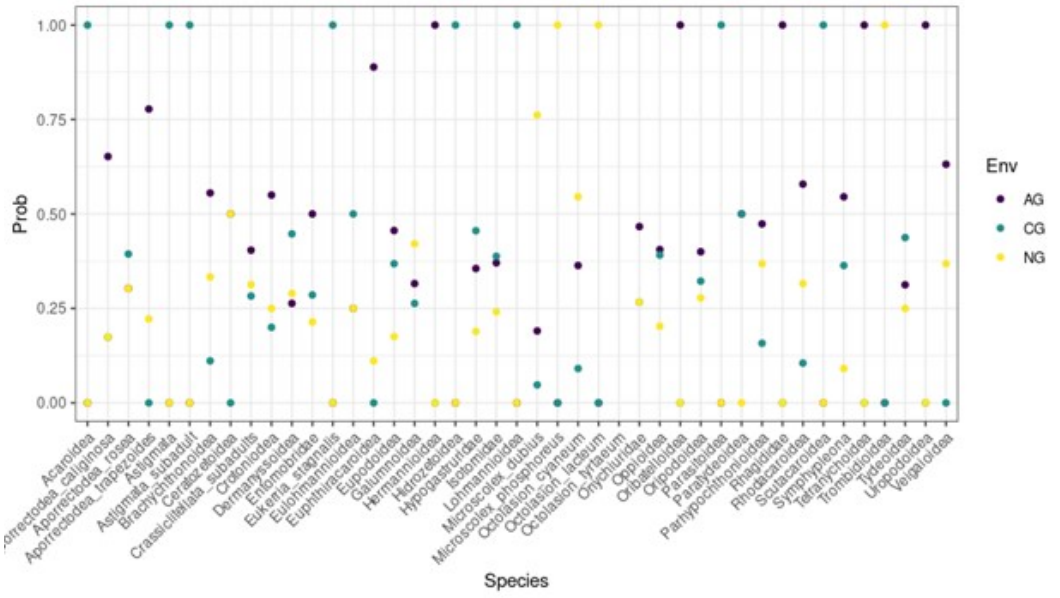

It shows the observed proportions in each environment, and they are represented by color dots.

a marked difference downwards in the CG environment.

CONCLUSIONS

Although this method was originally developed using a soil biota database (Sandler, 2019), it will work just the same in any other environment or ecosystem for which there is a suitable database of biological entities, associated with an environmental dataset. The algorithms developed and put together in this new method not only allow for the identification of indicator taxonomic units (depending on the taxonomic resolution available to the user), but also to approximate their ecological niches and, given a new sample, to estimate the physicochemical parameters of the site according of the species present in that sample. One of the main advantages of this method is that it can be used for any ecological system for which there is a suitable biological dataset associated to environmental factors. Another useful feature, is that it requires only presence/absence data. Researchers that also have density data, can modify and improve the method by tailoring it to their datasets. Thus, we feel that this contribution will be of interest for researchers developing indicators of ecosystem state. Moreover, the entire procedure was then converted to "Ecoindicators" Duhour et al. (2021), an R package that performs all the required tasks. The package (DOI: https://github.com/lsaravia/EcoIndicators) is free to use and to be improved by any researcher, with proper citation.

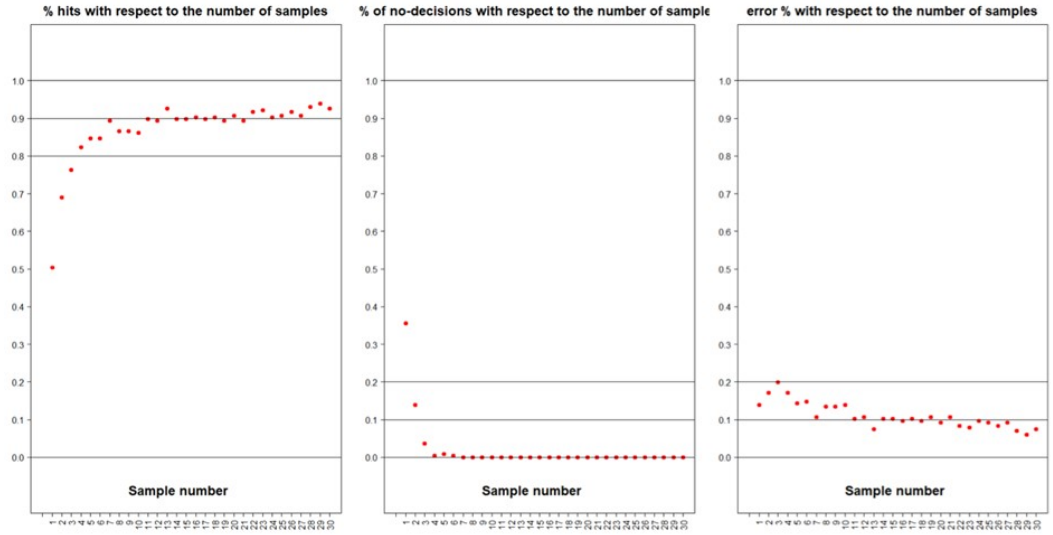

Figure 7: Percentages of hits, no-decisions, and misses calculated.

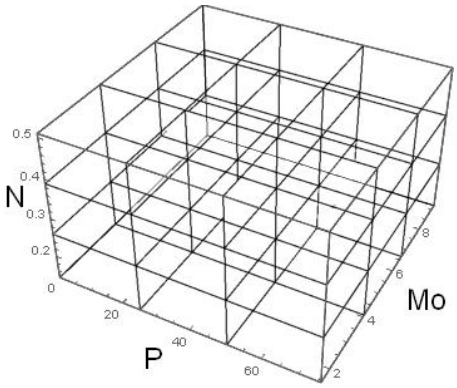

Figure 8: Cube built with Nitrogen (N), Phosphorous (P), and Organic matter (OM) environmental factors.

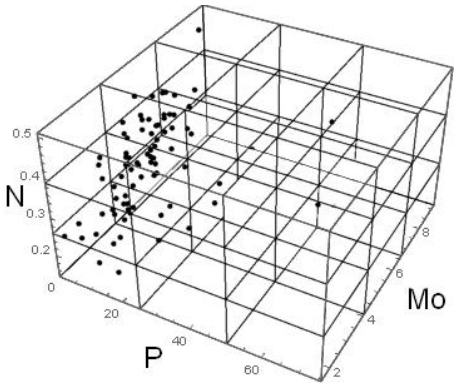

Figure 9: Cube built with N, P, and OM, showing the presence of the Onychiuridae taxon in a grid of the environmental variables N, P and OM.

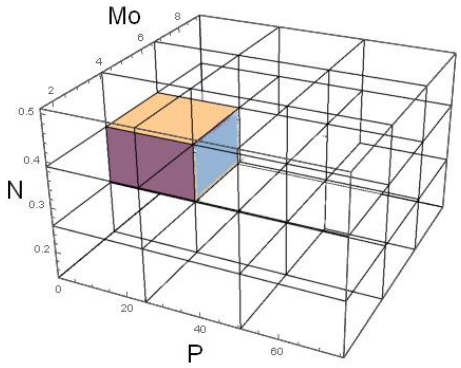

Figure 10: Simultaneous occurrence of taxonomic units Onychiuridae, Isotomidae, Eupodoidea and Aporos.

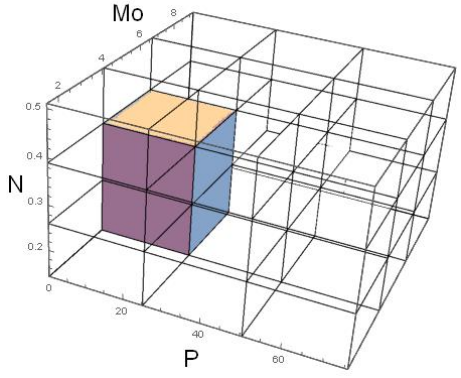

Figure 11: Simultaneous occurrence of taxonomic units Hypogastruridae, Crotoniodea, and Juveniles.

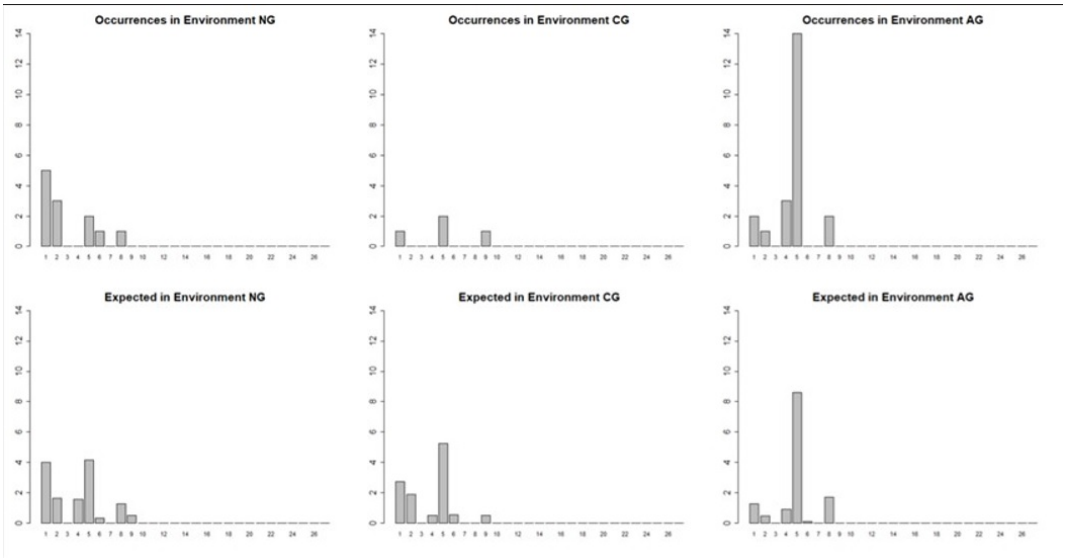

Figure 12: Observed (upper panels) and expected (lower panels) occurrence of unit Rhodacaroidea in the three environments being compared. Natural grassland (NG), Cattle grazing (CG), and Agriculture (AG).

REFERENCES

[1] Dufrêne, M. and Legendre, P. (1997). "Species assemblages and indicator species:the need for a flexible asymmetrical approach". *Ecological Monographs*, 67(3):345–366.

[2] Duhour, A., Falco, L., Saravia, L., Sandler, R., de la Vega, A. E., and Coviella, C. E.*lsaravia/EcoIndicators: First release*. title.

[3] European-Parliament (2000). "Eu water framework directive. directive 2000/60/ec of the european parliament and of the council of 23 october 2000 establishing a framework for community action in the field of water policy". *Official Journal*, L 327:0001 – 0073.

[4] Fortin, M.-J., Dale, M. R. T., and Brimacombe, C. (2021). "Network ecology in dynamic landscapes". *Proc. R. Soc. B.*, 288(20201889).

[5] Guerra, C. A., Bardgett, R. D., Caon, L., Crowther, T. W., Delgado-Baquerizo, M., Montanarella, L., Navarro, L. M., Orgiazzi, A., Singh, B. K., Tedersoo, L., Vargas-Rojas, R., Briones, M. J. I., Buscot, F., Cameron, E. K., Cesarz, S., Chatzinotas, A., Cowan, D. A., Djukic, I., van den Hoogen, J., Lehmann, A., Maestre, F. T., Marín, C., Reitz, T., Rillig, M. C., Smith, L. C., de Vries, F. T., Weigelt, A., Wall, D. H., and Eisenhauer, N. (2021). "Tracking, targeting, and conserving soil biodiversity". *Science*, 371(6526):239–241.

[6] Hutchinson, G. E. (1957). "Concluding remarks". *Cold Spring Harbor Symposium in Quantitative Biology*, 22:415–427.

[7] Potapov, A. M., Tiunov, A. V., and Scheu, S. (2019). "Uncovering trophic positions and food resources of soil animals using bulk natural stable isotope composition". *Biological Reviews*, 94(1):37–59.

[8] Sandler, R. V. (2019). *Indicadores de sustentabilidad del suelo basados en la estructura y funcionamiento de la fauna edáfica*. Universidad Nacional de General Sarmiento, Argentina.

[9] Velásquez, E., Patrick, L., and Mercedes, A. (2007). "Giqs: a multifunctional indicator of soil quality". *Soil Biology & Biochemistry*, 39:3066–3080.

When shape matters: using a simple mathematical model to estimate critical area sizes in conservation

‘Cuando la forma importa: uso de un modelo matemático simple para estimar los tamaños de áreas críticas en la conservación

Raul Abreu de Assis[1], Mazílio Coronel Malavazi, Rubens Pazim, Gustavo Canale, Moiseis Cecconello[2] and Odair José Teixeira da Fonseca[3]

[1] *Faculdade de Ciências Exatas, Universidade do Estado de Mato Grosso, Mato Grosso, Brazil*
[2] *Universidade Federal do Mato Grosso, Mato Grosso, Brazil*
[3] *Universidade Federal de Rondônia, Rondônia, Brazil*

Reception date of the manuscript: 14/junio/2022
Acceptance date of the manuscript: 09/agosto/2022
Publication date: 31/agosto/2022

Abstract—In the analysis of anthropogenic impact on the environment arises the question of whether the shapes of preserved habitat fragments play an important role in the conservation of wild species. In this work we use a very simple mathematical model based on a reaction-diffusion equation to analyze the effects of geometric shape and area on the permanence of populations in habitat fragments. Our results indicate that a dimensionless quantity calculated from a combination of biological variables is the main component that determines if the species survives in the preserved fragment and whether its geometric shape is important. We provide a methodology to calculate critical area sizes for which population size is most affected by fragment shape. The methodology is illustrated in a preliminary study, in which the model is used to estimate threshold area sizes for habitat fragments of a threatened species *Sapajus xanthosternos*.

Keywords—Area, Conservation, Fragment, Geometric Shape, Mathematical Model, Threshold.

Resumen—En el análisis del impacto antrópico sobre el medio ambiente surge la pregunta de si las formas de los fragmentos de hábitat conservados juegan un papel importante en la conservación de las especies silvestres. En este trabajo utilizamos un modelo matemático muy simple basado en una ecuación de reacción-difusión para analizar los efectos de la forma geométrica y el área sobre la permanencia de poblaciones en fragmentos de hábitat. Nuestros resultados indican que una cantidad adimensional calculada a partir de una combinación de variables biológicas es el componente principal que determina si la especie sobrevive en el fragmento preservado y si su forma geométrica es importante. Proporcionamos una metodología para calcular los tamaños de áreas críticas para las cuales el tamaño de la población se ve más afectado por la forma de los fragmentos. La metodología se ilustra mediante un estudio preliminar, en el que el modelo se utiliza para estimar el tamaño del área límite de los fragmentos de hábitat para la manutención de la especies amenazada, *Sapajus xantosternos*

Palabras clave— Área, Conservación, Fragmento, Forma geométrica, Modelo matemático.

INTRODUCTION

Landscape ecology studies traditionally use landscape pattern indices, a.k.a landscape metrics, to predict ecological responses, they are mostly associated to patch size, shape and habitat amount and aggregation (Gustafson, 2019). Detailed ecological research on patch-scale alterations on biodiversity were never as relevant, considering that half of the forests of the planet are less than 500 m from the forest edge, and mostly are patches smaller than 10 ha (Haddad et al., 2015). Moreover, habitat fragmentation, isolation and creation of edge environments initiate long-term responses of organisms and ecosystems processes that percolate through the landscape (Haddad et al., 2015).

The edge of forests may be a barrier to animal movements (Tuff et al., 2016; Boesing et al., 2018), thus, the area and

shape of forest patches are appropriate metrics to assess the effects of spatiotemporal changes in the landscape configuration over biodiversity measures, such as, species richness, community structure and organisms' abundance (Ramalho et al., 2014; Han et al., 2019). These alterations in landscape patterns are also used as predictors of ecological processes, namely the probability of population extinctions and migrations (Xu et al., 2014).

Recently, a vivid debate on the importance of considering several spatial scales to assess the changes in biodiversity has arisen and most studies indicate that scale selection is species-sensitive (Moraga et al., 2019). It is well-known that anthropogenic and natural landscape alterations disproportionately impact forest-core species, which are almost four times more prone to extinction than edge-tolerant and habitat generalist species (Pfeifer et al., 2017). Accordingly, it has been shown that forest-core species are vulnerable to hunting and predation when moving through non-forest habitats, and that abundance of forest-core animals is consistently larger at about 400 m away from the edge, confirming that edge effects operate at a small spatial scale (Pfeifer et al., 2017).

The impacts of edge effects on populations of forest-dependent species are influenced by the ratio of forest core in relation to forest edge. Thus, edge effects are strongly related to the shape of forest fragments, but they are less intensive in the core of larger forests fragments (Nogueira et al., 2021; Banks-Leite et al., 2010). Forest-core species are more strongly affected in small forest fragments with convoluted shapes (Ewers and Didham, 2008; Banks-Leite et al., 2010). The population abundance of these forest species tend to decline under edge effects and ultimately increase the risk of local extinction (Pfeifer et al., 2017).

Traditional approaches in landscape ecology use diversity measures, such as species richness and equitability, to explore how changes in habitat structure and landscape configuration may lead to species loss, alterations in the animal community composition, and biodiversity erosion (Watling et al., 2020). Fewer landscape ecology studies address the influence of those landscape modifications on population dynamics. Here we use population dynamics models (partial differential equations) to understand the population vulnerabilities associated to changes in the spatial configuration of forest patches. This approach allows us to study the link between the spatial configuration of the habitat and the population dynamics (Nabe-Nielsen et al., 2010).

The mathematical model used in the present work may be included in the broad class of KISS models (Cantrell and Cosner, 1994) and, although some discussion has already been developed on the theme of critical patch size (Cantrell and Cosner, 2001), many of the results can be computed explicitly only when applied to patches with a relatively simple geometry. Our analysis uses a different approach, which is based on numerical simulations over a wide variety of geometrical shapes and the use of field data to fit the model parameters. Combining the strong theoretical results present in Cantrell and Cosner (2001) with field data and precise numerical simulations is a work reserved for the future.

The paper is subdivided in three other essential sections besides this introduction. In the section "Material and Methods" we present the model, the biological hypotheses and parameters, and quickly review some metrics of fragment shape. In the section "Results" we deduce general ecological results from the model and illustrate its application in a particular preliminary study directed to a particular species (*Sapajus xanthosternos*). Finally, in the conclusion section we discuss some of the general and particular results, delineating also directions for future research.

MATERIALS AND METHODS

The model

The main focus of this paper is to deduce conditions in which the shape of a habitat fragment does have a significant impact on the chances of conservation of a certain species that occupies it. Since this question is quite general, we are immediately caught in a tension, trying to avoid two opposing dangers: oversimplification of biological traits and narrowness of results due to an excessive number of hypotheses.

For the particular model used in this work, each species may be represented by a combination of five basic biological parameters: the time it would take a population to be doubled under the most favorable conditions (T_r in time units), the carrying capacity in an undisturbed/preserved environment (K in number individuals per area unit), the time that it would be necessary for the population to be halved in a disturbed/hostile environment (T_m in time units), a dispersion coefficient (D units of area per unit of time) and a non-dimensional coefficient of mobility (η) that identifies if individuals tend to disperse faster or slower in the disturbed environment when compared to its movement in the preserved areas.

Of course, under many aspects, this is an oversimplification of any biological species, but here we argue for this approach, underlying the following points:

1. If our objective is to gain insight, from a broad perspective, on the effects of shape and area size on the survival of species, we cannot rely on detailed dynamics which are species-dependent.

2. This generality allows for an easier application in specific cases, requiring just a few biological parameters to adequately apply the methodology outlined by the model. Detailed models often require the estimation of a much higher number of parameters, many of which may demand intricate experiments to be successfully determined.

3. As long as the model and methodology is not considered as an absolute tool and is used only as a guideline to provide rough estimates of threshold area sizes, there should be no harm in approximating the complex population dynamics of the real populations for the simplified one presented here.

It is worth to mention that the model is effective in illustrating the importance of the relations between certain scales that are connected with mobility, reproduction rates and area of the fragment. In this sense, the model should provide some insight from the perspective of ecological theory and conservation, going beyond the simple applications of statistical methods of analysis, which, of course, have their own importance and scope.

The biological hypotheses

In the process of mathematical modeling it is important to clarify the biological hypotheses assumed so that we know exactly what is included and what is not in the dynamics presented by the model. The main assumptions considered in our model are enumerated below:

1. The model describes the dynamics of one particular species at a time. No interspecific relations are modeled.
2. The region to be analyzed can be divided into two clearly different landscapes. One represents a preserved and favorable environment to the species while the other corresponds to a hostile ambient, where the population could be sustained only for an definite amount of time (extinction is unavoidable in the hostile ambient).
3. Within the preserved environment the species grows logistically up to a carrying capacity.
4. In the hostile ambient the population decays exponentially.
5. Individuals are forced to move around in the environment in both types of landscapes, either due to overpopulation forces, foraging or other species-dependent factors. The particular details are not taken into account in the model, instead, those forces are represented by two parameters, one for movement in the preserved region and other for the hostile one.

The first hypothesis simply means that we are not explicitly describing complex ecological relations between species. These relations, of course, are very important in the real biological system and may be the decisive factor between the survival or the extinction of a particular population. In our approach, those relations are "embedded" in the form of the division of the region in a preserved or hostile environment. In the preserved region, all the ecological relations necessary for the survival of the population are present while in the hostile region those conditions are absent. In this way, the analysis can be focused in just one species.

The second hypotheses is related to a very frequent occurrence in the study of anthropogenic impact on wild populations. In many instances is is possible to observe a "natural" landscape, where wild populations reproduce and a "disturbed" one, that has been modified to serve another purpose, for instance, raising of cattle or agriculture (Gollnow et al., 2018). Although the biological hypotheses do not explicitly account for a continuous transition between those types of environment, in the sense that each location is either classified as "preserved" or "disturbed", the mathematical formulation does provide a certain smoothness in the transition from one scenario to the other. In this type of model, populations that live closer to the transition frontier tend to reproduce, on average, slower than those in more "interior" areas.

Referring to the third hypothesis, although some species tend to conform to the specific form of Logistic growth (Barlow, 1992), in our model, this particular form of dynamics is used just to represent the factual observation that every population has its growth limited to the natural resources available. In this case, those are supposed to be directly proportional to the size of the preserved area. Similar models with analogous limited-growth functions (a generalized Logistic model was used (Tsoularis and Wallace, 2002)) were tested and very close results were obtained, providing some evidence that our analysis is independent of the particular choice of a Logistic growth function, but rather that the fundamental fact is the limited carrying capacity of the environment.

The fourth hypothesis accounts for mortality in the hostile environment. It can be proved (Tijms, 2003) that if each individual has a fixed probability of dying per time unit then the dynamics of the whole population can be approximated by an exponential decay. The important factor here is that the species is tending to extinction in the hostile environment.

The last hypothesis involves the dispersion of the individuals. Animal movement is an extremely complex topic and many factors do contribute to the observed movement pattern at the population level. When enough data is available, precise mathematical models can be fitted to describe complex inter and intra-specific interactions that affect movement. In particular, Moorcroft et al. (2006) have successfully used a reaction-diffusion equation to model wolf pack territory formation in Yellowstone Park, being able to closely fit the model to empirical data on population distributions. Due to its generality, the model we propose is much less detailed and we do not expect such model to precisely describe the microscopic individual movement dynamics. Instead, we rely on a macroscopic parameter, the diffusion (or dispersion) coefficient, to represent a general tendency of dispersion, whatever is the particular biological mechanics behind it. Particular population estimates in well-known regions may then be used to fit the dispersion coefficient, avoiding the need of intricate empiric research on the movement pattern of the modeled species (see the Case Study Section for further details).

Finally, there is the observation that individuals may move at different speeds depending if they are in a preserved or hostile area. While the precise estimation of such difference may be subject to technical difficulties, we find this assumption necessary, given the generality of the model, which could be applied to many different species and terrains. In Section "Sensitivity Analysis" we show that parameter η, which is related to this difference in movement, is a parameter that does not have a very strong impact on the equilibrium population. Since the results are fairly robust to this factor, the model may still be applicable even if it is not possible to estimate precisely the difference in mobility between hostile and preserved areas.

The variables and the simulation space

The dynamics proposed occurs in a three-dimensional space ($\mathbb{R}^3$), having two Cartesian coordinates, $(x,y) \in \mathbb{R}^2$, for the spatial distribution and another one for time, $t \in \mathbb{R}$. The population is then described by a density function $u(x,y,t)$, so if $\Omega \subset \mathbb{R}^2$ represents a fragment, $P(\Omega) = \iint_\Omega u(x,y,t)\, dxdy$ is the total population in it the fragment at time instant t. The dimensions of x and y are compatible with length (kilometer, mile, meter), while u may be expressed in individuals per area using convenient units of population and area compatible with x and y (thousands, hundreds for population; square meters, miles or kilometers for area). The time variable may be measured in years, months or other useful scale.

The domain of simulation was chosen as a rectangular set $L = [a,b] \times [c,d]$. Each point inside the domain was classified as being either favorable to the species (preserved habitat) or hostile to it (impacted environment). We defined $\Omega \subset L$ as the set that represents the fragment of preserved habitat while $L - \Omega$ stands for the hostile environment. Figure 1 illustrates an example of this type of separation.

The reaction-diffusion equation

Reaction–diffusion models are applied to the study of a wide variety of natural systems. Pattern formation in animal coats (Murray, 1989), spatial distribution of slime molds and formation of galaxies (Lin and Segel, 1988), ecological invasion by alien species (Shigesada and Kawasaki, 1997), chemical signalization in insects (Bonabeau et al., 1999) and even evolutionary phenomena (Assis et al., 2018) are some examples of applications. For an excellent review of its use in Mathematical Ecology, we indicate the book by Okubo and Levin (2001).

To model the population dynamics in L, we propose the following equations:

$$\frac{\partial u}{\partial t} = \begin{cases} \operatorname{div}(D\nabla u) + ru(1-u/K) & \text{if } (x,y) \in \Omega \\ \operatorname{div}(D_H \nabla u) - \mu u & \text{if } (x,y) \in L - \Omega \end{cases} \quad (1)$$

where D and D_H are the dispersion coefficients in the preserved habitat and the hostile environment, respectively, r is the per capita reproduction rate in the habitat, μ is the per capita mortality rate in the hostile environment and K is the carrying capacity in the preserved habitat.

The dynamics is separated in two regions, Ω and $L - \Omega$. The first term in both equations represents the mobility of the population in each environment, so the ratio $\eta = D_H/D$ indicates where the movement is faster, if $\eta > 1$ individuals move faster in the hostile environment while $\eta < 1$ means the opposite.

The use of a diffusion equation to incorporate the characteristics of complex movement patterns may be criticized as an oversimplification. While it is true that this type of equation may be deduced in many different ways (Perthame, 2007), a common misconception is to think that it can only represent Brownian motion, that is, the movement displayed by particles randomly colliding and moving in every direction. One way to interpret differently this equation is to suppose that, in microscopic scale, individuals carefully avoid overcrowded regions, moving in the direction of less populated areas in a velocity that is proportional to the stimulus given by the Weber-Fechner law (Laming, 1989). Under such assumptions, the resulting macroscopic dynamics is exactly a diffusion equation[1].

This can be seen by simply writing the term corresponding to the flux of individuals, $\vec{z} = D\nabla u$ as $\vec{z} = Du\vec{v}$, where

$$\vec{v} = \frac{\nabla u}{u}; \quad u \neq 0.$$

The biological interpretation is clear now: individuals move on the opposite direction of the gradient, but with a a speed/probability that is proportional to the ratio of the concentration difference perceived and the concentration of individuals. This ratio incorporates the effect described by the Weber-Fechner law, that the perception of changes in the intensity of stimuli is relative to the total present stimulation. Just to give a simple concrete example of this psychophysical law: a match lighted in total darkness provides a much higher stimulus than one lighted in plain daylight. So the model can be interpreted as implying that the population is trying to avoid overcrowded areas, moving in the opposite direction of increasing population density. Although the Weber-Fechner is not an "absolute" natural law and has been subject to criticism and also that alternatives formulations have been proposed for modeling stimuli perception (Krueger, 1989; Nutter and Esker, 2006), recent results seen to find new evidence supporting it (Dehaene, 2003). In any case, here it serves the purpose of illustrating how the diffusion equation may be reinterpreted as portraying a more complex behavior than just Brownian motion.

As stated in a previous section, the domain of the equation is $L = [a,b] \times [c,d]$. This choice of domain was made for the following reasons:

1. A rectangular domain facilitates the implementation of numerical methods to solve the differential equation.

2. The domain is chosen in a way so that it included that fragment of interest (Ω) and that the boundary conditions do not have a significant impact on the results.

The boundary conditions for the mathematical problems may be homogeneous Dirichilet conditions:

$$u|_{\partial L} = 0 \quad (2)$$

where ∂L stands for the boundary of L. Another possibility is to use the Robin homogeneous condition is given by:

$$\left.\frac{\partial u}{\partial n}\right|_{\partial L} = k_r u \quad (3)$$

where $\partial u/\partial n$ is the normal derivative (pointing outwards region L) and $k_r > 0$ is a constant that defines the intensity of the flux.

Homogeneous Dirichilet conditions imply that individuals die at the boundaries while Robin homogeneous conditions represents a migration that is proportional to the population density at boundaries We will not stress too much the role of the boundary conditions because the focus of the model is to analyze the effect of the geometric shape and area of Ω. The domain L, in this case is just a convenient choice that allows for an easier numerical simulation. We tested our results using both conditions and a variety of values for k and the results were very similar, independently of the boundary conditions used..

One last technical observation on the model is that there is a discontinuity in the diffusion coefficient. This is not a relevant modeling problem for our particular case since, in this work, the solution of the differential equation is approximated using a discretized version of the domain, where discontinuities are not an issue.

[1] This interpretation came to our knowledge through personal communication with Prof. Wilson Castro Ferreira Jr. Up to date we are not aware of any publication that treats this topic in detail

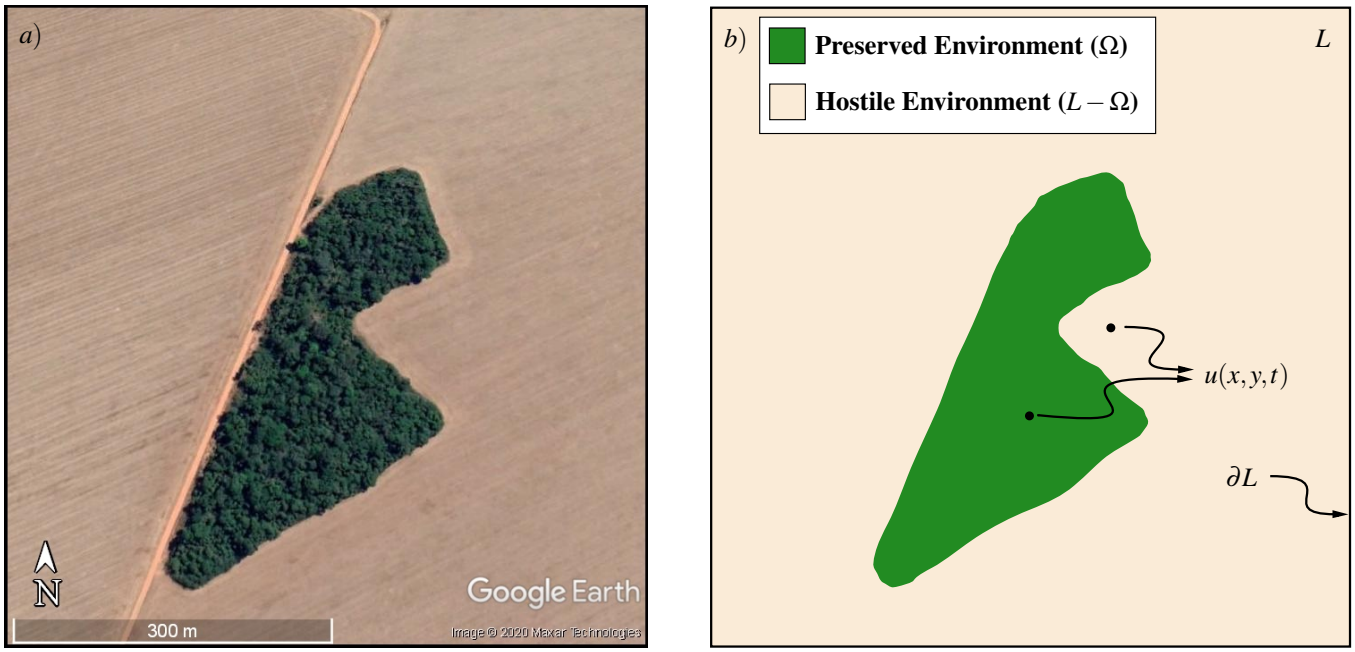

Figure 1: The image used in this example is merely illustrative. *a*) Rectangular satellite image of a preserved environment and surrounded by a hostile environment. The geographical coordinates $(12°0'49{,}60''S\ 55°24'29{,}35''W)$ belong to the highlighted region. Source: Google Earth. *b*) The domain of the model is a rectangular box L that includes a region of preserved environment represented by Ω and the complementary region $L-\Omega$ that stands for the hostile environment.The population is described by a density function $u \equiv u(x,y,t)$ that depends on the position in a two-dimensional space, (x,y) and a time variable t. The boundary of the domain is denoted by ∂L and is composed only of the four sides of the rectangle L.

Numerical methods

To simulate the model we first divided the domain L into the two regions Ω and $L-\Omega$ and, observing that D and D_H are constant, obtained the two partial differential equations:

$$\frac{\partial u}{\partial t} = D\Delta u + ru(1-u/K), \quad x \in \Omega \tag{4}$$

and

$$\frac{\partial u}{\partial t} = D_H \Delta u - \mu u, \quad x \in L-\Omega \tag{5}$$

where Δ stands for the two-dimensional Laplacian operator.

To approximate the solution of those equations, we adopted a finite-difference scheme (centered, second order) for the spatial Laplacian operator (Δ) and Runge-Kutta methods of combined orders 2 and 3 to solve the resulting system of ordinary differential equations. The application of these methods is considered routine in numerical analysis and can be consulted, for example, in Burden and Faires (2010).

To implement such numerical schemes we used two softwares: Matlab R2016b (registered for academic use under license number 1115837) and the open source Scilab (version 6.1.0). Two independent teams worked on the codes, each using a different software for comparison of results and avoidance of coding errors. For the Runge-Kutta methods we used the built-in functions provided by both softwares: `ode23` for Matlab and `ode` (with method option rk") for Scilab.

Estimates for r, μ and η

The model uses five mathematical parameters to simulate the dynamics: r, μ, K, D and D_H. To estimate those parameters, we need some biological estimates, as mentioned in the Section “The model":

1. T_r: supposing the conditions are very favorable to the population (resource abundance, low competition), T_r is the time the population takes to double its numbers.
2. T_m: supposing the whole region was transformed into a hostile environment, T_m is how long would it take for the population to be halved.
3. η: if we denote by d the average daily displacement of individuals in the preserved habitat and d_H in the hostile environment, then η may be interpreted as an estimate of d_H/d. Here the time scale of one day was mentioned, but it can be adapted according to the biological convenience.

The exact method for providing those estimates are left to the expert biologists for each case. From these three biological parameters and some population estimates in known areas and a least squares fit it is possible to estimate the remaining parameters (K and D). Further ahead in this paper we provide a case study as a guideline.

Parameter r: From the estimate of T_r, and taking into account that, for populations that are small relative to the carrying capacity, the Logistic growth can be approximated by a Malthusian one, we obtain r as:

$$r = \frac{\ln(2)}{T_r} \tag{6}$$

Parameter μ: Since the population decays exponentially on

the hostile environment, the instantaneous rate of decay μ can be directly obtained from the estimate T_m:

$$\mu = \frac{\ln(2)}{T_m} \tag{7}$$

Measures of compactness

One of the central questions approached in this paper is to evaluate how important fragment shape is to the conservation of populations. To conduct a mathematical analysis we need, then, some measure of "compactness" that can be used to represent the characteristics of a certain shape, so that its impact on population can be quantified. A discussion of the roles of such measures and a review of some particular formulas can be consulted in Li et al. Li et al. (2013). Other authors (Rutledge, 2003; McGarigal et al., 2012) present also some shape measures commonly used in landscape ecology analysis. Below, we briefly review some of the measures and choose which suits best the scope of this work.

If Ω is the two-dimensional set that represents the fragment we denote by $p(\Omega)$ as the perimeter (we suppose that the boundary of Ω can be described as a smooth function) and $a(\Omega)$ its area.

McGarigal et al. (2012)[p.104] present two of the most common measures of compactness, PARA:

$$\text{PARA} = \frac{p}{a} \tag{8}$$

and a Shape Index (SHAPE):

$$\text{SHAPE} = \frac{0{,}25p}{\sqrt{a}}. \tag{9}$$

Another possible measure is the IPQ (Osserman, 1978), given by:

$$\text{GE}_{IPQ} = \frac{4\pi a}{p^2}. \tag{10}$$

The measure given by PARA is not convenient because it is scale-dependent, so it was not adopted in this work. SHAPE is not dependent on scales and it is directly related to the IPQ.

In the IPQ measure a circle has the maximum measure of compactness value of 1. The intuition is simple, as the perimeter increases for the same area, the measure decreases, resulting in a value between 0 and 1. The use of the square of the perimeter avoids the impact of scaling factors (units of length), resulting in a reliable measure. To make the results more intuitive, we use the acronym GE to stand for "geometric efficiency" as the measure of compactness.

Here we propose a slight modification of the IPQ, using for the measure of compactness the following formula:

$$\text{GE} = \frac{16a}{p^2}. \tag{11}$$

The change is only a re-scaling of IPQ but, in our simulations, the discretization of the domain causes the regions to be transformed into a union of small squares, which also affects the length of its perimeter and, to a minor degree, its area. Due to this slight deformation of regions, we find it useful to use the square as the reference figure instead of the circle. In this measure, the square has a compactness measure of value 1.

SHAPE is directly related to GE:

$$\text{SHAPE} = \frac{1}{\sqrt{\text{GE}}}. \tag{12}$$

so any results obtained in terms of GE can be easily converted to SHAPE and vice-versa.

RESULTS

This section divided in two parts. The first is dedicated to general results and the second to a case study of the species *Sapajus xanthosternos*.

General results

For a clearer presentation, we separated the general results into three further sections. First, the combination of parameters that are important to the simulations are identified, then a sensitivity analysis is performed and finally the impact of geometric shape on species population is discussed.

Identifying the key parameters

Before we addressed the question relative to the impact of geometric shape of a fragment on populations, it was important to analyze the role of the parameters when shape was fixed. We chose a fragment as a circle and used six parameters to simulate the model: A_t (total area of the fragment), r (per capita reproduction rate in the preserved habitat), K (carrying capacity), μ (per capita mortality rate in the hostile environment), η (mobility coefficient) and D (dispersion coefficient).

Each simulation was conducted for a time limit of $100T_r$, that is, if the population is doubled in a year under the most favorable conditions, then the model was simulated for 100 years. For each simulation, we evaluated the total final population $P_\Omega(A_t, r, \mu, K, D)$ and then re-scaled it according to the maximum possible population $P_{\text{MAX}} = A_t \cdot K$, obtaining:

$$P^* = \frac{P_\Omega}{P_{\text{MAX}}}. \tag{13}$$

This re-scaling provides an estimate of the border effects on the fragment. For instance, if $P^* = 0{,}8$, this implies that the influence of the outside hostile environment causes a decrease of 20% of the maximum potential population in the fragment.

By simulating the model it was possible to obtain the re-scaled population as a function: $P^*(A_t, r, \mu, K, D)$ and we used this relation to study how the parameters affected the survival of the species. Allowing all parameters to vary in each simulation, the trend was not clear P^* when we looked individually at parameters A_t, r, μ, η or D, while parameter K had no impact at all in P^*. Instead, we found that P^* is dependent on the non-dimensional groupings:

$$\begin{aligned} \alpha &= \sqrt{\frac{A_t r}{D}} \\ \lambda &= \frac{\mu}{r} \end{aligned} \tag{14}$$

and the non-dimensional parameter η.

To illustrate such dependency, we chose three different values of λ (1/10, 1 and 10) and for each value of λ, the following distributions for the other parameters was chosen:

$$\begin{array}{ll} A_t \sim \mathscr{U}(0{,}25,3), & D \sim \mathscr{U}(0{,}001,0{,}25) \\ r \sim \mathscr{U}(0{,}25,1{,}4), & \eta \sim \mathscr{U}(0{,}5,2) \end{array} \tag{15}$$

where $\mathscr{U}(a,b), a,b \in \mathbb{R}$ stand for a uniform distribution between a and b. Note that once r and D are established, μ and D_H are automatically determined by the relations $\mu = \lambda r$ and $D_H = \eta D$.

These intervals were conveniently chosen to illustrate the relations and similar results are obtained with other intervals that comprise a similar spectrum for α. It is worth to stress that since α, λ and η are non-dimensional, they are not affected by the choice of units used to describe population density. A total of 250 random combination of parameters was chosen for each fixed value of λ. In Figure 2 we present illustrations of how P^* behaves in relation to some of the parameters, this illustrates the important role of λ and α. The results were robust to the choice of both initial and boundary conditions.

Another way to analyze the impact of the parameter is to measure the correlation between the parameters and P^*. In Table 1 we present the Spearman coefficient Kendall (1948) of correlation for the parameters and the variable P^*. The results confirm that α is the most important factor in the determination of P^*.

Another way of deriving the importance of α, λ and η is to write a non-dimensional version of the model. By defining new non-dimensional variables as $w = x/\sqrt{D/r}$, $v = y/\sqrt{D/r}$, $\tau = rt$ and $h = u/K$, model 1 is transformed to:

$$\frac{\partial h}{\partial \tau} = \begin{cases} \dfrac{\partial^2 h}{\partial w^2} + \dfrac{\partial^2 h}{\partial v^2} + h(1-h) & \text{if } (w,v) \in \bar{\Omega} \\ \eta\left(\dfrac{\partial^2 h}{\partial w^2} + \dfrac{\partial^2 h}{\partial v^2}\right) - \lambda h & \text{if } (w,v) \in \bar{\Omega} \in \bar{L} - \bar{\Omega} \end{cases} \tag{16}$$

where $\bar{L}$ and $\bar{\Omega}$ are transformations of the domain L and the fragment region Ω to (w,v) mapping. For the particular case of the simulations in this section, Ω was taken as a circle of area A_t having a radius of $R = \sqrt{A_t/\pi}$, so the transformed region $\bar{\Omega}$ is a circle of radius $\bar{R} = R/\sqrt{D/r} = \sqrt{A_t r/(D\pi)}$. Re-arranging the terms, we obtain:

$$\bar{R} = \frac{1}{\sqrt{\pi}}\sqrt{\frac{A_t r}{D}} = \frac{\alpha}{\sqrt{\pi}}. \tag{17}$$

Equations 16 and 17 show that the behavior of the non-dimensional model (which is independent of scaling) depends only on the non-dimensional groupings η, λ and α (which shall be called parameters henceforth).

The results of both the simulations and the dimensional analysis show clearly that parameters α and λ are essential to the survival of the species. These results are biologically intuitive: α^2 is proportional to both A_t and r, meaning larger areas and fast reproduction rates favor the survival of the species (hence the positive correlations between α and P^*). Also, α^2 inversely proportional to D, meaning that large mobility associated with a hostile surrounding environment impacts negatively the population. Parameter λ indicates how hostile is the environment outside the environment, being proportional to μ and inversely proportional to r, with more hostile environments leading to lower populations. Parameter η had a smaller influence on the final results, as can be seen in the curves in Figure 2-d), for each fixed curve with fixed λ, η was allowed to vary between 0,5 and 2, with little impact on the final re-scaled population P^* which was also confirmed by the analysis of the correlation coefficients in Table 1.

To analyze the relative impact of parameters α, λ and η we performed a sensitivity analysis of model 16, presented in the section below.

Sensitivity analysis

In this section we consider P^* as a function of α, λ and η. The simulations are analogous to the ones in Figure 2. We chose the shape of the fragment as a circle (with radius given by Equation 17), taking all parameters with the same distribution:

$$\alpha \sim \lambda \sim \eta \sim \mathscr{U}(0{,}05,20). \tag{18}$$

To evaluate the sensitivity we used the slopes of the direct one-dimensional regressions ($P^* \times \alpha$, $P^* \times \lambda$ and $P^* \times \eta$, from the multilinear regression ($P^* = a\alpha + b\lambda + c\eta + d$), the standardized regression coefficients and the Spearman coefficient. In Table 2 we display the results of the analysis. They clearly confirm the strong influence of parameter α, with λ and η playing a secondary role.

The impact of geometric shape

In the previous sections it was clearly established that α and λ are key parameters that define species survival in the model. The simulations indicated that, for each fixed λ, it is possible to divide the region of variation of α in three quite distinct regions. For very low values of α, the population is unable to survive, with $P^* \to 0$. For very high values, boundary effects have little impact on the dynamics, so $P^* \approx 1$ with the population approaching the maximum value possible. Finally, there is an intermediate region where P^* makes a transition between those extreme values, and in this region, the population total is strongly related to the effect of geometric shape.

For very large or very small values of α, geometric shape in unimportant, because either the area size is too big or too small in relation to the scales of reproduction and mobility (which is the measure that parameter α incorporates). In the intermediate region the geometric shape plays crucial role in determining how strong is the boundary effect, which may lead either to extinction or preservation.

The central problem analyzed in this paper can now be addressed as a very precise question: for each point in the two-dimensional parameter space (α,λ), is it possible to determine if geometric shape affects significantly the population estimates by the model? To answer this question we designed procedures do create random shapes and also to deform a preexisting shape, affecting its measure of compactness (as defined in the Section “Measures of Compactness").

For each point in the (α,λ) map we took an initial geometric shape for the region Ω, which we defined as S_0. This

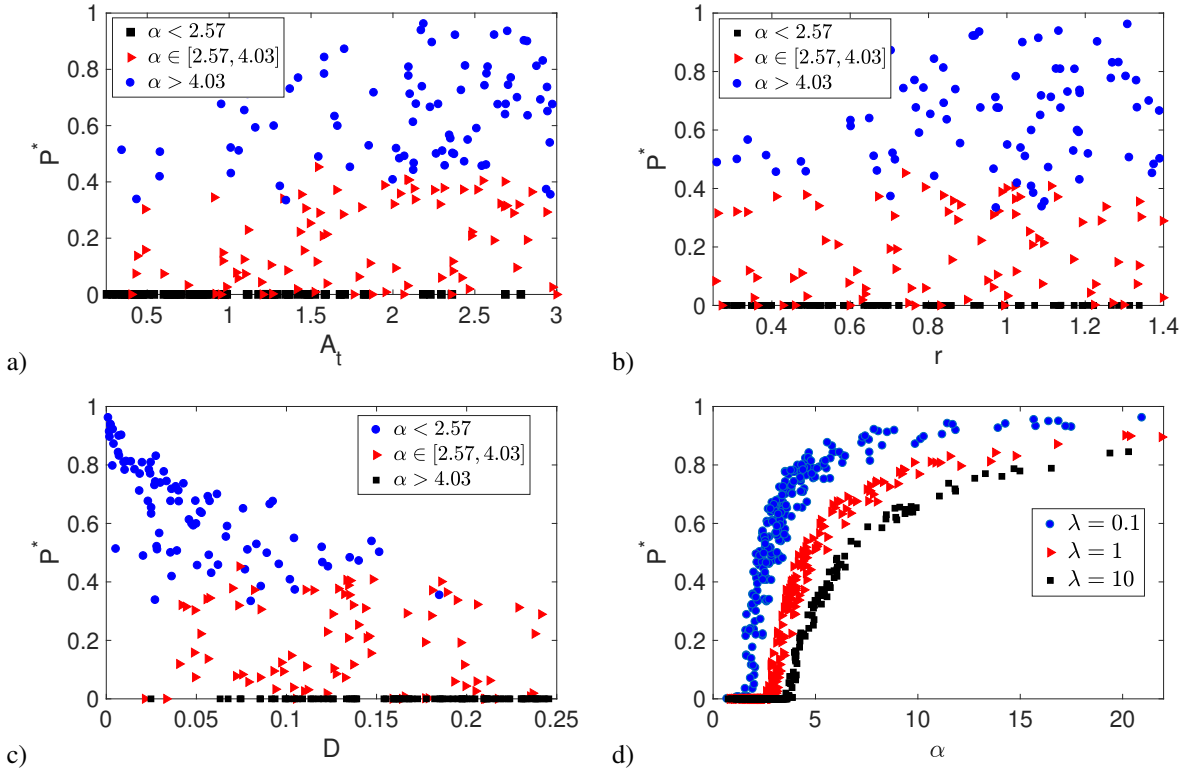

Figure 2: Seven hundred and fifty simulations of $P^* = P_\Omega / P_{\text{MAX}}$, the re-scaled population inside Ω. Parameters r (per capita reproduction rate), η (mobility outside the fragment), A_t (fragment area) and D (dispersion coefficient) were allowed to vary randomly according to the distributions given in Equation 15. a) Results of P^* in relation with A_t, the behavior is strongly dependent on the values of the other parameters. b) Results of P^* in relation with r. c) Results of P^* in relation with D. d) Results of P^* in relation with α, for each value of λ, a clear trend can be observed, indicating that α and λ are key parameters to the survival of the species in the fragment.

shape had a total area equal to α^2 to correspond to a dimensional simulation of a figure of area A_t and a initial GE, $G_0 = \text{GE}(S_0)$ larger than 0,65, to allow for variation. By applying deformations on this initial shape we generated a set of 30 other shapes, $S_1, \ldots, S_{30}$, with the same area but with compactness measures $G_1, G_2, \ldots, G_{30}$ in the set $(0{,}05 \cdot G_0, G_0)$. In the appendix we discuss in more detail the methods used to create deformations of the initial figure as to obtain shapes with smaller compactness values GE. This process is then repeated 10 times, so we obtain a collection of 300 shapes for each (α, λ) point.

For this set of shapes we simulated the non-dimensional model for a time horizon of $\tau = 100$ (which corresponds to the time horizon of $T = 100/r$ in the dimensional model) calculating the final re-scaled population $P_i^* = P(S_i)/\alpha^2$ for each shape, where $P(S_i)$ denotes the total population inside S_i after the simulation of the model. We obtained thus numbers between between 0 and 1 that correspond to the fraction of the maximum possible population achieved by that particular combination of parameters and geometric shape.

Given the series of points (G_j, P_j^*) relating figures with different measures of compactness and the final re-scaled population, it is possible then to calculate regressions of P^* by G that estimate the impact of the measure of compactness in the final re-scaled population. Since both variables are non-dimensional and are scaled between 0 and 1, we adopted the slope of the linear regression to estimate the correlation, obtaining the impact of geometric shape as a function of α and λ, $S \equiv F(\alpha, \lambda)$.

In Figure 3 we present a scheme that illustrates the whole process described in this section.

In Figure 4 we present examples of distributions of G_j, P_j^* and a curve $F(\alpha, \lambda)$ for $\lambda = 1$. The distributions clearly illustrate that, when $\lambda = 1$, we have the maximum impact of the geometric shape for values of $\alpha \in (5, 10)$.

In Figure 5 we present the map of slopes obtained from the simulations, $F(\alpha, \lambda)$. In the map is drawn also two curves $f(\alpha) = 0{,}1348 e^{0{,}007490604\alpha^3}$ (C^*) and $g(\alpha) = 0{,}0096 e^{0{,}2494\alpha}$ ($C_{0,4}$). C^* is used to estimate area sizes that are greatly impacted by fragment shape. To estimate this curve, for each fixed value of λ we estimated the corresponding α for which $F(\lambda, \alpha)$ was at it maximum value, next using a least squares fit, we adjusted a curve to fit the points. In this way C^* represents critical points where fragment shape has maximum impact and can be used to estimate areas sizes (A^*) for which fragment shape is very important. Finally, $C_{0,4}$ represents a part of the level set $F(\alpha, \lambda) = 0{,}4$. This line allows us to estimate, area sizes ($A_{0,4}$) for which fragment shape is relatively weak ($F = 0{,}4$ and smaller for larger areas).

If we recall that $\alpha = \sqrt{A_t r / D}$ we can establish approximate formulas for the critical area size (A^*) and relatively safe area size ($A_{0,4}$):

$$A^* \approx \frac{D}{r} \left(\frac{\ln(\lambda / 0{,}1348648)}{0{,}007490604} \right)^{2/3} \tag{19}$$

$$A_{0,4} \approx \frac{D}{r} \left(\frac{\ln(\lambda / 0{,}0096)}{0{,}2494} \right)^{2}. \tag{20}$$

TABLE 1: SPEARMAN CORRELATION COEFFICIENT FOR THE SIMUATIONS OF THIS SECTION. α, HAS THE LARGEST VALUE, ILLUSTRATING ITS IMPORTANCE TO THE SURVIVAL OF THE SPECIES. SINCE PARAMETERS A_t, r AND D ARE DIRECTLY RELATED TO α, THERE ARE ALSO A SIGNIFICANT CORRELATION.

	Spearman correlation coefficient for		
Parameter	$\lambda = 0{,}1$	$\lambda = 1$	$\lambda = 10$
α [1]	0.9622	0.9748	0.8486
A_t [1]	0.5264	0.5417	0.4037
D [1]	-0.7330	-0.6660	-0.6196
r [1]	0.3219	0.3308	0.4039
η [2]	0.2020 (0.1)	-0.0113 (0.85)	0.0723 (0.26)

[1] All coefficients have a p-value smaller than 10^{-8}.
[2] p-value inside parenthesis.

TABLE 2: RESULTS OF SENSITIVITY ANALYSIS OF MODEL 16 FOR PARAMETERS α, λ AND η, $P^* = P_\Omega/P_{\mathrm{MAX}}$ IS THE DEPENDENT VARIABLE. THE SPEARMAN COEFICCIENT AND THE SLOPES OF THE LINEAR, MULTILINEAR AND STANDARDIZED REGRESSIONS INDICATE THAT α PLAYS THE LEADING ROLE IN THE SURVIVAL OF THE SPECIES, FOLLOWED BY λ AND η THAT HAVE A MUCH WEAKER IMPACT.

	Slope by Method of Regression			
Parameter	**Linear [1]**	**Multilinear [2]**	**Standardized [3]**	**Spearman [4]**
α	0.0482	0.0479	0.8414	0.8864 ($< 10^{-4}$)
λ	-0.0095	-0.0081	-0.1365	-0.2889 ($< 10^{-4}$)
η	0.0091	0.0081	0.1319	0.2195 ($< 10^{-3}$)

[1] Individual linear regression in each parameter.
[2] Simultaneous linear regression in all parameters.
[3] Multilinear regression on the standardized variables $\left(x_i^* = (x_i - \bar{x})/\sqrt{\mathrm{var}(x)}\right)$.
[4] Upper bound for p-values inside the parenthesis.

Please note that the relatively small effects produced by variations in η are not included in these equations.

A preliminary case study

In this section we present a case study for the species *Sapajus xanthosternos*, a photo of an individual and a map of its geographic distribution are provided in Figure 6. We must stress that this study has the main purpose of illustrating the application of the model and how to interpret its results. For more robust biological conclusions concerning the species, further empirical work in estimating the parameters should be conducted.

It is possible to estimate r the maximum per capita growth rate if the maximum annual growth rate of the species is known. For this particular species, it was estimated that, given the most favorable conditions, the population would have a maximum growth rate of 13 % per year (da Silva et al., 2016), which leads to a correspondent logistic growth rate of

$$r = \ln 1{,}13 \approx 0{,}1222/\text{year}. \tag{21}$$

Mortality rates in the hostile environment are harder to estimate, and we had to rely on an educated guess by the expert (co-author Gustavo Canale) to arrive at a reference value. The information provided is that a group of 64 individuals could not last longer than a year, if exposed continuously to the hostile environment in this time interval. With such information and, considering an exponential decay in the hostile environment it is possible to obtain:

$$\mu = \ln 64 \approx 4{,}1588/\text{year}. \tag{22}$$

Since *Sapajus xanthosternos* is an arboreal species and the hostile environment, in this particular case, is considered to be mostly deforested areas dedicated monoculture, individuals tend to move and disperse faster in the impacted than in the preserved areas. The meaning here is that even though the individuals might move faster in arboreal environment, they tend to move more often in deforested areas, always looking for forest cover, resulting in a higher average speed in the open areas. Considering this information and also by expert advice, we adopted then a value of $\eta = 2$, meaning that, on average, individuals move two times faster outside the preserved areas.

To estimate the remaining parameters, D and K, we collected information on population estimates of populations of *Sapajus xanthosternos* (Culot et al., 2019) living in ecological sanctuaries near hostile environments. Since these population estimates are based on extrapolation from number of individuals sighted, we selected only those studies that were conducted in smaller regions (total area below 1000 ha) so that these estimates can be considered more precise. It is also worth to mention that 1000 ha is the largest forest area size in which *Sapajus xanthosternos* was recorded (Canale et al., 2013). After this process we obtained 5 fragments with different area sizes, shapes and populations. Such data can be consulted in Table 3.

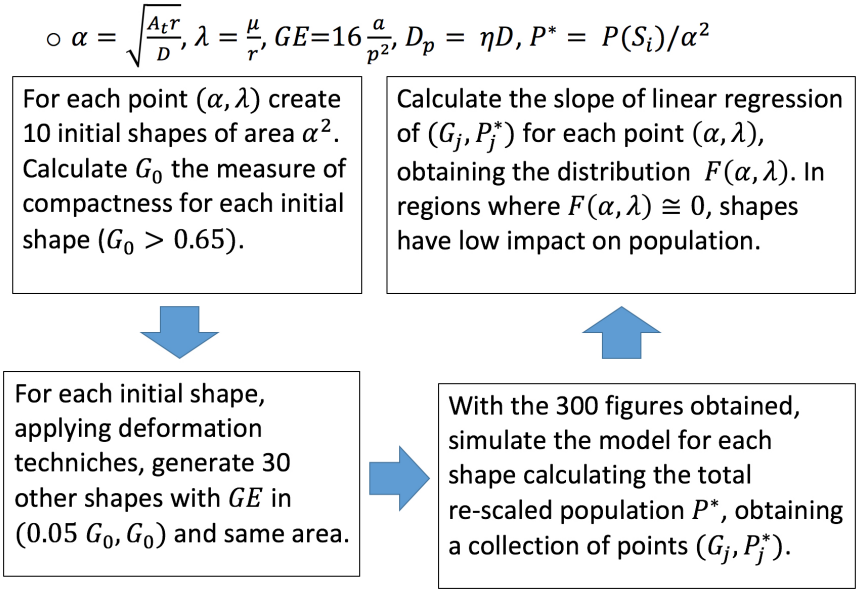

Figure 3: Scheme for the simulations of geometric shape impact on population. Each initial shape is deformed, reducing its compactness, and the impact on population recorded.The distribution $S(\alpha, \lambda)$, of linear regression slopes, measures the relation between compactness and population levels.

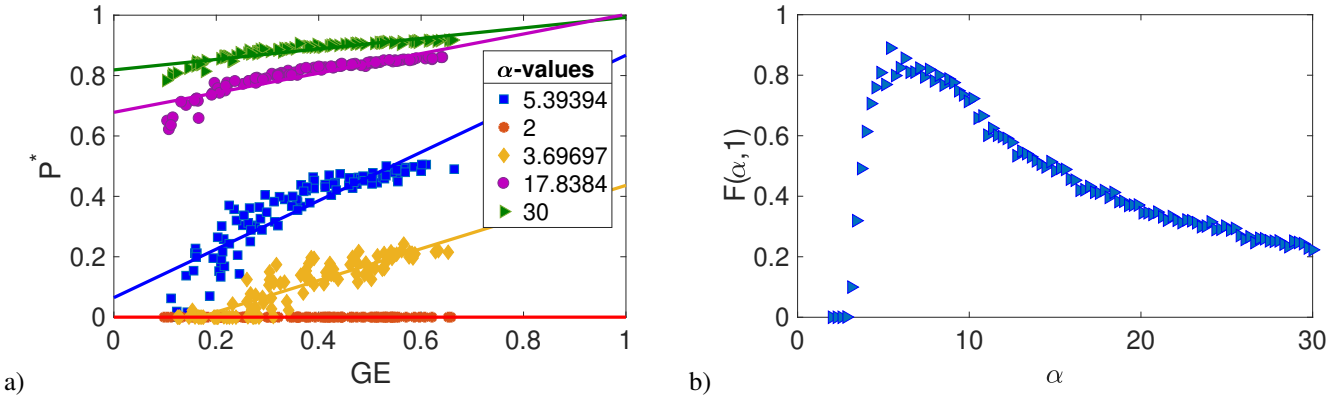

Figure 4: a) Five examples of collections of points (G_j^*, P_j^*), for different values of α and fixed $\lambda = 1$. For each collection we calculate the slope of the linear regression, $F(\alpha, 1)$. b) $F(\alpha, 1)$ denotes the values of the slope of linear regression of (G_j^*, P_j^*), for $\lambda = 1$ and $\alpha \in (2, 30)$.

To obtain images of the fragment shapes we used the software QGIS, using the CBERS4A downloader plugin, which provides access to the online database of CBERS4A satellite images. The images used correspond to the years in which the population estimates studies were conducted at each individual fragment. These are displayed In Figure 7. For each region, the model was simulated until the population reached an equilibrium. At the end of the simulation we calculated the total population *inside* the protected region, as in Figure 7, obtaining thus a vector with five population estimates provided by the mathematical model. We then used the least squares method to determine the optimal values of D and K that led to the best fit.

In Table 3 we present the results from simulations using the least squares fit for D and K. The optimal value for D was $D^* \approx 9{,}1746 \times 10^{-4}$ year$^{-1} \cdot$ km^{-2} and for K was $K^* \approx 26{,}8033 \times 10^{-4}$ individuals $\cdot$ km^{-2}. This particular value of K^* was considered biologically plausible by the expert biologist and within his own estimates.

With the estimated value of D^* now it is possible to use Equations 19 and 20 to establish to estimate the most sensible (A^*) and a relatively safe ($A_{0,4}$) area sizes for the species *Sapajus xanthosternos*. Results are presented in Table 4.

DISCUSSION

The simple model developed and the simulations allowed us to identify clearly the most important parameters that determine how strongly populations are affected by fragment shape. The results show clearly that these parameters are associated with mobility of the species, reproduction rate, area of the fragment and mortality rate in the hostile environment. All these parameters are combined in the two non-dimensional groupings α and λ.

The two-dimensional mapping of the behavior of the model in relation to parameters α and λ allowed us to establish functional relationships (i.e. 19 and 20) for A^*, the area size for which the population is very sensible to geometric shape,

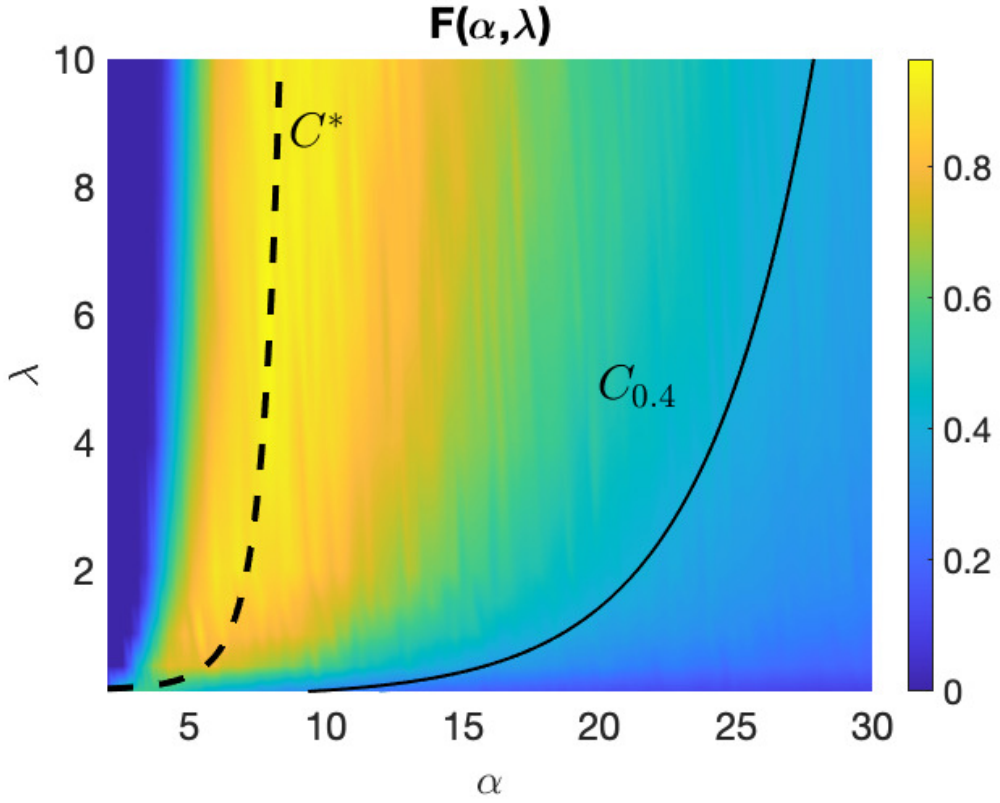

Figure 5: Two-dimensional mapping of the impact of geometric shape on the population. $F(\alpha,\lambda)$ denotes the values of the slope of linear regression of (G_j^*, P_j^*). Two curves $\lambda(\alpha)$ are drawn in the mapping: C^* given by the equation: $f(\alpha) = 0{,}1348e^{0{,}007490604\alpha^3}$ and $C_{0,4}$, with equation $g(\alpha) = 0{,}0096e^{0{,}2494\alpha}$. Curve C^* is constructed by estimating, for each fixed value of λ the corresponding value of α that leads to the highest value for $F(\lambda,\alpha)$ while $C_{0,4}$ is a part of the level set $F(\alpha,\lambda) = 0{,}4$. C^* represent critical values where fragment shape has maximum impact while $C_{0,4}$ represent a point where the impact of shape is already low.

and $A_{0,4}$, an estimate of a sufficient large are where geometric shape does not have much impact on population size. These relations show that the area threshold is proportional to the mobility (represented by D) and inversely proportional to r (rate of reproduction), reflecting the intuitive ideas that more mobile species need larger areas and those who reproduce faster need smaller ones. Also, the fact that the parameter that represents mortality in the hostile environment (λ or μ) is present as an argument of a logarithm function reflects the fact, also shown in the sensitivity analysis, that its impact on the area threshold is smaller.

Another, somewhat obvious, biological result that can be derived from the equations is that species with smaller body sizes should also need smaller areas for their preservation. This is because smaller species tend to reproduce faster (Dobson and Oli, 2007), meaning that parameter r should be greater for these species, leading to smaller critical areas. Finally, more lethal hostile environments also lead to increase in the area needed for preservation of the species. This is demonstrated in the results simply by recalling that $\lambda = \mu/r$, so any increase in μ leads to a correspondent increase in λ and, since both A^* and $A_{0,4}$ are increasing functions of λ, any increase in mortality rates in the hostile environment also leads to larger areas needed for preservation.

Previous work on KISS models and critical patch size (Cantrell and Cosner, 1994, 2001) present a more robust mathematical treatment of the stability of the zero solution (which represents extinction), while our approach (based on simulations) provides for more flexibility in dealing with complex geometric patch shapes. Another difference, is that our approach does not aim to calculate a particular area size in which the population is able to survive, instead, we identify a critical area in which geometrical shape exerts the strongest influence on the total population. Finally, the case study shows clearly how to use the model to estimate such critical areas, establishing a clear methodology to use field data.

Finally, we highlight a few points where further improvement of the model and results can be made:

1. Incorporate the use of finite element methods for the simulations of the model, since those can incorporate better the details of geometric shape of fragments.

2. Apply the model to a number of different species and fragments.

3. Improve the quality of parameter estimation, either by using larger data bases with information on fragment populations or better/more numerous estimates of reproduction/mortality rates and mobility.

4. Incorporate the mathematical methodology of estimating critical patch size using eigenvalues as in Cantrell and Cosner (1994) and Cantrell and Cosner (2001).

a) 

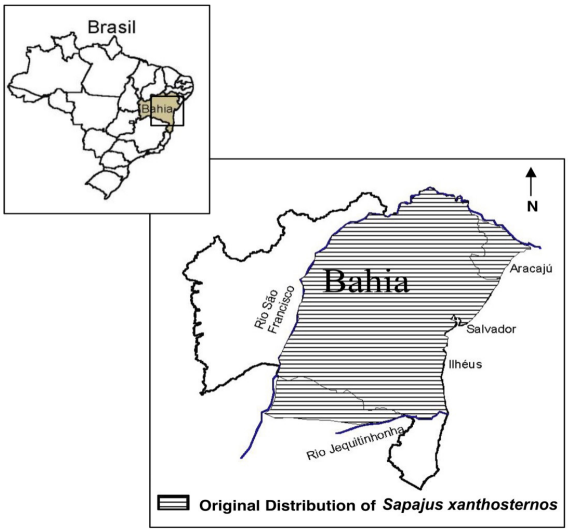

b)

Figure 6: a) An individual of the species *Sapajus Xanthosternos*. b) Map that reproduces appoximately the geographic distribution of the species.

TABLE 3: DATA ON *Sapajus xanthosternos* POPULATIONS IN PRESERVED FRAGMENTS, AVAILABLE IN CULOT *et al.* (2019) (CULOT ET AL., 2019) AND COMPARISON WITH SIMULATIONS OF THE MODEL WITH OPTIMAL VALUES $D^* \approx 9{,}1746 \times 10^{-4}$ YEAR$^{-1}\cdot$KM^{-2}, $K^* \approx 26{,}8033 \times 10^{-4}$ INDIVIDUALS$\cdot$KM^{-2}.

Region name/number	Total Area (ha)	Population estimate | Simulation [1]	Geographical Coordinates [2]
Água Sumida - 1	240	52,80 | 51,22	(−48,29082778, −22,63317778)
Monal - 2	374	164,48 | 85,76	(−48,08360278, −22,69596944)
Pouso Alegre - 3	350	26,98 | 70,02	(−45,96666667, −22,21666667)
Mata São José - 4	230	56,35 | 44,68	(−47,47743300, −22,35881600)
Sara - 5	501	76,85 | 114,69	(−48,19536111, −22,66642222)

[1] Number of individuals. Left: estimates based on number of sightings. Right: estimates based on simulations of the mathematical model.
[2] (Longitude, Latitude)

ACKNOWLEDGMENTS

The authors thank an anonymous referee for the suggestions that helped improve the original manuscript.

Funding

The authors declare that no funds, grants, or other support beyond their regular salaries were received during the preparation of this manuscript.

Conflicts of interest/Competing interests

The authors have no relevant financial or non-financial interests to disclose.

Consent for publication

The article does not use any third-part sensitive information that needs consent to be published. The authors consent to the publishing of the manuscript.

Availability of data and material

All the relevant data used in the manuscript is available in the published scientific references. The software used in the simulations is licensed for academic use and is registered in the name of the first author.

Author contributions

Raul Abreu de Assis elaborated the model, directed the analysis, helped create codes for the simulations, and led the writing of the manuscript. Gustavo Cannale proposed the biological problem, provided biological references, estimated part of the parameters for *Sapajus xanthosternos*, provided advice in biological issues and helped writing the manuscript. Mazilio Coronel Malavazi, Rubens Pazim, Odair Fonseca and Moiseis Cecconello created routines in both MATLAB and Scilab, executed numerical simulations and provided mathematical criticism for the model and simulations. All authors contributed critically to the drafts and gave final approval for publication.

GEOMETRICAL METHODS OF SHAPE DEFORMATION

To generate figures with various values of GE, we adopted three methods. Method 1 is based on “stretching” the figure in one direction, method 2 is based on adding irregularities

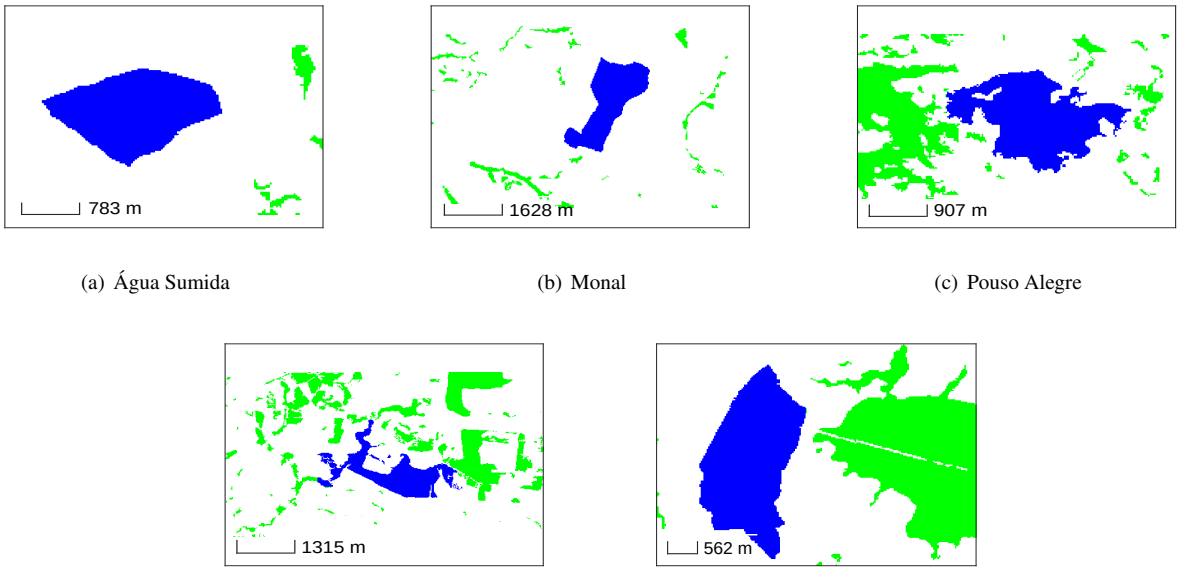

(a) Água Sumida (b) Monal (c) Pouso Alegre

(d) São José (e) Sara

Figure 7: Images of preserved fragments for the *Sapajus xanthosternos* case study. The blue area represents an ecological reserve with preserved environment where we have estimates for the population, the green area stands for preserved environment but not within the reserve while the white area corresponds to the hostile environment. Name of the reserves **a)** Água Sumida (1) **b)** Monal (2) **c)** Pouso Alegre (3) **d)** Mata São José (4) **e)** Sara (5). Simulations of the model were performed in these domains and the results were compared with the field estimates for the populations (see Table 3).

TABLE 4: RESULTS FOR THE SPECIES *Sapajus xanthosternos*. AREAS WERE ESTIMATED USING PARAMETERS ESTIMATED THROUGH SIMULATIONS (D), EXPERT ADVICE (λ) AND BIBLIOGRAPHICAL RESEARCH (r) COMBINED WITH EQUATIONS 19 AND 20. A^* STANDS FOR THE SIZE ESTIMATE IN WHICH THE POPULATION IS MOST SENSIBLE TO CHANGES IN FRAGMENT SHAPE. $A_{0,4}$ IS AN ESTIMATE FOR A FRAGMENT SIZE IN WHICH GEOMETRIC SHAPE DOES NOT HAVE MUCH IMPACT ON THE POPULATION.

Type of area (critical/safe)	**km^2**	**ha**
A^* [1]	0,6132	61,32
$A_{0,4}$ [2]	8,062	806,20

[1] Calculated using $A^* \approx \frac{D}{r}\left(\frac{\ln(\lambda/0{,}1348648)}{0{,}007490604}\right)^{2/3}$.

[2] Calculated using $A_{0,4} \approx \frac{D}{r}\left(\frac{\ln(\lambda/0{,}0096)}{0{,}2494}\right)^{2}$.

at the boundaries, increasing the perimeter without stretching the figure in any direction, finally, the method 3 is a combination of the first two. In Figure 8 we present some examples of figures generated by the three methods.

Given a target area ar_0, a polygon P with nv vertices is generated using polar coordinates, with angle $a_i = \frac{2\pi i}{nv+1},$, and ray ρ_i, $i = 0,1,\cdots,nv-1$, such that the area of P is ar_0. For each region P, two preserving area geometric transformations are applied on P in order to modify its measure of geometric efficiency (GE). One of these transformation consists in stretching P alongside one of the axis. The second one consists in stretching np (out of nv) vertices for a factor $r_i, i = 1,2\cdots,np$.

The data used in this article was create according to the following steps:

1. Initially, for a given ar_0, a region P is created with nv vertices, following a uniform distribution $U([a,b])$ and following a uniform distribution $U([c,d])$ such that $GE > 0{,}65$;
2. Using the first transformation method on P, ten regions R_i are created with geometric efficiency $\frac{iGE}{10}, i = 1,2,\cdots,10$;
3. Using the second transformation method on P, ten regions S_i are created with geometric efficiency $\left(0{,}2+\frac{i-1}{12}\right)GE, i = 1,2,\cdots,10$. In this case, np is a random variable following a uniform distribution $U([e,f])$ and r_i follows a uniform distribution $U([g,h])$;
4. Using a combination of those two methods, ten regions T_i are created like this: first, $\tilde{T}_i$ is created, using the second transformation method, with geometric efficiency $\tilde{EG} = \left(0{,}2+\frac{i-1}{12}\right)EG$ and then T_i is created, using the first transformation method, with geometric efficiency $\gamma\tilde{EG}$, $\gamma < 1$.

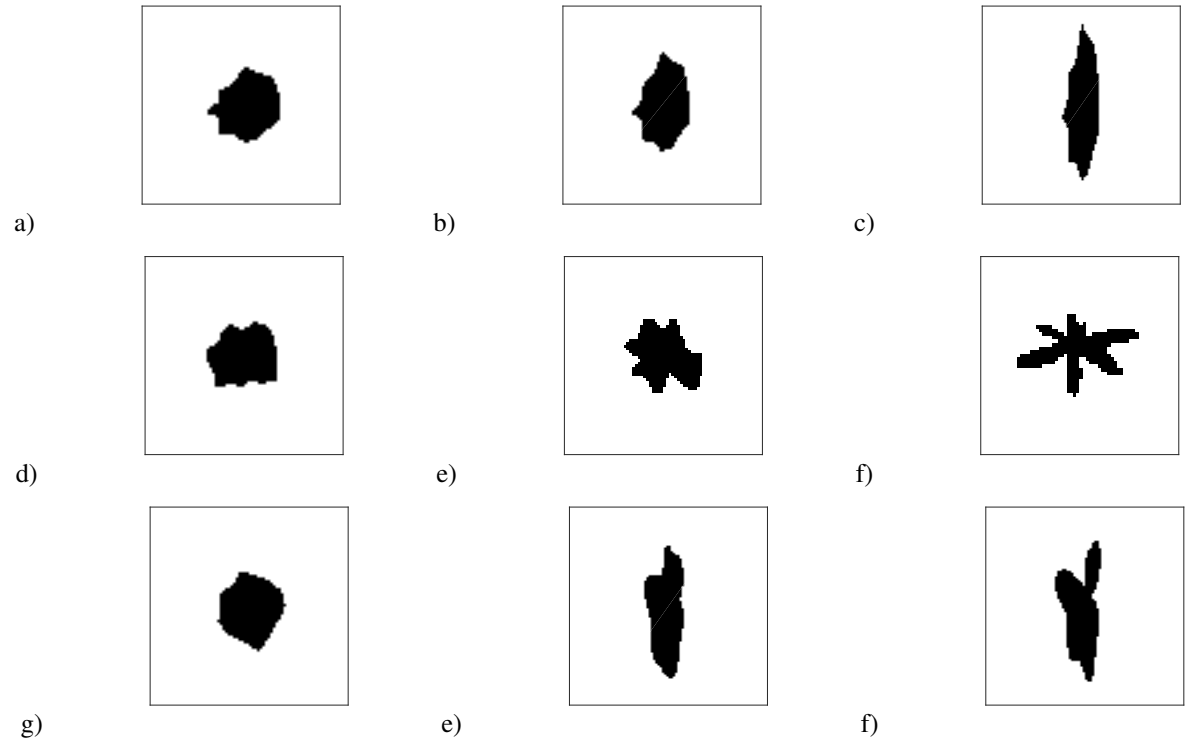

Figure 8: a) b) and c): figures generated using method 1, the measures of compactness (GE) are 0.65, 0.58 and 0.39, respectively. d) e) and f) figures generated using method 2, the measures of compactness (GE) are 0.67, 0.42 and 0.16, respectively. g) h) and i) figures generated using method 3, the measures of compactness (GE) are 0.65, 0.45 and 0.32, respectively. .

For a given ar_0, steps 1-4 previously describe are repeated ten times so that, for such ar_0, thirty regions are created.

REFERENCES

[1] Assis, R. A., Cecconello, M. S., Casacci, L. P., Barbero, F., Assis, L. M. E., Venturino, E., and Bonelli, S. (2018). "A theory and a mathematical model for the evolution of single and multiple host behavior in a parasite-host system (maculinea-myrmica)". *Ecological Complexity*, 34:178–187.

[2] Banks-Leite, C., Ewers, R. M., and Metzger, J.-P. (2010). "Edge effects as the principal cause of area effects on birds in fragmented secondary forest". *Oikos*, 119(6):918–926.

[3] Barlow, J. (1992). "Nonlinear and logistic growth in experimental populations of guppies". *Ecology*, 73(3):941–950.

[4] Boesing, A. L., Nichols, E., and Metzger, J. P. (2018). "Land use type, forest cover and forest edges modulate avian cross-habitat spillover". *Journal of Applied Ecology*, 55(3):1252–1264.

[5] Bonabeau, E., Dorigo, M., and G., T. (1999). *Swarm Intelligence: From Natural to Artificial Systems*. Oxford University Press, New York.

[6] Burden, R. and Faires, J. D. (2010). *Numerical Analysis*. Cengage, Boston, ninth edition ed.

[7] Canale, G. R., Kierulff, M. C. M., and Chivers, D. J. (2013). "A critically endangered capuchin monkey (sapajus xanthosternos) living in a highly fragmented hotspot". In: *Primates in fragments*, pages 299–311. Springer.

[8] Cantrell, R. and Cosner, C. (1994). "Insular biogeographic theory and diffusion models in population dynamics". *Theoretical Population Biology*, 45(2):177–202.

[9] Cantrell, R. and Cosner, C. (2001). "Spatial heterogeneity and critical patch size: area effects via diffusion in closed environments". *Journal of Theoretical Biology*, 209(2):161–171.

[10] Culot, L., Pereira, L. A., Agostini, I., De Almeida, M. A. B., Alves, R. S. C., Aximoff, I., Bager, A., Baldovino, M. C., Bella, T. R., Bicca-Marques, J. C., et al.*ATLANTIC-PRIMATES: a dataset of communities and occurrences of primates in the Atlantic Forests of South America*. title.

[11] da Silva, F. A., Canale, G. R., Kierulff, M. C. M., Duarte, G. T., Paglia, A. P., and Bernardo, C. S. (2016). "Hunting, pet trade, and forest size effects on population viability of a critically endangered neotropical primate, sapajus xanthosternos (wied-neuwied, 1826)". *American journal of primatology*, 78(9):950–960.

[12] Dehaene, S. (2003). "The neural basis of the weber–fechner law: a logarithmic mental number line". *Trends in cognitive sciences*, 7(4):145–147.

[13] Dobson, F. S. and Oli, M. K. (2007). "Fast and slow life histories of mammals". *Ecoscience*, 14(3):292–299.

[14] Ewers, R. M. and Didham, R. K. (2008). "Pervasive impact of large-scale edge effects on a beetle community". *Proceedings of the National Academy of Sciences*, 105(14):5426–5429.

[15] Gollnow, F., Hissa, L. B. V., Rufin, P., and Lakes, T. (2018). "Property-level direct and indirect deforestation for soybean production in the amazon region of mato grosso, brazil". *Land use policy*, 78:377–385.

[16] Gustafson, E. J. (2019). "How has the state-of-the-art for quantification of landscape pattern advanced in the twenty-first century?" *Landscape Ecology*, 34(9):2065–2072.

[17] Haddad, N. M., Brudvig, L. A., Clobert, J., Davies, K. F., Gonzalez, A., Holt, R. D., Lovejoy, T. E., Sexton, J. O., Austin, M. P., Collins, C. D., et al. (2015). "Habitat fragmentation and its lasting impact on earth's ecosystems". *Science advances*, 1(2):e1500052.

[18] Han, Y., Kang, W., Thorne, J., and Song, Y. (2019). "Modeling the effects of landscape patterns of current forests on the habitat quality of historical remnants in a highly urbanized area". *Urban Forestry & Urban Greening*, 41:354–363.

[19] Kendall, M. G. (1948). "Rank correlation methods."

[20] Krueger, L. E. (1989). "Reconciling fechner and stevens: Toward a unified psychophysical law". *Behavioral and Brain Sciences*, 12(2):251–267.

[21] Laming, D. (1989). "Experimental evidence for fechner's and stevens's laws". *Behavioral and Brain Sciences*, 12(2):277–281.

[22] Li, W., Goodchild, M. F., and Church, R. (2013). "An efficient measure of compactness for two-dimensional shapes and its application in regionalization problems". *International Journal of Geographical Information Science*, 27(6):1227–1250.

[23] Lin, C. C. and Segel, L. A. (1988). *Mathematics Applied to Deterministic Problems in the Natural Sciences*. SIAM, Philadelphia.

[24] McGarigal, K., Cushman, S. A., and Ene, E. (2012). "Spa-

tial pattern analysis program for categorical and continuous maps". *Computer software program produced by the authors at the University of Massachusetts, Amherst. FRAGSTATS v4. See http://wwwumassedu/landeco/research/fragstats/fragstatshtml*.

[25] Moorcroft, P. R., Lewis, M. A., and Crabtree, R. L. (2006). "Mechanistic home range models capture spatial patterns and dynamics of coyote territories in yellowstone". *Proceedings of the Royal Society B: Biological Sciences*, 273(1594):1651–1659.

[26] Moraga, A. D., Martin, A. E., and Fahrig, L. (2019). "The scale of effect of landscape context varies with the species' response variable measured". *Landscape Ecology*, 34(4):703–715.

[27] Murray, J. D. (1989). *Mathematical Biology*. Springer, New York.

[28] Nabe-Nielsen, J., Sibly, R. M., Forchhammer, M. C., Forbes, V. E., and Topping, C. J. (2010). "The effects of landscape modifications on the long-term persistence of animal populations". *PloS one*, 5(1):e8932.

[29] Nogueira, O. M. A., Palmeirim, A. F., Peres, C. A., and Dos Santos-Filho, M. (2021). "Synergistic effects of habitat configuration and land-use intensity shape the structure of bird assemblages in human-modified landscapes across three major neotropical biomes". *Biodiversity and Conservation*, pages 1–19.

[30] Nutter, F. W. and Esker, P. D. (2006). "The role of psychophysics in phytopathology: The weber–fechner law revisited". *European Journal of Plant Pathology*, 114:199–213.

[31] Okubo, A. and Levin, S. A. (2001). *Diffusion and Ecological Problems: Modern Perspectives*. Springer, New York.

[32] Osserman, R. (1978). "The isoperimetric inequality". *Bulletin of the American Mathematical Society*, 84(6):1182–1238.

[33] Perthame, B. (2007). *Transport Equations in Biology*. Birkhäuser-Verlag, Basel-Boston-Berlin.

[34] Pfeifer, M., Lefebvre, V., Peres, C., Banks-Leite, C., Wearn, O., Marsh, C., Butchart, S., Arroyo-Rodríguez, V., Barlow, J., Cerezo, A., et al. (2017). "Creation of forest edges has a global impact on forest vertebrates". *Nature*, 551(7679):187–191.

[35] Ramalho, C. E., Laliberté, E., Poot, P., and Hobbs, R. J. (2014). "Complex effects of fragmentation on remnant woodland plant communities of a rapidly urbanizing biodiversity hotspot". *Ecology*, 95(9):2466–2478.

[36] Rutledge, D. T. (2003). "Landscape indices as measures of the effects of fragmentation: can pattern reflect process?"

[37] Shigesada, N. and Kawasaki (1997). *Biological Invasions: Theory and Practice*. Oxford University Press, New York.

[38] Tijms, H. C. (2003). *A first course in stochastic models*. John Wiley and sons.

[39] Tsoularis, A. and Wallace, J. (2002). "Analysis of logistic growth models". *Mathematical biosciences*, 179(1):21–55.

[40] Tuff, K., Tuff, T., and Davies, K. (2016). "A framework for integrating thermal biology into fragmentation research". *Ecology letters*, 19(4):361–374.

[41] Watling, J. I., Arroyo-Rodríguez, V., Pfeifer, M., Baeten, L., Banks-Leite, C., Cisneros, L. M., Fang, R., Hamel-Leigue, A. C., Lachat, T., Leal, I. R., et al. (2020). "Support for the habitat amount hypothesis from a global synthesis of species density studies". *Ecology letters*, 23(4):674–681.

[42] Xu, C., Huang, Z. Y., Chi, T., Chen, B. J., Zhang, M., and Liu, M. (2014). "Can local landscape attributes explain species richness patterns at macroecological scales?" *Global ecology and biogeography*, 23(4):436–445.

Temporal dynamics of alcohol consumption patterns: The peer pressure and binge drinkers' role

Dinámica temporal de los patrones de consumo de alcohol: presión de pares y el rol de bebedores compulsivos

Rodrigo Gutiérrez[1], J.G. Vergaño-Salazar[2], Claudio Rojas-Jara[3] and Nicole Martínez-Jeraldo[4]

[1] *Facultad de Ciencias Básicas, Departamento de Matemática, Física y Estadística, Universidad Católica del Maule, Talca, Chile*
[2] *Escuela de Investigación en Biomatemáticas, Universidad del Quindío, Quindío, Colombia*
[3] *Facultad de Ciencias de la Salud, Departamento de Psicología, Universidad Católica del Maule, Talca, Chile*
[4] *Doctorado en Modelamiento Matemático Aplicado, Universidad Católica del Maule, Talca, Chile*

Reception date of the manuscript: 01/08/2022
Acceptance date of the manuscript: 30/08/2022
Publication date: 31/08/2022

Abstract—Alcohol consumption is a problem of both social and health interest since consumption at an early age increases the probability of developing alcohol dependence, along with a series of risks associated with diseases, violence, and injuries. In young people, the first episode and recurrence of alcohol consumption usually occur in the form of binge drinking, in which peers assume a protective or risky role. Mathematical modeling of binge drinking has frequently been performed based on interactions with other consumption patterns, defined in terms of quantity and frequency, without considering that the periodicity of excessive (or compulsive) alcohol consumption is associated with specific social contexts, such as parties, where mainly social drinkers adopt this pattern. Our objective is to analyze the influence exerted by social drinkers on their peers who adopt excessive alcohol consumption, as well as the recurrence and persistence of harmful consumption. We formulate a mathematical model described by a Filippov system, where the "contagion" dynamic is based on two transfer sequences according to the workweek and weekend. Our findings establish that depending on the parameter values of the model, four asymptotic periodic dynamics can arise. In addition to this, the existence of a trade-off between protective and risk factors is evidenced, allowing evaluation of the effect of social variables on binge drinking prevalence.

Keywords—Alcohol abuse, Excessive alcohol consumption, Filippov system, Trade-off

Resumen—El consumo de alcohol es un problema de interés tanto social como sanitario, ya que un consumo a edades tempranas aumenta la probabilidad de desarrollar dependencia al alcohol, junto con una serie de riesgos asociados a enfermedades, violencia y lesiones. En los jóvenes, el primer episodio y la recurrencia del consumo de alcohol suelen darse en forma de borracheras, en las que los pares asumen un rol protector o de riesgo. La modelización matemática del consumo excesivo de alcohol ha sido realizada habitualmente a partir de interacciones con otros patrones de consumo, definidos en función de cantidad y frecuencia, sin considerar que la periodicidad del consumo excesivo (o compulsivo) está asociada a contextos sociales específicos, tales como fiestas, donde principalmente bebedores sociales adoptan este patrón. Nuestro objetivo es analizar la influencia que ejercen bebedores sociales en sus pares, quienes adoptan un consumo excesivo de alcohol, además de la recurrencia y la persistencia hacia un consumo nocivo. Formulamos un modelo matemático descrito por un sistema de Filippov, donde la dinámica de "contagio" se basa en dos secuencias de transferencia en correspondencia a la semana laboral y el fin de semana. Nuestros hallazgos establecen que, dependiendo de los valores de los parámetros del modelo, pueden surgir cuatro dinámicas periódicas asintóticas. Además de eso, se evidencia la existencia de un trade-off entre los factores protectores y de riesgo, lo que permite evaluar el efecto de las variables sociales en la prevalencia del consumo excesivo de alcohol.

Palabras clave— Abuso de alcohol, Consumo excesivo de alcohol, Sistema de Filippov, Compromiso

INTRODUCTION

Alcohol is a drug highly consumed worldwide due to legal character and regulatory frameworks based on permissive laws and policies (Brown et al., 2008; Margozzini and Sapag, 2015). Harmful alcohol consumption is responsible for multiple diseases and injuries (World Health Organization, 2019), whose consequences affect the person who consumes it and their immediate environments, such as family, friends, co-workers, and neighbors (Bernstein et al., 2007; Sophie, 2019).

Based on a drink standard unit established by World Health Organization, equivalently to 10 grams of pure alcohol (World Health Organization, 2019), a person who consumes alcohol can be categorized as a Social drinker (also termed moderate drinker), Risk drinker (also termed frequent drinker), Harmful drinker, or Alcoholic drinker (also termed, Dependent drinker) according to the quantity, frequency, and duration of alcohol consumption (Benedict, 2007; Sánchez et al., 2007; Brauer, 2008). The change in the consumption pattern from one individual to another of a higher hierarchy, ascending both in quantity and frequency of alcohol consumption, has followed the medical/health model where a drug user is a sick person who must be cured. In this approach, the drug is an infectious-contagious agent that acts on the individual (Leiva-Vásquez and Rojas-Jara, 2018) and, therefore, potentially transmissible to other individuals, often called susceptible, which in this framework corresponds to social drink and abstainers.

The mathematical modeling used in studying temporal dynamics of alcohol consumption patterns has followed principles and guidelines of the mathematical modeling approach in infectious and contagious diseases (Benedict, 2007), based on ordinary differential equations (An der Heiden et al., 1998; Sánchez et al., 2007; Benedict, 2007; Manthey et al., 2008; Santonja et al., 2010; Sharma and Samanta, 2013; Walters et al., 2013; Bani et al., 2013; Buonomo and Lacitignola, 2014; Sharma and Samanta, 2015; Adu et al., 2017; Giacobbe et al., 2017; An et al., 2020; Crokidakis and Sigaud, 2021; Bentout et al., 2021) and difference equations (Khajji et al., 2020d,c; Labzai et al., 2020; El Youssoufi et al., 2021; Gutiérrez et al., 2022). In addition, these models also incorporate delay processes (Ma et al., 2015; Hai-Feng et al., 2017; Buonomo et al., 2018; Zhang et al., 2020; Ma et al., 2021; Djillali et al., 2021), stochastic processes (Wang et al., 2017; Anwarud and Yongjin, 2021), impulsive processes (Scribner et al., 2009; Lakshmikantham et al., 1989), or optimal processes (Bonyah et al., 2019; Khajji et al., 2020a; Pérez, 2020; El Youssoufi et al., 2021). Traditionally, the interconnection among consumption patterns follows a transference sequence: Social drinkers $\hookrightarrow$ Risk drinkers $\hookrightarrow$ Harmful drinkers (or Binge drinkers) $\hookrightarrow$ Alcoholic drinkers, with the possibility of returning to previous categories or being removed depending on the successful application of detoxification practices (Khajji et al., 2020c,b). In addition, the co-abuse of substances (*e.g.*, alcohol and smoking or alcohol and methamphetamine) (Bhunu and Mushayabasa, 2012; Orwa and Nyabadza, 2019) and the role of alcohol consumption in the transmission and progression of various diseases (Thomas and Lungu, 2009; Bowong et al., 2011; Mushayabasa and Bhunu, 2011; Bonyah et al., 2019) have been analyzed from mathematical models that incorporate the drinking patterns in its formulation.

Several studies on alcohol consumption reveal concern about excessive alcohol consumption (Parada et al., 2011; Llerena et al., 2015), characterized by consumption of 60/50 grams of alcohol pure per man/woman, carried out episodically and concentrated in a short period (two hours) by adolescent groups without gender differentiation on weekend nights (Parada et al., 2011). Furthermore, socio-medical investigations closely link this consumption pattern with social drinker individuals (Reifman et al., 1998; Adan et al., 2017; Llerena et al., 2015), stand out the role of peers in the first drunk episode and behavioral persistence (Borsari and Carey, 2001; Christiansen et al., 2002; Duncan et al., 2005; Rojas-Jara and Leiva-Vásquez, 2018; González-Araya and Rojas-Jara, 2020). Thus, the binge drinker label can be understood as a momentary behavior that social drinkers mainly adopt in specific drink circumstances such as parties and familiar or friend meetings (Sudhinaraset et al., 2016; Bahr et al., 1995). Importantly, the consequences of excessive alcohol consumption on health vary, highlighting long-term memory loss and muscle problems in the long-term (Crews et al., 2016; Hermens and Lagopoulos, 2018; Föger-Samwald et al., 2018; Voskoboinik et al., 2021; Degerud et al., 2021).

In the mathematical modeling framework, and based on the quantity consumption criterion for defining the compartments into a supposed alcoholic population, the Binge drinker and Harmful drinker classes are equivalents. The Binge drinking pattern has been studied from interconnections with the other compartments, particularly influencing social drinkers (Mulone and Straughan, 2012; Huo and Song, 2012; Anwarud and Yongjin, 2021) or being influenced by Risk drinkers (Hai-Feng et al., 2017; Zhang et al., 2020; Anwarud and Yongjin, 2021). However, when considering both the frequency and duration of consumption in specific circumstances, binge drinking behavior emerges mainly from Social drinkers (Parada et al., 2011). The above approach is conceptually correct and has not been widely explored. On this matter, in Gutiérrez et al. (2022) using a discrete-time mathematical model, analyzing the proportion of social drinkers who engage in excessive drinking behavior in social contexts based on parameters associated with social vulnerability (Rimal and Real, 2005; Margozzini and Sapag, 2015). Their findings, apart from the analysis and dynamic richness of the proposed model, establish parametric relationships that guarantee the predominance of social consumption, where peer pressure plays an important role. Outstanding research has considered peer pressure, inserting it into the point prevalence as a function dependent on external variable information that favors or discourages binge drinking (Giacobbe et al., 2017; Buonomo et al., 2018) and whose mechanism is inspired by imitation of inappropriate behavior and social conformity (Buonomo and Lacitignola, 2014; Straughan, 2019).

We formulate a switch and impulsive mathematical model (a Filippov system) to represent the alcohol consumption "contagion" dynamics based on two transference sequences according to the work week and weekend interactions:

(1) Social drinkers $\hookrightarrow$ Risk drinkers $\hookrightarrow$ Harmful drinkers,

(2) Social drinkers $\hookrightarrow$ Binge drinkers and Risk drinkers $\hookrightarrow$ Harmful drinkers,

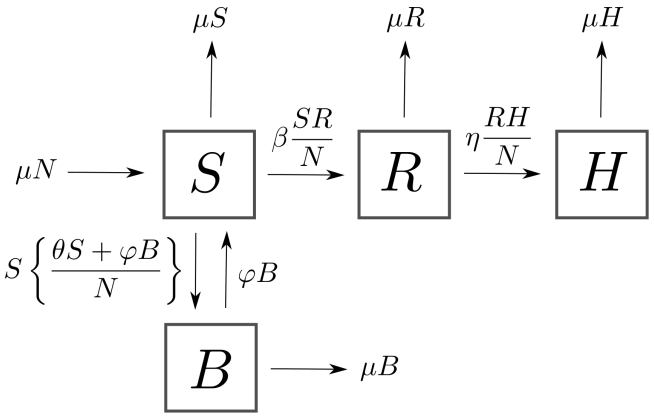

Figure 1: Progression diagram for alcoholic drinking compartmental mathematical model where S, R, H, and B correspond to Social drinkers, Risk drinkers, Harmful drinkers, and Binge drinkers, respectively.

Our goal is to analyze (i) the negative peer influence induced by social drinkers on other social drinkers for binge drinking adopt, (ii) the effect of binge drinkers on social drinkers, (iii) the recurrence of binge drinking, and (iv) the persistence on harmful consumption from a binge consumption on the temporal dynamics of alcohol.

The organization of this paper is as follows. In Section 2, a preliminary alcohol consumption mathematical model based on ordinary differential equations is formulated, and its qualitative analysis is carried out, from which a switch and impulsive model emerges as a consequence of differentiating the interrelations among drinking classes based on periodicity and contexts that favor the binge drinking by social drinkers. Then, in Section 3, a parametric sensibility analysis of temporal dynamics of Social and Binge drinking patterns is carried out. Finally, our findings are discussed in Section 4 as possibilities for future work.

MATHEMATICAL MODEL FORMULATION

A preliminary model and main results

Let be $S(t)$, $R(t)$, $H(t)$, and $B(t)$ compartments of Social drinkers, Risk drinkers, Harmful drinkers, and Binge drinkers at time t, respectively. We assumed a constant population size denoted by N, such that $S(t)+R(t)+H(t)+B(t)=N$ is obtained. New drinkers adopt social drinking at a rate proportional to N, with a constant given by μ, where μ is a unique vital rate used to represent both inflow and outflow of individuals in the compartments. From the traditional mathematical approach used for modeling the infectious and contagious disease dynamics (Brauer, 2017), alcohol drinking patterns are formulated (Sánchez et al., 2007). Thus, a social drinker individual becomes a risk drinker. In turn, a risk drinker individual becomes a harmful drinker by the negative influence, defined by effective contact between individuals of different compartments at rates $\beta S(R/N)$ and $\eta R(H/N)$ respectively, that promote the change of alcohol consumption pattern. In turn, social drinkers adopt a binge drinking pattern at a rate $S\{(\theta S+\varphi B)/N\}$ where θ is the peer pressure rate, and φB is the rate of returning to social consumption. Figure 1 illustrates the interconnections among these drinkers classes.

Therefore, the following model is proposed

$$\left\{\begin{array}{rcl} S'(t) &=& \mu N-\beta S(t)\dfrac{R(t)}{N}-S(t)\left\{\dfrac{\theta S(t)+\varphi B(t)}{N}\right\}+ \\ & & +\varphi B(t)-\mu S(t) \\ R'(t) &=& +\beta S(t)\dfrac{R(t)}{N}-\eta R(t)\dfrac{H(t)}{N}-\mu R(t) \\ H'(t) &=& +\eta R(t)\dfrac{H(t)}{N}-\mu H(t) \\ B'(t) &=& +S(t)\left\{\dfrac{\theta S(t)+\varphi B(t)}{N}\right\}-\varphi B(t)-\mu B(t) \end{array}\right., \tag{1}$$

with $S(0)+R(0)+H(0)=N$ and $B(0)=0$.

We observed that not exist alcohol-free equilibrium point due to $\theta\neq 0$. Even more, the equilibrium points of the normalized model (1) are:

(1) $E_1=(S_1^*,0,0,1-S_1^*)$ where

$$S_1^*=\frac{2(\mu+\varphi)}{\mu+2\varphi+\sqrt{\mu^2+4\theta(\mu+\varphi)}}.$$

(2) $E_2=(S_2^*,1-S_2^*-B_2^*,0,B_2^*)$ where

$$S_2^*=\frac{\mu}{\beta},\quad \text{and}\quad B_2^*=\frac{\theta\mu^2}{\beta[\beta(\mu+\varphi)-\mu\varphi]},$$

with $\beta/\mu>1$.

(3) $E_3=(S_3^*,R_3^*,H_3^*,B_3^*)$ where

$$\begin{array}{rcl} S_3^* &=& \dfrac{2\eta(\mu+\varphi)}{(\beta+\eta)(\mu+\varphi)+\varphi\eta+\sqrt{[\beta(\mu+\varphi)+\mu\eta]^2+4\theta\eta^2(\mu+\varphi)}}, \\ R_3^* &=& \dfrac{\mu}{\eta},\quad H_3^*=\dfrac{\beta S_3^*-\mu}{\eta},\quad B_3^*=\dfrac{\theta {S_3^*}^2}{\mu+\varphi(1-S_3^*)}, \end{array}$$

with $\eta/\mu>1$. In addition, note that $0<S_3^*<1$. Indeed, taking $\xi=\beta/\eta$, then

$$S_3^*=\frac{2(\mu+\varphi)}{\xi(\mu+\varphi)+\mu+2\varphi+\sqrt{[\xi(\mu+\varphi)+\mu]^2+4\theta(\mu+\varphi)}}.$$

Defining S_3^* as a function of $\xi>0$, we have that $dS_3^*/d\xi<0$. Thus,

$$S_3^*<\frac{2(\mu+\varphi)}{\mu+2\varphi+\sqrt{\mu^2+4\theta(\mu+\varphi)}}=S_1^*<1$$

is obtained, such that $S_3^*\to 0$ as ξ increases.

Let be threshold values

$$\begin{array}{rcl} \mathscr{U} &=& \dfrac{2\beta(\mu+\varphi)}{\mu\{\mu+2\varphi+\sqrt{\mu^2+4\theta(\mu+\varphi)}\}}, \\ \mathscr{V} &=& \dfrac{\eta}{\mu}\left\{1-\dfrac{\mu}{\beta}-\dfrac{\theta\mu^2}{\beta[\beta(\mu+\varphi)-\mu\varphi]}\right\}. \end{array}$$

Then, the following result establishes the stability of each equilibrium point.

Proposition 1 *Consider model (1). Thus,*

(1) If $0<\mathscr{U}<1$, then the equilibrium point E_1 is locally asymptotically stable.

(2) If $\mathscr{U} > 1$ and $0 < \mathscr{V} < 1$ then the equilibrium point E_2 is locally asymptotically stable.

(3) If $\mathscr{U} > 1$ and $\mathscr{V} > 1$ then the equilibrium point E_3 is locally asymptotically stable.

Proof 1 *Let be $J(E)$ the Jacobian matrix associate with model (1) at equilibrium point $E = (S,R,H,B)$.*

(1) The eigenvalues of $J(E_1)$ are

$\left\{-\mu,-\mu,\lambda_0,-\sqrt{\mu^2+4\theta(\mu+\varphi)}\right\}$ *where*

$$\lambda_0 = \frac{2\varphi(\beta-\mu)^2 - 2\mu[(\beta+\theta)\mu-\beta^2]}{\beta(\mu+2\varphi)+2\mu(\theta-\varphi)+\beta\sqrt{\mu^2+4\theta(\mu+\varphi)}}.$$

Taking $\beta = \xi\mu$, $\theta = \tau\mu$ and $\varphi = \phi\mu$ we have

$$\begin{aligned}\lambda_0 &= \mu\frac{-[\xi+2\tau+2\phi(\xi-1)]+\xi\sqrt{1+4\tau(1+\phi)}}{2(\tau-\phi)},\\ &= -\mu\frac{2\{\tau+(1-\xi)[\xi(1+\phi)-\phi]\}}{2(\tau-\phi)+\xi(1+2\phi)+\xi\sqrt{1+4\tau(1+\phi)}}.\end{aligned}$$

From $0 < \mathscr{U} < 1$, follows

$$\xi < \frac{1}{2}\left\{1+\frac{\phi+\sqrt{1+4\tau(1+\phi)}}{1+\phi}\right\}.$$

Let be $\rho > 0$ such that

$$\xi = \frac{1}{2}\left\{1+\frac{\phi+\sqrt{1+4\tau(1+\phi)}}{1+\phi}\right\}-\rho.$$

Then,

$$\lambda_0 = -\mu\rho\frac{2(1+\phi)}{1+2\varphi+\sqrt{1+4\tau(1+\phi)}} < 0.$$

Therefore, E_1 is locally asymptotically stable.

(2) The eigenvalues of $J(E_2)$ are

$$\left\{-\mu,\lambda_1,\lambda_2,-\mu\underbrace{\left[1-\frac{\eta}{\mu}\left(1-\frac{\mu}{\beta}-\frac{\theta\mu^2}{\beta[\beta(\mu+\varphi)-\mu\varphi]}\right)\right]}_{1-\mathscr{V}}\right\},$$

where λ_1 and λ_2 are roots of $P(\lambda) = \lambda^2 + p_1\lambda + p_2$ with

$$\begin{aligned}p_1 &= \frac{\beta^2\varphi^2-\mu^2\varphi(\theta-\varphi)+\beta^3(\mu+\varphi)+\beta\mu(\theta-\varphi)(\mu+2\varphi)}{\beta[\beta(\mu+\varphi)-\mu\varphi]},\\ p_0 &= \frac{\beta^2(\mu+\varphi)-\mu[\mu(\tau-\varphi)+\beta(\mu+2\varphi)]}{\beta}.\end{aligned}$$

Taking $\beta = \xi\mu$ (Here, $\xi > 1$), $\theta = \tau\mu$, $\varphi = \phi\mu$ and from $\mathscr{U} > 1$, we have

$$\xi > \frac{1}{2}\left\{1+\frac{\phi+\sqrt{1+4\tau(1+\phi)}}{1+\phi}\right\}.$$

Let be $\rho > 0$ such that

$$\xi = \frac{1}{2}\left\{1+\frac{\phi+\sqrt{1+4\tau(1+\phi)}}{1+\phi}\right\}+\rho,$$

then $p_1 = 2\mu\{\rho^2(1+\phi)[2\rho(1+\phi)+3(1+\sqrt{1+4\tau(1+\phi)})+2\phi(3+\phi)]+(1+\phi)+(1+\phi)[\sqrt{1+4\tau(1+\phi)}+2\tau(2+2\phi+\sqrt{1+4\tau(1+\phi)})]+4\rho\tau(1+\phi)(2+\phi)+\rho[3(1+\sqrt{1+4\tau(1+\phi)})+2\phi(2+\phi+3\sqrt{1+4\tau(1+\phi)}+\phi\sqrt{1+4\tau(1+\phi)})]\}/\{(1+2\rho(1+\phi)+\sqrt{1+4\tau(1+\phi)})(1+2\phi+2\rho(1+\phi)+\sqrt{1+4\tau(1+\phi)})\}$ and $p_0 = 2\rho\mu^2(1+\phi)[\rho(1+\phi)+\sqrt{1+4\tau(1+\phi)}]/\{1+2\phi+2\rho(1+\phi)+\sqrt{1+4\tau(1+\phi)}\}$, both positive values. Then, by the Routh–Hurwitz criterion, E_2 is locally asymptotically stable.

(3) The eigenvalues of $J(E_3)$ are $\{-\mu,\lambda_3,\lambda_4,\lambda_5\}$, where

λ_3, λ_4 and λ_5 are roots of $Q(\lambda) = \lambda^3 + q_2\lambda^2 + q_1\lambda + q_0$ with

$$\begin{aligned}q_2 &= \frac{r(S_3^*)}{\mu+\varphi(1-S_3^*)}+\frac{\beta\mu}{\eta},\\ q_1 &= \frac{\mu\{(\beta S_3^*-\mu)\eta+\beta[\beta S_3^*+\varphi(1-S_3^*)]\}}{\eta},\\ q_0 &= \frac{\mu(\beta S_3^*-\mu)\{\beta[\mu+\varphi(1-S_3^*)]^2+\eta r(S_3^*)\}}{\eta[\mu+\varphi(1-S_3^*)]},\end{aligned}$$

and $r(S) = -\varphi(\theta-\varphi)S^2 + 2(\theta-\varphi)(\mu+\varphi)S + (\mu+\varphi)^2$ which satisfies

(i) If $\theta = \varphi$, then $r(S) = (\mu+\varphi)^2 > 0$,

(ii) If $\theta > \varphi$, then $r(S) > \min\{r(0),r(1)\}$ with $r(0) = (\mu+\varphi)^2 > 0$ and $r(1) = \mu^2 + \theta(2\mu+\varphi) > 0$.

(iii) If $\theta < \varphi$ then $r(S) \geq (3\theta+\varphi)(\mu+\varphi)^2/(4\varphi) > 0$ for any $S > 0$.

Consequently, $q_2 > 0$. On the other hand, $q_1 > 0$ and $q_0 > 0$ if and only if $\beta S_3^* - \mu > 0$ (i.e., the existence condition of equilibrium point E_3, positivity of component B_3^*). Indeed,

$$\begin{aligned}\beta S_3^*-\mu &= \frac{\beta[\beta(\mu+\varphi)+(\mu+2\varphi)\eta]-2\mu[(\beta+\eta)\varphi-\theta\eta)]-\beta\sqrt{\beta^2(\mu+\varphi)^2+2\beta\eta\mu(\mu+\varphi)+[\mu^2+4\theta(\mu+\varphi)]\eta^2}}{2[(\beta+\eta)\varphi-\theta\eta)]},\\ &= \frac{2\{\beta^2(\mu+\varphi)(\eta-\mu)+\mu^2(\varphi-\theta)\eta-\beta\mu[2\varphi\eta+\mu(\eta-\varphi)]\}}{\underbrace{\beta[\beta(\mu+\varphi)+(\mu+2\varphi)\eta]-2\mu[(\beta+\eta)\varphi-\theta\eta)]}_{N}+\underbrace{\beta\sqrt{\beta^2(\mu+\varphi)^2+2\beta\eta\mu(\mu+\varphi)+[\mu^2+4\theta(\mu+\varphi)]\eta^2}}_{L}} = \frac{M}{N+L},\end{aligned}$$

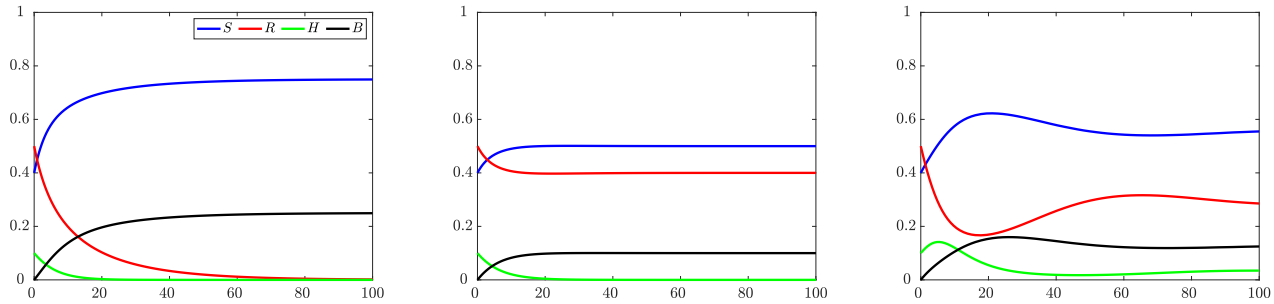

(a) (b) (c)

Figure 2: Temporal dynamics of model (1) in correspondence to outcomes in Proposition 1. We assumed $N = 1$ and initial conditions $S(0) = 0.4$, $R(0) = 0.5$, $H(0) = 0.1$, and $B(0) = 0$, with common parameters: $\mu = 0.2$, $\varphi = 0.1$, and $\theta = 0.1$. In particularly, (a) $\beta = 0.2$ and $\eta = 0.1$ with $\mathscr{U} = 0.75$, (b) $\beta = 0.4$ and $\eta = 0.1$ with $\mathscr{U} = 1.5$ and $\mathscr{V} = 0.2$, and (c) $\beta = 0.4$ and $\eta = 0.7$ with $\mathscr{U} = 1.5$ and $\mathscr{V} = 1.4$.

where clearly $L > 0$. *Let be* $\beta = \xi\mu$ *(Here,* $\xi > 1$*),* $\theta = \tau\mu$*,* $\varphi = \phi\mu$ *and* $\eta = \kappa\mu$. *Because* $\mathscr{V} > 1$*, exist* $\sigma > 1$ *such that*

$$\kappa = \sigma\left(1 - \frac{1}{\xi} - \frac{\tau}{\xi[\xi(1+\phi)-\phi]}\right)^{-1}.$$

Then,

$$\begin{aligned} M &= 2\mu^4(\sigma-1)\xi[\xi+(\xi-1)\varphi] > 0, \quad \textit{and} \\ N &= \mu^4\{\xi[\phi(\xi-2)+\xi]+ \\ &\quad +\kappa(\sigma,\xi,\phi)[2\tau+2\phi(\xi-1)+\xi]\}. \end{aligned}$$

Now, if $\mathscr{U} > 1$ *exist* $\rho > 0$ *such that*

$$\xi = \frac{1}{2}\left\{1 + \frac{\phi + \sqrt{1+4\tau(1+\phi)}}{1+\phi}\right\} + \rho,$$

we have $N = \{[1+2\rho+2\phi(1+\rho)+\sqrt{1+4(1+\phi)\tau}][2(1+\phi)^2\rho^3 + (1+\phi)\rho^2(1+2\sigma+2\phi(2\sigma-1)+3\sqrt{1+4(1+\phi)\tau}+\sigma(1+\sqrt{1+4(1+\phi)\tau}+2\tau(2+2\phi+\sqrt{1+4(1+\phi)\tau}))+\rho(1+4(1+\phi)\tau+\sqrt{1+4(1+\phi)\tau}+2\sigma(1+\phi+2(1+\phi)\tau+\sqrt{1+4(1+\phi)\tau})+2\phi(2\sigma-1)\sqrt{1+4(1+\phi)\tau})]\}/\{4\rho(1+\phi)[\rho(1+\phi)+\sqrt{1+4(1+\phi)\tau}]\} > 0.$

Finally, $q_2q_1 - q_0 = \{\beta^2\mu S_3^*[\mu+\varphi(1-S_3^*)]+\eta\varphi(1-S_3^*)[2\mu(\theta S_3^*+\mu)+\theta\varphi(2-S_3^*)S_3^*+3\mu\varphi(1-S_3^*)+\varphi^2(1-S_3^*)^2]+\beta[\varphi\mu(1-S_3^*)(\mu+\varphi(1-S_3^*))+\eta S_3^* h(S_3^*)]\}/\{\eta[\mu+\varphi(1-S_3^*)]\}$ *where* $h(S) = -\theta\varphi S^2 + [2\theta(\mu+\varphi)-\mu\varphi]S + \mu(\mu+\varphi) > \min\{h(0),h(1)\}$ *for any* $S \in (0,1)$ *with* $h(0) = \mu(\mu+\varphi) > 0$ *and* $h(1) = \mu^2 + \theta(2\mu+\varphi) > 0$.

Thus, $q_2q_1 - q_0 > 0$. *Therefore, by the Routh–Hurwitz criterion,* E_3 *is locally asymptotically stable.*

Importantly, the local stability of equilibrium point E_i implies the unstably of equilibrium point E_j with $i \neq j \in \{1,2,3\}$. Even more, and in some cases, the very existence of the other equilibrium points. Figure 2 illustrates model (1) trajectories according to Proposition 1 results.

A switch and impulsive type model

The kth week is divided into the work week and weekend in correspondence with temporal intervals $(kT,(k+l)T)]$ and $((k+l)T,(k+1)T]$, respectively. Particularly, $T = 7$ days and $l = 4/7$ are assumed. The flows shown in Figure 1 are divided and defined in the previous temporalities according to two transference sequences:

(1) Social drinkers $\hookrightarrow$ Risk drinkers $\hookrightarrow$ Harmful drinkers, and

(2) Social drinkers $\hookrightarrow$ Binge drinkers and Risk drinkers $\hookrightarrow$ Harmful drinkers.

During weekends, the alcohol consumption prevalence is estimated from new drinkers that adopt social or binge-drinking. We assumed that input flow μN is divided into complementary rates given by $\mu\alpha N$ and $\mu(1-\alpha)N$ towards Social drinking and Binge drinking compartments, respectively. The proportion $\alpha = \alpha(t) \in (0,1)$ is represented by

$$\alpha' = \lambda(1-\alpha) - \frac{\theta S}{S+B}\alpha, \quad \alpha((k+l)T) = 1 \qquad (2)$$

and inspired from Cabrera et al. (2021), Gutiérrez-Jara et al. (2022), Gutiérrez Jara and Muñoz Quezada (2022), and Gutiérrez-Jara and Saracini (2022), which modeling is associated with risk perception. The rate $\lambda \geq 0$ is a measure of the protective factors that promote a social drinking pattern through an increase of proportion α to its maximum value. Thus, in $\theta = 0$, the proportion α is equivalent to one, meaning that the first episodic alcohol consumption is with responsibility and control, typically of social drinkers. On the contrary, if $\theta > 0$, the rate λ contributes to compensating for peers' negative influence, represented by the point prevalence level. Figure 3 illustrates the interconnections among these compartments according to temporality.

Importantly, during the working week, binge drinkers do not interactions with the other compartments due to the periodicity of this pattern of consumption is exhibited by social drinkers only during the weekend that once the consumption social context is over, such as a party, binge drinkers return to initial social consumption or persist in harmful consumption. At the beginning of each work week and weekend, represented respectively by instants $t = kT$ and $t = (k+l)T$, a fraction $\delta \in (0,1)$ of binge drinkers return to social drinking, and the complementary fraction adopts harmful drinking. In turn, social drinkers adopt binge drinking a fraction $\omega \in (0,1)$. Therefore, the following model is proposed

$$
\begin{cases}
\left.\begin{aligned}
S'(t) &= \mu N - \beta S(t)\frac{R(t)}{N} - \mu S(t)\\
R'(t) &= +\beta S(t)\frac{R(t)}{N} - \eta R(t)\frac{H(t)}{N} - \mu R(t)\\
H'(t) &= +\eta\frac{R(t)}{N}H(t) - \mu H(t)\\
B'(t) &= 0
\end{aligned}\right\} & \text{, if} \quad t \in (kT,(k+l)T]\\
\left.\begin{aligned}
S(t^+) &= (1-\omega)S(t)\\
R(t^+) &= R(t)\\
H(t^+) &= H(t)\\
B(t^+) &= B(t)+\omega S(t)
\end{aligned}\right\} & \text{, if} \quad t = (k+l)T\\
\left.\begin{aligned}
S'(t) &= \mu\alpha N - S(t)\left\{\frac{\theta S(t)+\varphi B(t)}{S(t)+B(t)}\right\} - \mu S(t)\\
R'(t) &= -\eta R(t)\frac{H(t)}{R(t)+H(t)} - \mu R(t)\\
H'(t) &= +\eta R(t)\frac{H(t)}{R(t)+H(t)} - \mu H(t)\\
B'(t) &= \mu(1-\alpha)N + S(t)\left\{\frac{\theta S(t)+\varphi B(t)}{S(t)+B(t)}\right\} - \mu B(t)
\end{aligned}\right\} & \text{, if} \quad t \in ((k+l)T,(k+1)T]\\
\left.\begin{aligned}
S(t^+) &= S(t)+\delta B(t)\\
R(t^+) &= R(t)\\
H(t^+) &= H(t)+(1-\delta)B(t)\\
B(t^+) &= 0
\end{aligned}\right\} & \text{, if} \quad t = kT
\end{cases}
\tag{3}
$$

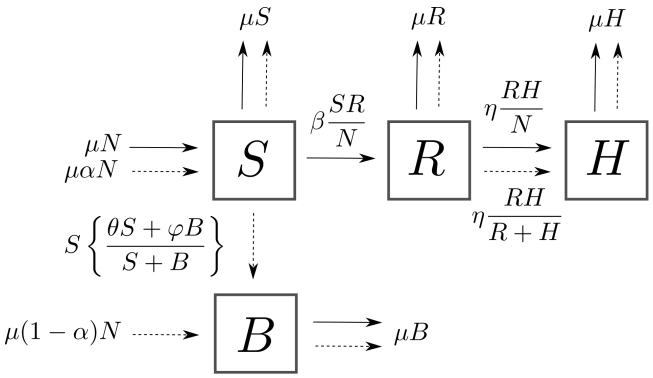

Figure 3: Progression diagram for alcoholic drinking compartmental mathematical model of switch type. The continuous lines indicate the work week, and the dashed lines the weekend flows.

such that $S(0)+R(0)+H(0)=N$ and $B(0)=0$.

RESULTS

The temporal dynamics of alcohol consumption patterns obtained from model (3) correspond to periodic trajectories that heuristically are of four types according to the persistence of the states: (i) Persistence of S and B, (ii) Persistence of S, R, and B, (iii) Persistence of S, H, and B, and (iv) all states persistence (See Figure 4).

The trajectories shape indicates the existence of maximum and minimum values of S and B during the weekends. They will tend to increase or decrease depending on the value of the parameters involved in the model (3). Thus, we define the following values

$$X_{max} = \lim_{t\to\infty} \max_{t\in I}\{X(t)\} \quad \text{and} \quad X_{min} = \lim_{t\to\infty} \min_{t\in I}\{X(t)\}$$

for $X \in \{S,B,\alpha\}$ with $I = ((k+l)T,(k+1)T]$. Note that $\alpha_{max}=1$, and $B_{min}=0$ when $\omega=0$.

Therefore, How is the variation of X_{max} and X_{min} in the parametric plane $\lambda vs.\theta$ as $\rho \in \{\beta,\eta,\omega,\varphi,\delta\}$ increases? The parameters have default values according to Table 1, assuming a temporal limit $t_\infty = 350$ and $(\theta,\lambda) \in [0:0.05:1]^2$.

Peer influence on binge drinking

The alcohol consumption patterns dynamic of the weekend depends on the dynamics of the workweek, where β, η, and μ are relevant parameters. However, since μ is a parameter present in most of the equations of the model (3), the sensitivity study requires a more robust analysis, which is possible to perform using System Dynamics methodology (Aracil and Gordillo, 1997; Sterman, 2000).

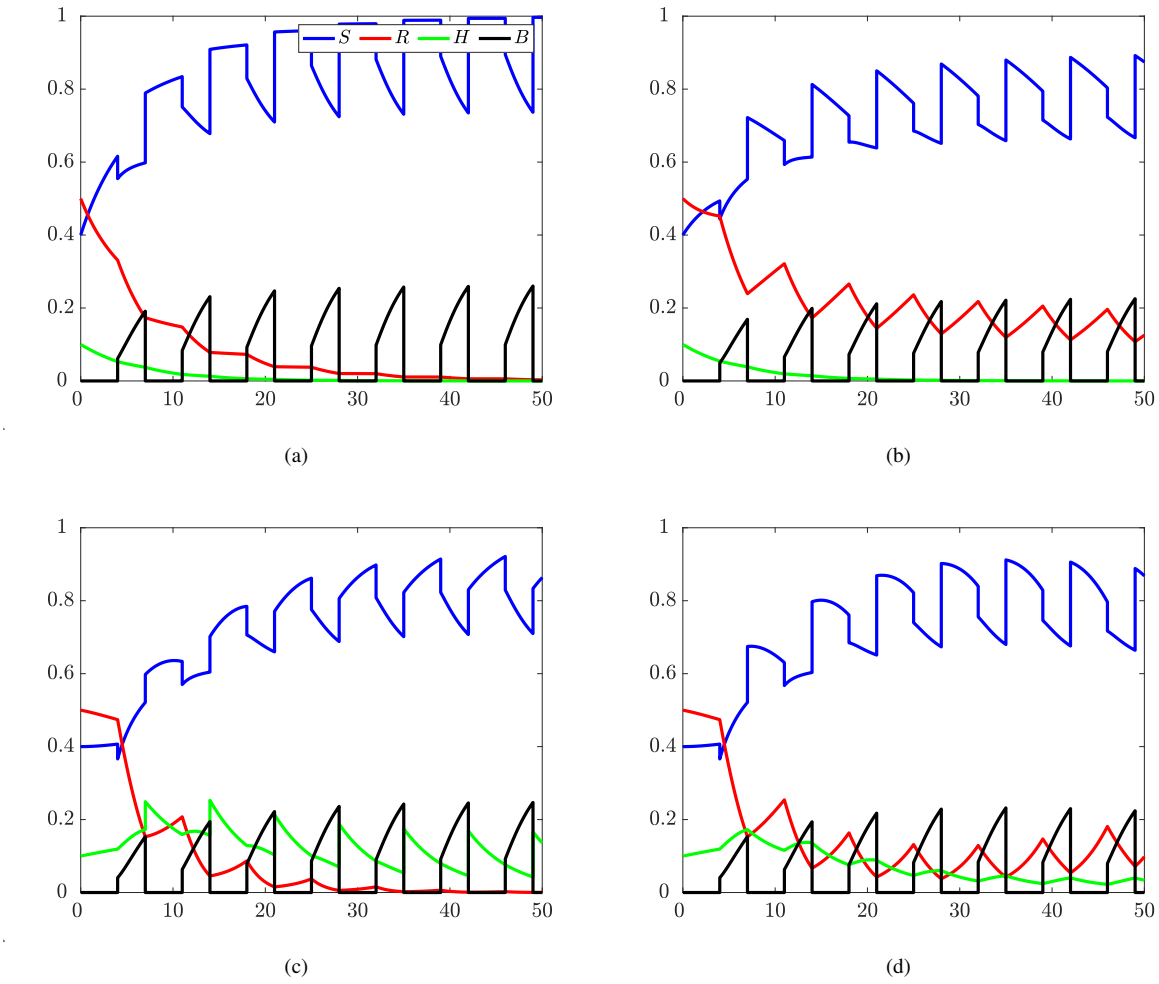

Figure 4: Temporal dynamics of model (3). We assumed $N = 1$ and initial conditions $S(0) = 0.4$, $R(0) = 0.5$, $H(0) = 0.1$ and $B(0) = 0$, with common parameters: $\mu = 0.2$, $\varphi = 0.1$, $\theta = 0.1$, $\omega = 0.1$ and $\lambda = 1$. In particularly, (a) $\beta = 0.2$, $\eta = 0.1$ and $\delta = 1$, (b) $\beta = 0.4$, $\eta = 0.1$ and $\delta = 1$, (c) $\beta = 0.6$, $\eta = 0.5$ and $\delta = 1$, and (d) $\beta = 0.6$, $\eta = 0.5$ and $\delta = 0.5$.

Effect of parameter β on the Social and Binge drinking dynamical patterns

Figure 5 shows the effect of the parameter β on values of S_{max}, S_{min}, B_{max}, and α_{min}. The red arrow indicates that the surfaces associated with the above values decrease as β increases. Importantly, for small values of θ the surfaces S_{max} and S_{min} vary, while for B_{max} it varies as θ increases. Additionally, Figure 5(d) shows a unique shape for α_{min}.

Such variations can be explained by the interactions between the state variables S and R in the model (3). As β increases, the higher the point prevalence of social drinkers by risk drinkers, which implies a decrease in social drinkers at the start of each weekend. Consequently, it decreases the relative size of S and thus the values S_{max}, S_{min} and B_{max} also.

Effect of parameter η on the Social and Binge drinking dynamical patterns

The effect of parameter η on the values of S_{max}, S_{min} and B_{max} is shown in Figure 6. The blue (respectively, red) arrow illustrates that as η increases, the surfaces S_{max} and B_{max} also increase (respectively, S_{min} decreases). Note that larger variations in S_{max} and S_{min} are obtained for small values of θ (See Fig.6(a)-(b)). However, B_{max} varies widely for large values of θ (See Fig.6(c)).

From model (3) follows that if η increases, the higher the point prevalence of risk drinkers by harmful drinkers, which implies a decrease and increase of risk drinkers and social drinkers at the start of each weekend, respectively. Consequently, the relative size of S increases, and therefore the value of S_{max} also increases. The decreasing of S_{min} and increase of B_{max} could be understood from the point prevalence of peer in equation (2) which increases due to the increase in S or θ.

Trade-off between protective and risk factors

Figure 7 shows the proportion of individuals who, in the long term, remain social drinkers at the end of each weekend, that is, those who socially start their consumption and end it the same way. In this case, its consumption pattern is not altered without succumbing to binge drinking. Consequently, the blue region is associated with the combination of high values of θ and low values of λ, indicating that a small proportion of individuals remain social drinkers at the end of each weekend. On the contrary, the red color accounts for a high proportion of individuals who remain social drin-

Parameter	Default value					
	Fig.5	Fig.6	Fig.7	Fig.8	Fig.9	Fig.10
β	0.5:0.1:0.9	0.5	0.5	0.5	0.5	0.5
η	0.5	0.3:0.1:0.7	0.5	0.3	0.3	0.3
ω	0.0	0.0	0.0	0.1:0.2:0.9	0.0	0.0
φ	0.0	0.0	0.0	0.0	0.1:0.2:0.9	0.0
δ	1.0	1.0	1.0	1.0	1.0	0.1:0.2:0.9

TABLE 1: THE PARAMETERS AND THEIR DEFAULT VALUES FOR THE SYSTEM (3) FOR VISUALIZING THE X_{max} AND X_{min} WITH $X \in \{S, B, \alpha\}$ TAKING INITIAL CONDITIONS $S(0) = 0.4$, $R(0) = 0.5$, $H(0) = 0.1$ AND $B(0) = 0$, AND THE COMMON VALUE $\mu = 0.2$.

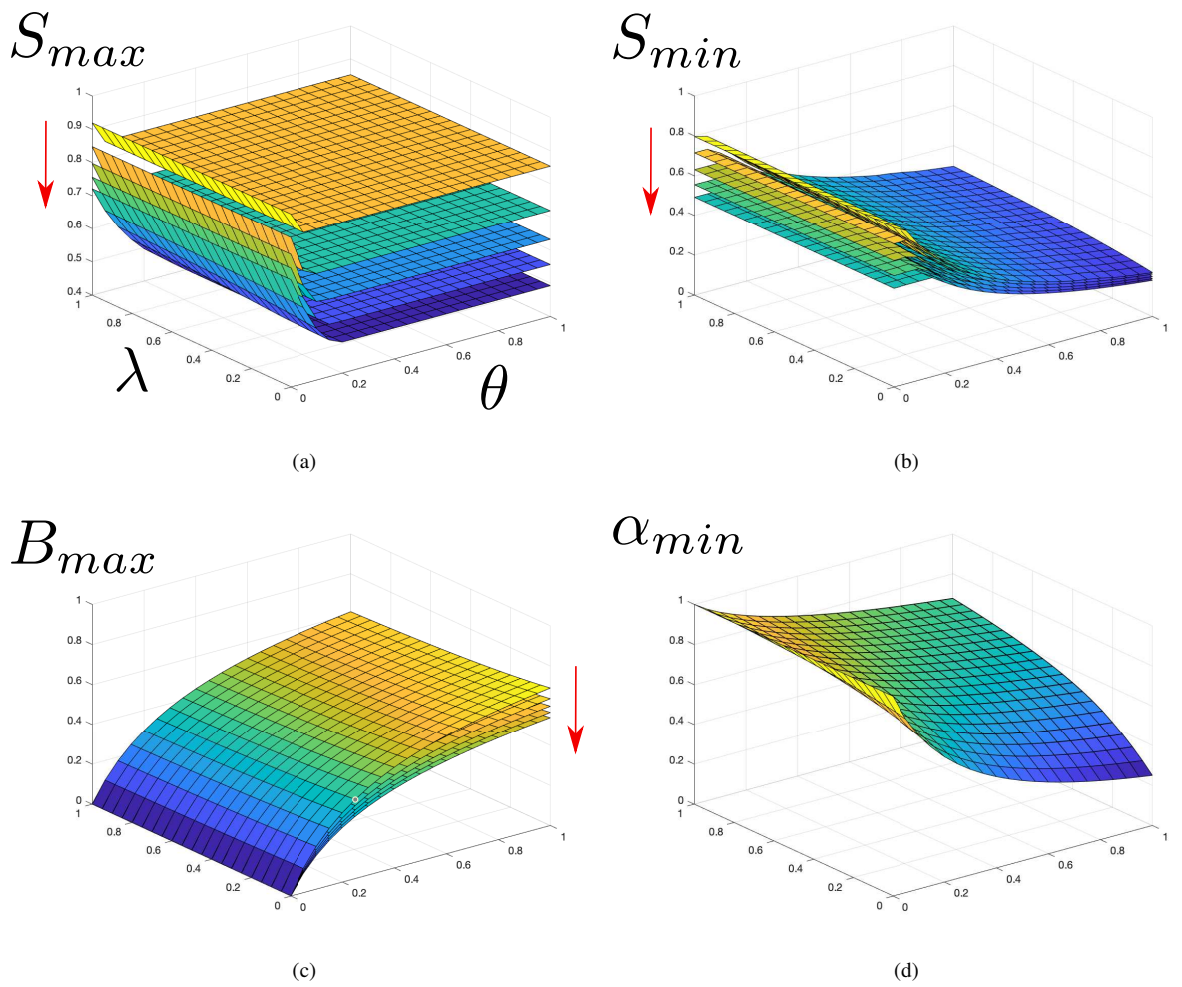

Figure 5: Influence of $\beta \in \{0.5, 0.6, 0.7, 0.8, 0.9\}$ on the surface (a) S_{max}, (b) S_{min}, (c) B_{max}, and (d) α_{min}. The red arrow indicates that the surfaces associated with the variables above decrease as β increases.

kers. To describe such an effect, the horizontal axis quantifies peer social pressure exerted by social drinkers on other social drinkers, and the vertical axis quantifies the factors of behavioral regulation, self-control, and behavior management of social drinking.

Recurrence to binge drinking

The recurrence of binge drinking is measured by the proportion $\omega \in (0, 1)$ of S. Figure 8 illustrates the effect of the parameter ω on the values of S_{max}, S_{min}, B_{max}, and α_{min}. As in the previous figures, the red arrow (respectively, blue) describes that as ω increases, the surfaces associated with the previous values decrease (increase, respectively). Note that S_{max} and S_{min} vary widely and for increasing values of θ. Conversely, B_{max} is variable for small values of θ. Additionally, as ω increases, α_{min} decreases slightly.

From the interrelations on the model (3) follows that if ω increases, a more significant proportion of social drinkers are predisposed to binge drinking at the beginning of each weekend. Thus, states B and S have high and low initial conditions, respectively. This could explains the decrease in S_{max}, S_{min} and α_{min} and the increase in B_{max}.

Dependent prevalence of binge drinkers

Model (3), with respect to model (1), does not consider the rate returning to social consumption given by φB. However, because the binge drinker label corresponds to a momentary state which is expressed in a single occasion, here during the

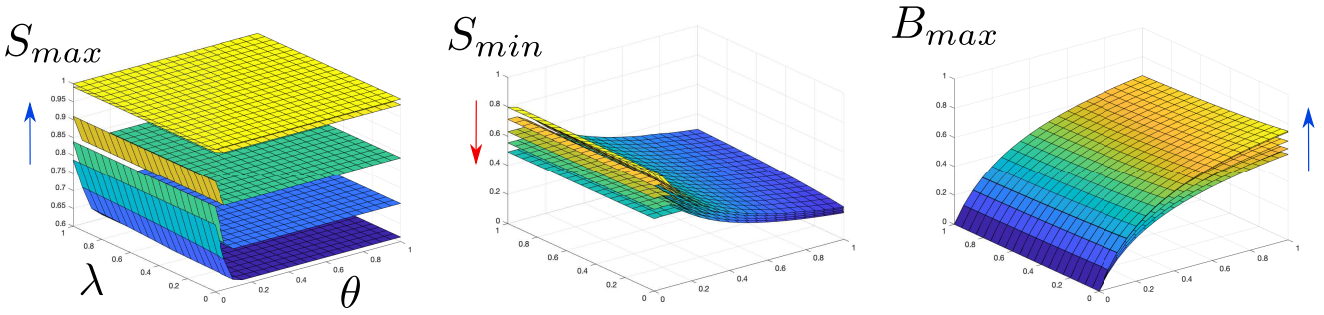

(a) (b) (c)

Figure 6: Influence of $\eta \in \{0.3, 0.4, 0.5, 0.6, 0.7\}$ on the surface (a) S_{max}, (b) S_{min} and (c) B_{max}. The red/blue arrow indicates that the surfaces associated with the variables above decrease/increase as η increases.

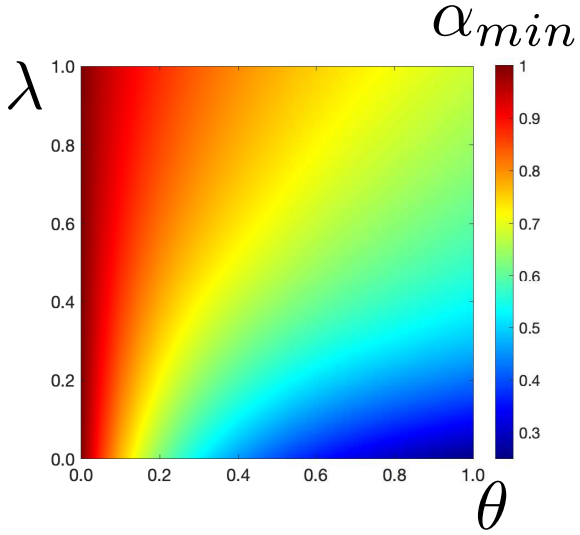

Figure 7: Value of $\alpha_{min} \in [0,1]$ according to color scale for the combination of parameters θ and λ.

weekend, such that once the drinking circumstance is over, the individual can return to social consumption (even abstemious) until the following weekend or maintain harmful drinking during the workweek.

The effect of parameter φ on the values of S_{max}, S_{min}, B_{max} and α_{min} is presented in Figure 9. As φ increases, the surfaces associated with S_{max} and S_{min} decrease. On the contrary, the surfaces associated with B_{max} and α_{min} increase when φ also increases. Note that the variability for S_{max} is highly concentrated towards small values of θ and with a rapid drop-off towards a constant value as θ increases. With respect to S_{min}, there is a homogeneous decrease in the surfaces with respect to φ increase and an increase in the surfaces associated with B_{max} and α_{min} for all the possible combinations of the θ and λ parameters. In particular, a subtle variation is observed for the α_{min} values as φ increases.

In model (3), the φ increase implies that the point prevalence of social drinkers by binge drinkers also increases. Thus, the S and B states decrease and increase, respectively. Finally, the increase of B implies a lower punctual prevalence of peers according to equation (2), where the increase of α_{min} is explained.

Harmful drinking from a sustained binge drinking

Extending binge drinking to the working week corresponds to adopting harmful consumption, which is measured by the proportion $\delta_c = 1 - \delta \in (0,1)$.

Figure 10 presents the effect of parameter δ on S_{max}, S_{min}, and B_{max} values. Considering the influence of θ, the surfaces associated with the previously mentioned values increase in all cases. For low values of θ, the S_{max} surfaces intersect. On the other hand, the surfaces S_{min} and B_{max} behave homogeneously as δ varies. Thus, increasing δ_c causes S_{max}, S_{min}, and B_{max} to decrease. The size of S and B will be low, and the drinking population will be concentrated in the harmful drinking pattern.

DISCUSSION AND CONCLUSIONS

The present research studies the temporal dynamics of different alcohol consumption patterns by formulating a compartmental mathematical model described by impulsive and change differential equations, a Filippov system. Based on the medical/health approach, dynamic "contagion" presents differences in the individual's social context. In the classical modeling of alcohol consumption, social drinkers define a class analogous to the formed by susceptible individuals in infectious-contagious disease modeling. However, we establish that social drinkers have the ability to influence the behavior of others, altering and modifying both their original patterns of alcohol consumption and that of their peers through social pressure (Buonomo and Lacitignola, 2014; Giacobbe et al., 2017; Buonomo et al., 2018; Straughan, 2019; Gutiérrez et al., 2022).

Our findings establish that depending on the value of the parameters involved in the formulated mathematical model (3), four asymptotic periodic dynamics can emerge, one more than the continuous model (1). The dynamics analysis, numerically carried out, focuses on the Social drinking and Binge drinking states during weekends and the long term, bounded by their maximum and minimum values, denoted by S_{max} and S_{min} respectively. A sensitivity analysis allowed determining the positive, negative, or neutral effect of the parameter $\rho \in \{\beta, \eta, \omega, \varphi, \delta\}$ on S_{max}, S_{min}, B_{max} and α_{min} for $(\theta, \lambda) \in [0,1]^2$. The cases where surfaces are not shown for α_{min} are due to the fact that there are no significant observable changes between surfaces. The parametric influence is

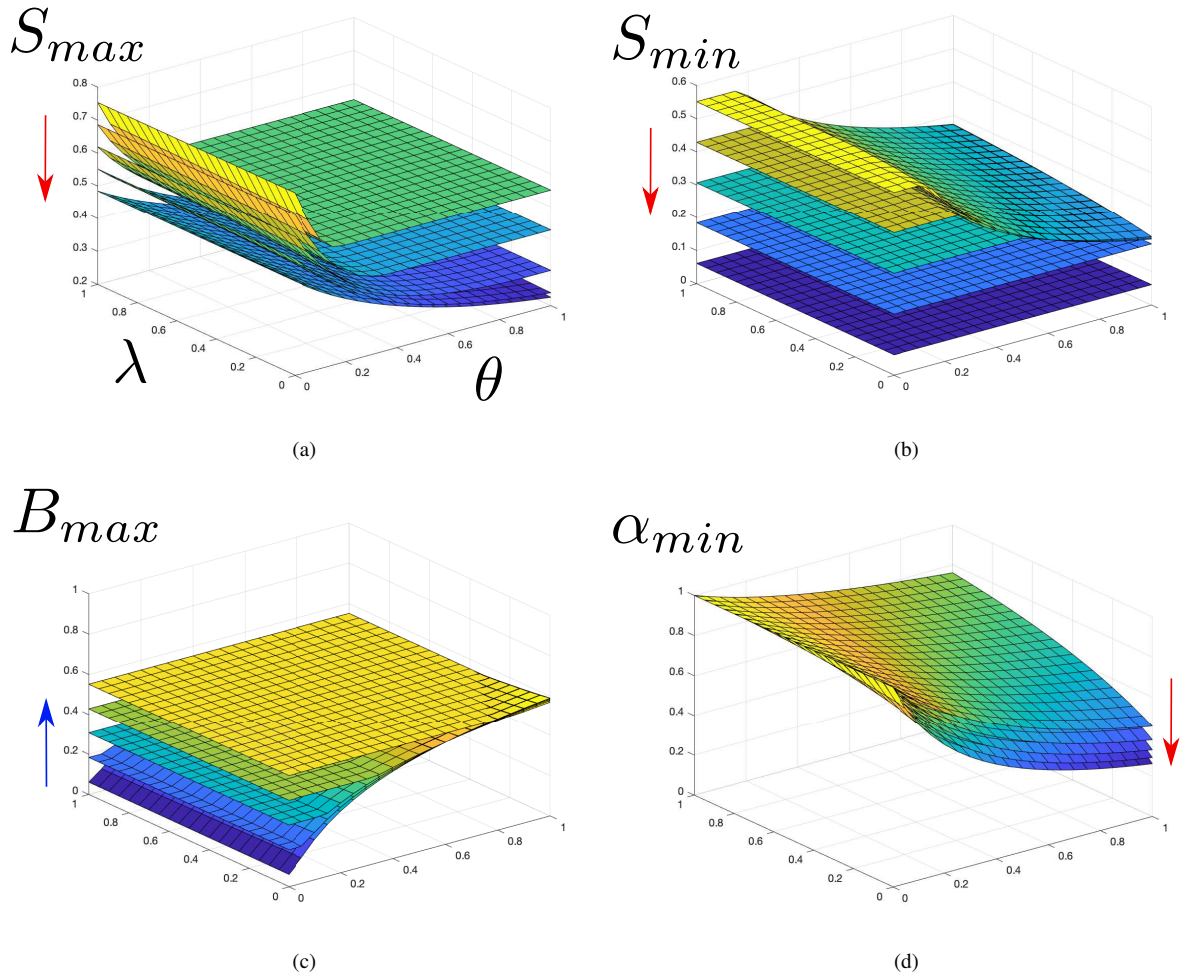

Figure 8: Influence of $\omega \in \{0.1, 0.3, 0.5, 0.7, 0.9\}$ on the surface (a) S_{max}, (b) S_{min}, (c) B_{max} and α_{min}. The red/blue arrow indicates that the surfaces associated with the variables above decrease/increase as ω increases.

summarized in Table 2.

Parameter	Influence			
	S_{max}	S_{min}	B_{max}	α_{min}
β	$-$	$-$	$-$	0
η	$+$	$-$	$+$	0
ω	$-$	$-$	$+$	$-$
φ	$-$	$-$	$+$	$+$
δ	$+$ ($\theta \gg 0$)	$+$	$+$	0

TABLE 2: INFLUENCE OF PARAMETER $\rho \in \{\beta, \eta, \omega, \varphi, \delta\}$ ON VALUES S_{max}, S_{min}, B_{max} AND α_{min} AS INCREASES IT: POSITIVE ($+$), NEGATIVE ($-$) AND NEUTRAL (0).

Our main finding corresponds to the existence of a trade-off between protective and risk factors. In Figure 8, a tension between protective and risk factors are observed, evidenced by the color scale (value of α_{min}), where a large proportion of individuals maintain a pattern of social consumption when peer pressure is low. In the face of peer social pressure, we can argue that a level of self-control regulates consumption behavior and causes the maintenance of the original pattern, social consumption. Furthermore, it is possible to determine thresholds of support and resistance to peer social pressure that is exerted in contexts of alcohol consumption. When peer pressure (θ) is greater than self-control (λ), the original consumption pattern may alter and establish a start toward new consumption patterns.

In this study, and as a limitation, only the effect caused by peer social pressure on consumption social patterns is considered, both positively and negatively, understanding that there may be other variables that also affect it, such as school and family (Rojas-Jara and Leiva-Vásquez, 2018). The latter is transformed into a proactive drift towards new studies on factors capable of altering alcohol consumption behaviors.

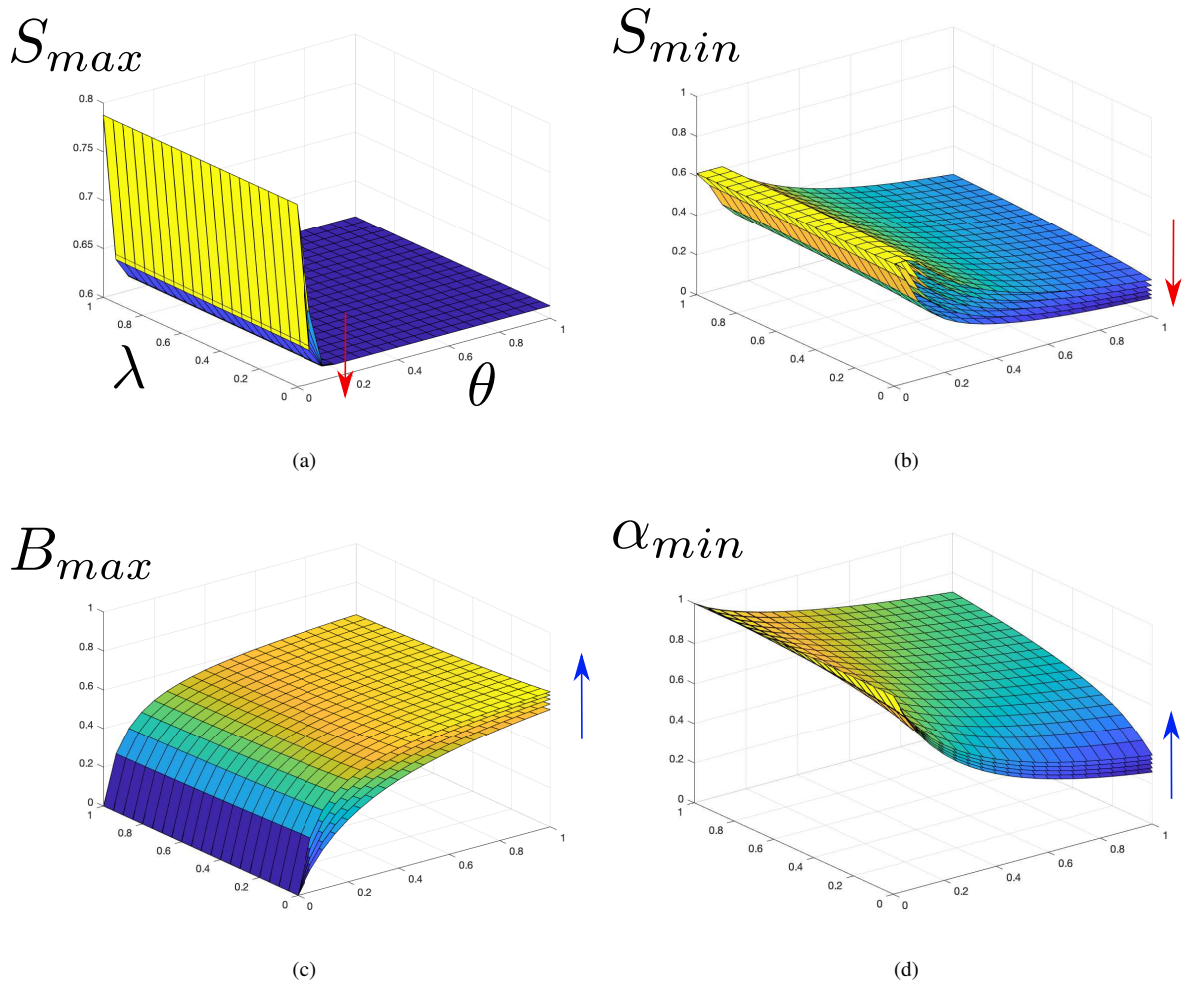

Figure 9: Influence of $\varphi \in \{0.1, 0.3, 0.5, 0.7, 0.9\}$ on the surface (a) S_{max}, (b) S_{min}, (c) B_{max} and (d) α_{min}. The red/blue arrow indicates the surfaces associated with the variables above decrease/increase as φ increases.

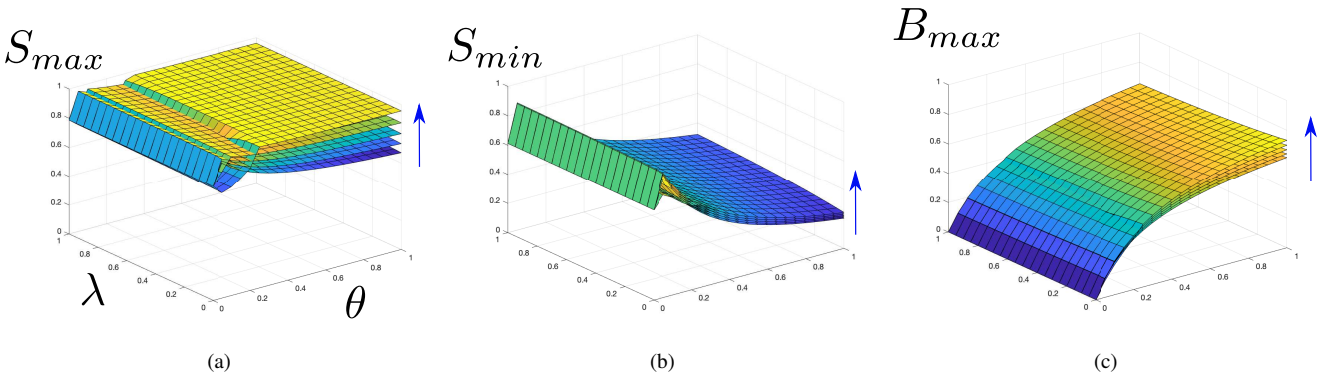

Figure 10: Influence of $\delta \in \{0.1, 0.3, 0.5, 0.7, 0.9\}$ on the surface (a) S_{max}, (b) S_{min} and (c) B_{max}. The blue arrow indicates the surfaces associated with the variables above increase as δ increases.

ACKNOWLEDGMENTS

N. M-J would like to thank Vicerrectoría de Investigación y Postgrado at Universidad Católica del Maule, Chile. C. R-J would like to thank R.G, J.G. V-S and N. M-J for allowing look at drug use from a dialogue between mathematics and psychology.

REFERENCES

[1] Adan, A., Forero, D. A., and Navarro, J. F. (2017). "Personality traits related to binge drinking: A systematic review". *Frontiers in Psychiatry*, 8(134):134.

[2] Adu, I. K., Osman, M., and Yang, C. (2017). "Mathematical model of drinking epidemic". *Br. J. Math. Computer Sci*, 22(5).

[3] An, Z., Zhang, S., and Xu, J. (2020). "Stability analysis of an alcoholism model with public health education and nsfd scheme". *Discrete Dynamics in Nature and Society*, 2020:1–15.

[4] An der Heiden, U., Schwegler, H., and Tretter, F. (1998). "Patterns

of alcoholism: a mathematical model". *Mathematical Models and Methods in Applied Sciences*, 8(03):521–541.

[5] Anwarud, D. and Yongjin, L. (2021). "The extinction and persistence of a stochastic model of drinking alcohol". *Results in Physics*, 28:104649.

[6] Aracil, J. and Gordillo, F. (1997). *Dinámica de sistemas*. Alianza Editorial.

[7] Bahr, S. J., Marcos, A. C., and Maughan, S. L. (1995). "Family, educational and peer influences on the alcohol use of female and male adolescents." *Journal of studies on alcohol*, 56(4):457–469.

[8] Bani, R., Hameed, R., Szymanowski, S., Greenwood, P., Kribs-Zaleta, C. M., and Mubayi, A. (2013). "Influence of environmental factors on college alcohol drinking patterns". *Mathematical Biosciences & Engineering*, 10(5-6):1281.

[9] Benedict, B. (2007). "Modeling alcoholism as a contagious disease: how infected drinking buddies spread problem drinking". *SIAM news*, 40(3):11–13.

[10] Bentout, S., Djilali, S., and Chekroun, A. (2021). "Global threshold dynamics of an age structured alcoholism model". *International Journal of Biomathematics*, 14(03):2150013.

[11] Bernstein, K. T., Galea, S., Ahern, J., Tracy, M., and Vlahov, D. (2007). "The built environment and alcohol consumption in urban neighborhoods". *Drug and alcohol dependence*, 91(2-3):244–252.

[12] Bhunu, C. P. and Mushayabasa, S. (2012). "A theoretical analysis of smoking and alcoholism". *Journal of Mathematical Modelling and Algorithms*, 11(4):387–408.

[13] Bonyah, E., Khan, M., Okosun, K., and Gómez-Aguilar, J. (2019). "Modelling the effects of heavy alcohol consumption on the transmission dynamics of gonorrhea with optimal control". *Mathematical biosciences*, 309:1–11.

[14] Borsari, B. and Carey, K. B. (2001). "Peer influences on college drinking: A review of the research". *Journal of Substance Abuse*, 13(4):391–424.

[15] Bowong, S., Moualeu, D., Tewa, J., and Aziz-Alaoui, M. (2011). "3. on the role of alcohol drinking on the dynamics transmission of hepatitis b". In: Steady, M. and Bhunu, C. P., editors, *Understanding the dynamics of emerging and Re-emerging infectious diseases using mathematical model*, chapter 3. Transworld Research Network.

[16] Brauer, F. (2008). "Compartmental models in epidemiology". In: Brauer, F., van den Driessche, P., and Wu, J., editors, *Lecture Notes in Mathematics*, chapter 2, pages 19–79. Springer, Berlin, Heidelberg.

[17] Brauer, F. (2017). "Mathematical epidemiology: Past, present, and future". *Infect Dis Model*, 2(2):113–127.

[18] Brown, S. A., McGue, M., Maggs, J., Schulenberg, J., Hingson, R., Swartzwelder, S., Martin, C., Chung, T., Tapert, S., Sher, K., and others. (2008). "A developmental perspective on alcohol and youths 16 to 20 years of age". *Pediatrics*, 121(Supplement 4):S290–S310.

[19] Buonomo, B., Giacobbe, A., and Mulone, G. (2018). "Analysis of an epidemic model with peer-pressure and information-dependent transmission with high-order distributed delay". *Ricerche di Matematica*, 68:453–468.

[20] Buonomo, B. and Lacitignola, D. (2014). "Modeling peer influence effects on the spread of high-risk alcohol consumption behavior". *Ricerche di Matematica*, 63(1):101–117.

[21] Cabrera, M., Córdova-Lepe, F., Gutiérrez-Jara, J., and Vogt-Geisse, K. (2021). "An sir-type epidemiological model that integrates social distancing as a dynamic law based on point prevalence and socio-behavioral factors". *Sci Rep*, 11(10170).

[22] Christiansen, M., Vik, P. W., and Jarchow, A. (2002). "College student heavy drinking in social contexts versus alone". *Addictive Behaviors*, 27(3):393–404.

[23] Crews, F. T., Vetreno, R. P., Broadwater, M. A., and Robinson, D. L. (2016). "Adolescent alcohol exposure persistently impacts adult neurobiology and behavior". *Pharmacological reviews*, 68(4):1074–1109.

[24] Crokidakis, N. and Sigaud, L. (2021). "Modeling the evolution of drinking behavior: A statistical physics perspective". *Physica A: Statistical Mechanics and its Applications*, 570:125814.

[25] Degerud, E., Høiseth, G., Mørland, J., Ariansen, I., Graff-Iversen, S., Ystrom, E., Zuccolo, L., Tell, G. S., and Naess, P. (2021). "Associations of binge drinking with the risks of ischemic heart disease and stroke: A study of pooled norwegian health surveys". *American Journal of Epidemiology*, 190(8):1592–1603.

[26] Djillali, S., Bentout, S., Touaoula, T. M., and Tridane, A. (2021). "Global dynamics of alcoholism epidemic model with distributed delays". *Math Biosci Eng*, 18(6):8245–8256.

[27] Duncan, G. J., Boisjoly, J., Kremer, M., Levy, D. M., and Eccles, J. (2005). "Peer effects in drug use and sex among college students". *Journal of Abnormal Child Psychology*, 33(3):375–385.

[28] El Youssoufi, L., Khajji, B., Balatif, O., and Rachik, M. (2021). "A discrete mathematical modeling for drinking alcohol model resulting in road accidents and violence: an optimal control approach". *Commun. Math. Biol. Neurosci.*, 2021.

[29] Föger-Samwald, U., Knecht, C., Stimpfl, T., Szekeres, T., Kerschan-Schindl, K., Mikosch, P., Pietschmann, P., and Sipos, W. (2018). "Bone effects of binge alcohol drinking using prepubescent pigs as a model". *Alcoholism: Clinical and Experimental Research*, 42(11):2123–2135.

[30] Giacobbe, A., Mulone, G., Straughan, B., and Wang, W. (2017). "Modelling drinking with information". *Mathematical Methods in the Applied Sciences*, 40(12):4400–4411.

[31] González-Araya, J. and Rojas-Jara, C. (2020). "Prevención y abordaje del consumo de drogas en adolescentes: intervención motivacional breve en contextos educativos". In: Concha, P. and García, F., editors, *La adolescencia hoy: problemas y soluciones para terapeutas*, chapter 15, pages 97–111. Nueva Mirada Ediciones, Talca, Chile.

[32] Gutiérrez, R., Cuesta-Herrera, L., Torres-Mantilla, H., and Martínez-Jeraldo, N. (2022). "Mathematical modeling of binge drinking from social influence". *Journal of Difference Equations and Applications*.

[33] Gutiérrez Jara, J. P. and Muñoz Quezada, M. T. (2022). "Modeling of hantavirus cardiopulmonary syndrome". *Medwave*, 22(03).

[34] Gutiérrez-Jara, J., Vogt-Geisse, K., Cabrera, M., Córdova-Lepe, F., and Muñoz-Quezada, M. (2022). "Effects of human mobility and behavior on disease transmission in a covid-19 mathematical model". *Sci Rep*, 12(10840).

[35] Gutiérrez-Jara, J. P. and Saracini, C. (2022). "Risk perception influence on vaccination program on covid-19 in chile: A mathematical model". *International Journal of Environmental Research and Public Health*, 19(4).

[36] Hai-Feng, H., Yong-Lan, C., and Hong, X. (2017). "Stability of a binge drinking model with delay". *Journal of Biological Dynamics*, 11(1):210–225.

[37] Hermens, D. F. and Lagopoulos, J. (2018). "Binge drinking and the young brain: A mini review of the neurobiological underpinnings of alcohol-induced blackout". *Frontiers in psychology*, 9:12.

[38] Huo, H.-F. and Song, N.-N. (2012). "Global stability for a binge drinking model with two stages". *Discrete Dynamics in Nature and Society*, 2012:1–15.

[39] Khajji, B., Kouidere, A., Balatif, O., and Rachik, M. (2020a). "Mathematical modeling, analysis and optimal control of an alcohol drinking model with liver complication". *Commun. Math. Biol. Neurosci.*, 2020.

[40] Khajji, B., Labzai, A., Balatif, O., and Rachik, M. (2020b). "Mathematical modeling and analysis of an alcohol drinking model with the influence of alcohol treatment centers". *International Journal of Mathematics and Mathematical Sciences*, 2020.

[41] Khajji, B., Labzai, A., Kouidere, A., Balatif, O., and Rachik, M. (2020c). "A discrete mathematical modeling of the influence of alcohol treatment centers on the drinking dynamics using optimal control". *Journal of Applied Mathematics*, 2020.

[42] Khajji, B., Moumine, E. M., Ferjouchia, H., Balatif, O., and Rachik, M. (2020d). "Optimal control and discrete-time modelling of alcohol model with physical and psychological complications". *J. Math. Comput. Sci.*, 10(5):1969–1986.

[43] Labzai, A., Kouidere, A., Khajji, B., Balatif, O., and Rachik, M. (2020). "Mathematical modeling and optimal control strategy for a discrete time drug consumption model". *Discrete Dynamics in Nature and Society*, 2020:1–10.

[44] Lakshmikantham, V., Bainov, D., and Simeonov, P. (1989). *Theory of Impulsive Differential Equation*. World Scientific, NJ.

[45] Leiva-Vásquez, J. and Rojas-Jara, C. (2018). "Uso de drogas y adolescentes en contextos escolares: un decálogo elemental para (re)pensar la prevención." In: Morgado, K., editor, *Puentes entre Psicología, Educación y Cultura.*, chapter 4, pages 53–69. Estero, Talca, Chile.

[46] Llerena, S., Arias-Loste, M. T., Puente, A., Cabezas, J., Crespo, J., and Fábrega, E. (2015). "Binge drinking: Burden of liver disease and beyond". *World journal of hepatology*, 7(27):2703–2715.

[47] Ma, S.-H., Huo, H.-F., and Meng, X.-Y. (2015). "Modelling alcoholism as a contagious disease: a mathematical model with awareness programs and time delay". *Discrete Dynamics in Nature and Society*,

2015.

[48] Ma, S. H., Huo, H. F., Xiang, H., and Jing, S. L. (2021). "Global dynamics of a delayed alcoholism model with the effect of health education". *Math. Biosci. Eng*, 18:904–932.

[49] Manthey, J., Aidoo, A., and Ward, K. (2008). "Campus drinking: an epidemiological model". *Journal of Biological Dynamics*, 2(3):346–356.

[50] Margozzini, P. and Sapag, M. J. (2015). "El consumo riesgoso de alcohol en chile: Tareas pendientes y oportunidades para políticas públicas". *Temas de la agenda pública*, 10(75):1–15.

[51] Mulone, G. and Straughan, B. (2012). "Modeling binge drinking". *International Journal of Biomathematics*, 5(1):1250005.

[52] Mushayabasa, S. and Bhunu, C. (2011). "Modelling the effects of heavy alcohol consumption on the transmission dynamics of gonorrhea". *Nonlinear Dynamics*, 66(4):695–706.

[53] Orwa, T. O. and Nyabadza, F. (2019). "Mathematical modelling and analysis of alcohol-methamphetamine co-abuse in the western cape province of south africa". *Cogent Mathematics & Statistics*, 6(1):1641175.

[54] Parada, M., Corral, M., Caamaño-Isorna, F., Mota, N., Crego, A., Rodríguez Holguín, S., and Cadaveira, F. (2011). "Definición del concepto de consumo intensivo de alcohol adolescente (binge drinking) [definition of adolescent binge drinking]". *Adicciones*, 23(1):53–63.

[55] Pérez, E. (2020). "Mathematical modeling of the spread of alcoholism among colombian college students". *Ingeniería Y Ciencia*, 16(32):195–223.

[56] Reifman, A., Barnes, G. M., Dintcheff, B. A., Farrell, M. P., and Uhteg, L. (1998). "Parental and peer influences on the onset of heavier drinking among adolescents". *Journal of Studies on Alcohol*, 53(3):311–317.

[57] Rimal, R. N. and Real, K. (2005). "How behaviors are influenced by perceived norms". *Communication Research*, 32(3):389–414.

[58] Rojas-Jara, C. and Leiva-Vásquez, J. (2018). "Prevención del uso de drogas en niños, niñas y adolescentes: objeto, sujeto y contexto." In: Castro, A., Rojas, C., and Saavedra, E., editors, *Familias y Niñez: nuevas tensiones, nuevas respuestas*, chapter 3, pages 43–53. Nueva Mirada Ediciones, Talca, Chile.

[59] Santonja, F.-J., Sánchez, E., Rubio, M., and Morera, J.-L. (2010). "Alcohol consumption in spain and its economic cost: a mathematical modeling approach". *Mathematical and Computer Modelling*, 52(7-8):999–1003.

[60] Scribner, R., Ackleh, A. S., Fitzpatrick, B. G., Jacquez, G., Thibodeaux, J. J., Rommel, R., and Simonsen, N. (2009). "A systems approach to college drinking: development of a deterministic model for testing alcohol control policies". *Journal of studies on alcohol and drugs*, 5(70):805–821.

[61] Sharma, S. and Samanta, G. (2013). "Drinking as an epidemic: a mathematical model with dynamic behaviour". *Journal of applied mathematics & informatics*, 31(1-2):1–25.

[62] Sharma, S. and Samanta, G. (2015). "Analysis of a drinking epidemic model". *International Journal of Dynamics and Control*, 3(3):288–305.

[63] Sophie, Y. (2019). ""an exercise in careful diplomacy": Talking about alcohol, drugs and family violence". *Policy Design and Practice*, 2(3):258–274.

[64] Sterman, J. (2000). *Business dynamics: Systems thinking and modeling for a complex world*. Boston: Irwin/McGraw-Hill.

[65] Straughan, B. (2019). "E-cigarette smoking with peer pressure". *Mathematical Methods in the Applied Sciences*, 42(6):2098–2108.

[66] Sudhinaraset, M., Wigglesworth, C., and Takeuchi, D. T. (2016). "Social and cultural contexts of alcohol use: Influences in a social-ecological framework". *Alcohol research: current reviews*, 38(1):35–45.

[67] Sánchez, F., Wang, X., Castillo-Chávez, C., Gorman, D. M., and Gruenewald, P. J. (2007). "16 - drinking as an epidemic—a simple mathematical model with recovery and relapse". In: Witkiewitz, K. A. and Marlatt, G. A., editors, *In Practical Resources for the Mental Health Professional, Therapist's Guide to Evidence-Based Relapse Prevention*, chapter 16, pages 353–368. Academic Press.

[68] Thomas, G. and Lungu, E. (2009). "The influence of heavy alcohol consumption on hiv infection and progression". *Journal of Biological Systems*, 17(04):685–712.

[69] Voskoboinik, A., McDonald, C., Chieng, D., O'Brien, J., Gutman, S., Ngu, P., Sugumar, H., Wong, G., Kalman, J. M., Taylor, A. J., and Kistler, P. (2021). "Acute electrical, autonomic and structural effects of binge drinking: Insights into the holiday heart syndrome". *International Journal of Cardiology*, 331:100–105.

[70] Walters, C. E., Straughan, B., and Kendal, J. R. (2013). "Modelling alcohol problems: total recovery". *Ricerche di Matematica*, 62(1):33–53.

[71] Wang, X.-Y., Zhang, P.-Z., and Yang, Q.-S. (2017). "On the stochastic dynamics of a social epidemics model". *Discrete Dynamics in Nature and Society*, 2017.

[72] World Health Organization (2019). *Global Status Report on Alcohol and Health 2018*. Geneva: World Health Organization.

[73] Zhang, Z., Zou, J., and Kundu, S. (2020). "Bifurcation and optimal control analysis of a delayed drinking model". *Advances in Difference Equations*, 2020(1):1–20.

Prey gathering may act as a counterattack measure against predators

El agrupamiento de presas puede actuar como una medida de contraataque contra los depredadores.

Martina Cossa[1], Ester Cravero[1], Masaki Pugliese[1] and Ezio Venturino[1]

[1] *Dipartimento di Matematica "Giuseppe Peano", Università di Torino, via Carlo Alberto 10, 10123 Torino, Italy*

Reception date of the manuscript: 07/agosto/2022
Acceptance date of the manuscript: 24/agosto/2022
Publication date: 31/agosto/2022

Abstract—Two generalist predators not interfering with each other and hunting the same single prey that gathers in a herd are here considered. The system allows only two possible final outcomes, the prey-free state in which both predators thrive at their own carrying capacities, an equilibrium that is always present, and coexistence, which is not guaranteed to exist. When it arises, it does it in pair, of which one point is a saddle. As a result, the phase space is partitioned into two domains of attraction corresponding to these two equilibria. If the prey represents a pest, this result would provide a theoretical tool for its eradication, provided that it is coupled with some human external action, such as insecticide spraying, which however can be administered just in a mild way, sufficient to push the system trajectories into the prey-free point domain of attraction. If it is a species to be preserved instead, corresponding measures for enhancing its survival should be taken, such as increasing its reproductivity or lowering the predators' pressure, so that the state of the system would fall into the attraction domain of the coexistence equilibrium.

Keywords—Mathematical Ecology, Mathematical Models, Population theory, Herding, Two-predators-one-prey

Resumen—Aquí se consideran dos depredadores generalistas que no interfieren entre sí y cazan la misma presa única que se reúne en una manada. El sistema permite solo dos posibles resultados finales, el estado libre de presas en el que ambos depredadores prosperan con sus propias capacidades de carga, un equilibrio que siempre está presente y la coexistencia, que no está garantizada. Cuando surge, lo hace en pareja, de las cuales un es un punto silla. Como resultado, el espacio de fases se divide en dos dominios de atracción correspondientes a estos dos equilibrios. Si la presa representa una plaga, este resultado proporcionaría una herramienta teórica para su erradicación, siempre que se acompañe de alguna acción externa humana, como la fumigación con insecticidas, que sin embargo puede administrarse de forma suave, suficiente para empujar las trayectorias del sistema en el dominio de atracción del punto libre de presas. Si en cambio se trata de una especie a. Si en cambio se trata de una especie a preservar, se deben tomar las medidas correspondientes para mejorar su supervivencia, como aumentar su reproductividad o disminuir la presión de los depredadores, de modo que el estado del sistema caiga en el dominio de atracción del equilibrio de coexistencia.

Palabras clave— Modelos Matemáticos, Ecología Matemática, Teoria de las Poblaciónes, Manadas, Dos-predatores-una-presa

INTRODUCTION

Several papers in the literature address the one-predator-several-prey situation, for instance in trophic chains as in (Baudrot et al., 2016a,b), where at times also the influence of contaminants and diseases are discussed, (Baudrot et al., 2018; Sieber et al., 2014).

Populations gathering in herds are well-known in nature. Herbivores usually have this habit and retain it also while wandering in the prairies in search for better feeding and pastures. Modeling this specific feature has been addressed in a number of papers, starting from (Ajraldi et al., 2011). Herding has been a subject of recent researches also with situations envisaging a disease affecting some population in the system, (Belvisi and Venturino, 2013; Cagliero and Venturino, 2016; Kooi and Venturino, 2016). In other contexts several investigations have dealt with different and even generic response functions (González-Olivares et al., 2022; Vil-

ches et al., 2018) or have studied herding populations diffusion in space (Souna et al., 2020; Jiang and Tang, 2019). One of the results that most distiguishes these models from the classical ones is in (Melchionda et al., 2018), where tristability is discovered to take place in two competing populations, allowing the simultaneous thriving of both, in contrast to the classical result that for such a system competitive exclusion must occur.

In this paper we continue the study of prey gathered in herds. We keep on using a particular form of the response function, namely the square root function, but it should be remarked that the latter is just a particular instance, a more general formulation has been introduced in (Bulai and Venturino, 2017; Djilali, 2019) leading perhaps to a slightly more difficult analysis, without however any significant change in the results. Here, in particular we assume that, if their numbers are large enough, prey can respond to predators' attacks by some form of retaliation, thereby reducing the chance of being hunted. The main idea is exposed in (Acotto and Venturino, 2022) and has further been explored in the parallel paper (Bondi et al., 2022). In the present situation we introduce a different ecological situation than those considered in the previous two investigations.

The paper is organized as follows. We describe the model construction in the next section and turn to its analysis in the subsequent section. A final discussion concludes the paper.

MODEL SETUP

We consider a prey population N that gather together. Herding facilitates the possible predators' X capturing of the prey on the boundary of the herd, expressed mathematically by the function $h(N,X)$. This is simply modeled via a square root function, assimilating the herd shape to a circle, although more general exponents other than $1/2$ can be taken, as discussed in (Bulai and Venturino, 2017), to account for more complicated domains, without any substantial changes in the results. Thus h has the form

$$h(N,X) = a\sqrt{N}X.$$

Here, specifically, two predators P and Q are present in the environment, and hunt the prey. The two predators are assumed to have also other food sources, and thereby do not explicitly compete with each other, only "mildly" through sharing the common prey N. Following the ideas of (Acotto and Venturino, 2022), the predators' attacks are reduced if the prey population attains a sufficiently large size. Therefore to model the functional response, we need a decreasing function of N, that vanishes in the limit when N tends to infinity. Thus, the function $h(N,X)$ should be a kind of modified Holling type II (HTII) response function, and thus must be modified as follows

$$h(N,X) = a\frac{\sqrt{N}X}{1+bN}. \tag{1}$$

These considerations lead to the system

$$\begin{aligned}
\frac{dP}{dt} &= n_P P\Big(1-\frac{P}{H_P}\Big)+\frac{e_P a_P\sqrt{N}P}{1+b_P N},\\
\frac{dQ}{dt} &= n_Q Q\Big(1-\frac{Q}{H_Q}\Big)+\frac{e_Q a_Q\sqrt{N}Q}{1+b_Q N},\\
\frac{dN}{dt} &= n_N N\Big(1-\frac{N}{H_N}\Big)-\frac{a_P\sqrt{N}P}{1+b_P N}-\frac{a_Q\sqrt{N}Q}{1+b_Q N}.
\end{aligned} \tag{2}$$

The first two equations for the predators are similar, containing a logistic term expressing the availability of other resources, and the benefit from hunting the prey N, scaled via suitable conversions coefficients e_P and e_Q, where the functional response of type (1) has been employed. The third equation for the prey N also has a logistic growth rate, but the additional terms express the harm suffered by the predators' attacks. All the parameters are assumed to be nonnegative, in particular the reproduction rates n_P and n_Q are here strictly positive:

$$n_P > 0, \quad n_Q > 0. \tag{3}$$

Table 1 lists all the model parameters and their interpretation.

Parameter	Interpretation
H_P	predator P carrying capacity
H_Q	predator Q carrying capacity
H_N	prey N carrying capacity
n_P	predator P reproduction rate
n_Q	predator Q reproduction rate
n_N	prey N reproduction rate
e_P	predator P conversion coefficient
e_Q	predator Q conversion coefficient
a_P	predator P hunting rate
a_Q	predator Q hunting rate
b_P	predator P handling time
b_Q	predator Q handling time

TABLE 1: PARAMETER INTERPRETATION FOR MODEL (2).

THE SYSTEM BEHAVIOR

We study here the dynamics of (2), focusing on its possible equilibria. The analysis will assess their feasibility and local stability.

Equilibria feasibility

The equilibrium equations obtained from (2) are highly nonlinear, but in some simple instances, analytic expressions for the equilibrium population values can be obtained. There are eight possible combinations, if we concentrate on the two alternatives that a population may or may not be present in the environment. All of them are at least conditionally admissible, as we will see below. This essentially follows from the assumption that the predators are generalist, which prevents the rejection of the points containing only such populations in the absence of their prey N based on the fact that for specialist predators this is their only food source.

Equilibria with just one population

Easily, the points $E_0 = (0,0,0)$, $E_N = (0,0,H_N)$, $E_Q = (0,H_Q,0)$ and $E_P = (H_P,0,0)$ are seen to be unconditionally feasible.

Equilibria with just two populations

The same results as for the single population points hold also for the prey-free point $E_{PQ} = (H_P,H_Q,0)$.

The other equilibria with two populations are more involved. But the symmetrical nature of the system (2) in terms of the two predators, allows us to investigate only one of them, as for the other one the results will follow by a simple change in the subscript.

Prey-one-predator equilibrium $E_{QN} = (0,\widetilde{Q}^*,\widetilde{N}^*)$

We thus investigate the point with $P = 0$, $Q \neq 0$, $N \neq 0$. From the last two equilibrium equations of (2), we obtain the nonlinear system

$$\Phi(N) = \Phi_Q(N) = \frac{H_Q}{n_Q}\Big(n_Q + \frac{e_Q a_Q\sqrt{N}}{1+b_Q N}\Big), \qquad (4)$$
$$\Psi(N) = \Psi_Q(N) = \frac{n_N}{a_Q}\sqrt{N}\Big(1-\frac{N}{H_N}\Big)(1+b_Q N).$$

The possible solution of this system will be investigated geometrically, as the intersections of the two curves $\Phi(N)$ and $\Psi(N)$. The height of these points therefore provide the predators equilibrium value $\widetilde{Q}^*$, while the abscissae those of $\widetilde{N}^*$, so that the point $E_{QN} = (0,\widetilde{Q}^*,\widetilde{N}^*)$ is known.

The function $\Phi(N)$ is defined over the whole positive line, with height at the origin given by H_N and a horizontal asymptote at the same level, in view of the following result

$$\lim_{N\to\infty}\Phi(N) = H_Q^+,$$

the asymptote being approached from above. Evaluating its derivative, we find

$$\Phi'(N) = \frac{H_Q e_Q a_Q(1-b_Q N)}{2n_Q\sqrt{N}(1+b_Q N)^2}$$

where the denominator is aways positive. To assess the sign of $\Phi'(N)$ we just need to study the one of the numerator, which is positive for $N < \frac{1}{b_Q}$. Thus for $0 < N < \frac{1}{b_Q}$ the function $\Phi(N)$ is increasing, and conversely decreasing in $N > \frac{1}{b_Q}$. The maximum is thus attained at the point

$$M_\Phi = \left[\frac{1}{b_Q}, \Phi\left(\frac{1}{b_Q}\right)\right].$$

In view of the above findings, it is apparent that near the origin $\Phi(N)$ is concave, because

$$\lim_{N\to 0^+}\Phi'(N) = +\infty,$$

and it becomes convex for large values of N, indicating the presence of an inflection point. To assess it better, we differentiate once more,

$$\Phi''(N) = \frac{e_Q a_Q H_Q(3N^2 b_Q^2 - 6Nb_Q - 1)}{4n_Q N\sqrt{N}(1+b_Q N)^3}.$$

Again, the denominator does not influence the sign of the second derivative. In the numerator the term $3N^2b_Q^2 - 6Nb_Q - 1$ is positive whenever $N < N^-_{\Phi''}$ and $N > N^+_{\Phi''}$, where $N^\pm_{\Phi''}$ are its zeros,

$$N^\pm_{\Phi''} = \frac{1}{3b_Q^2}\left[3b_Q \pm \sqrt{9b_Q^2 + 3b_Q^2}\right] = \frac{1}{3b_Q^2}\left[3b_Q \pm 2b_Q\sqrt{3}\right]$$

that always exist as the discriminant of the corresponding quadratic equation is always positive. Specifically,

$$N^-_{\Phi''} = \frac{1}{3b_Q}\left[3-2\sqrt{3}\right] < 0, \quad N^+_{\Phi''} = \frac{1}{3b_Q}\left[3+2\sqrt{3}\right] > 0.$$

In conclusion, $\Phi(N)$ is convex for $0 < N < N^+_{\Phi''}$ and it is concave for $N > N^+_{\Phi''}$.

Qualitatively, the behavior of $\Phi(N)$ is shown in Figure 1.

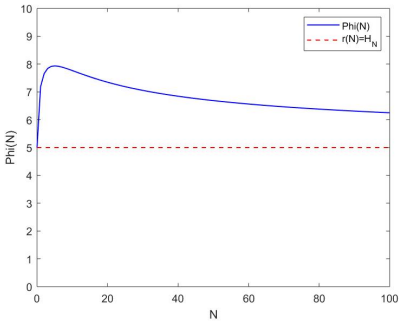

Figure 1: The function $\Phi(N)$ for the parameter choice $n_Q = 0{,}4$, $H_Q = 5$, $e_Q = 0{,}3$, $a_Q = 0{,}7$, $b_Q = 0{,}2$.

We now study the function $\Psi(N)$. It is defined for all $N \geq 0$ and

$$\lim_{N\to\infty}\Psi(N) = -\infty.$$

Its zeros are located at the origin and at $\psi_1 = H_N$, while the other vanishing point $\psi_2 = -b_Q^{-1} < 0$ lies outside the relevant domain of interest. On calculating its derivative, the denominator is found to be always positive,

$$\Psi'(N) = \frac{-n_N[5b_Q N^2 - 3N(b_Q H_N - 1) - H_N]}{2a_Q H_N\sqrt{N}},$$

and the sign of $\Psi'(N)$ depends just on the one of the numerator, which is the quadratic function

$$q(N) = -5b_Q N^2 + 3N(b_Q H_N - 1) + H_N.$$

Specifically $\Psi'(N) > 0$ within the interval of the roots $N^\pm_{\Psi'}$, with

$$N^-_{\Psi'} = -\frac{1}{10b_Q}[3(b_Q H_N - 1) - \sqrt{9(1-b_Q H_N)^2 + 20b_Q H_N}],$$
$$N^+_{\Psi'} = -\frac{1}{10b_Q}[3(b_Q H_N - 1) + \sqrt{9(1-b_Q H_N)^2 + 20b_Q H_N}].$$

Note that they are always real, because $q(0) = H_N > 0$ and $q(N)$ is a concave parabola. Also, we have $N^+_{\Psi'} < 0$ and $N^-_{\Psi'} > 0$, in both cases $b_Q H_N > 1$ and $b_Q H_N < 1$. Thus $\Psi(N)$ is increasing for $0 < N < N^-_{\Psi'}$ and decreasing in $[N^-_{\Psi'},\infty)$, so

that its maximum is located at the point $(N^+_{\Psi'}, \Psi(N^+_{\Psi'}))$. We study now the second derivative

$$\Psi''(N) = \frac{-n_N[15b_Q N^2 - 3N(b_Q H_N - 1) + H_N]}{4a_Q H_N N\sqrt{N}},$$

where the denominator is once more always positive in the domain of interest, $N > 0$. To assess convexity, we investigate the sign of the numerator, which is positive in case

$$p(N) = 15b_Q N^2 - 3N(b_Q H_N - 1) + H_N \leq 0.$$

The roots of $p(N) = 0$ are

$$N^{\pm}_{\Psi''} = \frac{1}{30b_Q}[3(b_Q H_N - 1) \pm \sqrt{\Delta}], \tag{5}$$

where Δ is regarded as a function of $b_Q H_N$:

$$\Delta = 9(b_Q H_N - 1)^2 - 60 b_Q H_N = 9(b_Q H_N)^2 - 78 b_Q H_N + 9.$$

In turn Δ is a quadratic function in $\delta = b_Q H_N$, with roots

$$\delta_{\pm} = \frac{1}{9}[39 \pm \sqrt{1521 - 81}] = \frac{1}{9}[39 \pm \sqrt{1440}] \approx \frac{1}{9}[39 \pm 37{,}95]$$

that are both positive. Thus $\Delta > 0$ in both the following alternative cases:

$$0 < b_Q H_N < \delta_- = \delta_1 \approx 0{,}12, \quad b_Q H_N > \delta_+ = \delta_2 \approx 8{,}55.$$

With these restrictions this guarantees the existence of real roots for the numerator of the second derivative of Ψ, namely $N^{\pm}_{\Psi''}$.

There are two cases:

- If $\Delta < 0$, $N^-_{\Psi''}$ and $N^+_{\Psi''}$ are both complex, the quadratic $p(N)$ is always positive and thus $\Psi''(N) < 0$ entailing that the function $\Psi(N)$ is always concave for $N > 0$.
- Alternatively for $\Delta > 0$, we may have either $0 < b_Q H_N < \delta_1 < 1$ or $b_Q H_N > \delta_2 > 8$.

  Note that for $b_Q H_N < 1$, from (5) we find $N^{\pm}_{\Psi''} < 0$, because $\Delta < 3(b_Q H_N - 1)$. In such case $\Psi''(N) < 0$ outside the interval $[N^-_{\Psi''}, N^+_{\Psi''}]$, and in particular for all $N > 0$. Hence in the domain of interest, Ψ is concave.

  If instead $b_Q H_N > 1$, again using (5) we have $N^{\pm}_{\Psi''} > 0$, once more because $\Delta < 3(b_Q H_N - 1)$. But this and $\Delta > 0$ imply that $b_Q H_N > \delta_2 > 8$, so that either

  $$0 < N^-_{\Psi''} < \delta_1 < 1, \quad N^+_{\Psi''} > \delta_2 > 8,$$

  or, alternatively

  $$N^{\pm}_{\Psi''} > \delta_2 > 8.$$

  In both cases, it turns out that $\Psi''(N) > 0$ for $N^-_{\Psi''} < N < N^+_{\Psi''}$, which implies that $\Psi(N)$ is convex in the same interval $[N^-_{\Psi''}, N^+_{\Psi''}]$, and concave for $0 < N < N^-_{\Psi''}$ as well as for $N > N^+_{\Psi''}$.

These possible inflection points lie in the first quadrant only if the condition $\Psi(N^{\pm}_{\Psi''}) > 0$ is satisfied.

The equilibrium E_{QN} is therefore a possible intersection of $\Phi(N)$ and $\Psi(N)$ in the first quadrant. Now, in view of the above analysis, this is not always guaranteed, as it is clear from Figure 2. It is also apparent that the two intersections, giving a pair of equilibria, occur via a saddle-node bifurcation.

A sufficient condition for the existence of such points is obtained when the maximum value of $\Psi(N)$ exceeds the value of $\Phi(N)$ for the corresponding abscissa. Obviously, the latter is located at the zero $N^+_{\Psi'}$ of $\Psi'(N)$ and thus the sufficient condition reads

$$\Phi(N^+_{\Psi'}) \geq \Psi(N^+_{\Psi'}). \tag{6}$$

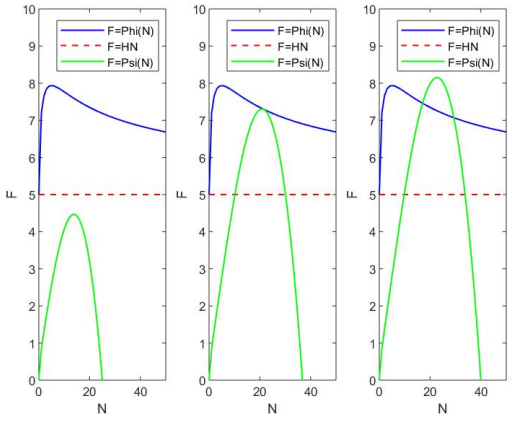

Figure 2: Graph of the functions $\Psi(N)$ and $\Phi(N)$ with the parameters $a_Q = 0{,}7$, $b_Q = 0{,}2$, $e_Q = 0{,}3$, $n_N = 0{,}5$, $n_Q = 0{,}4$, $H_Q = 5$. Left to right, $H_N = 25$, $H_N = 38{,}6$ and $H_N = 40$.

.

Equilibrium with the other predator absent $(\widehat{P}^*, 0, \widehat{N}^*)$

As stated above, this case can be investigated in the same way as for $E_{QN} = (0, \widetilde{Q}^*, \widetilde{N}^*)$, by suitably changing the notation. The sufficient condition (6) would be replaced by an analogous statement, where $\Phi(N)$ and $\Psi(N)$ would be meant to be the functions $\Phi_P(N)$ and $\Psi_P(N)$ with an obvious change of notation in (4).

Coexistence equilibrium

We study this equilibrium $E^* = E_{PQN} = (P^*, Q^*, N^*)$ by solving two of the equilibrium equations and substituting into the remaining one. From the first two equilibrium equations we find

$$P = \frac{H_P}{n_P}\left(n_P + \frac{e_P a_P \sqrt{N}}{1 + b_P N}\right)$$

and

$$Q = \frac{H_Q}{n_Q}\left(n_Q + \frac{e_Q a_Q \sqrt{N}}{1 + b_Q N}\right).$$

Substitution into the equilibrium equation for N we obtain the equation

$$\beta(N) = 0,$$

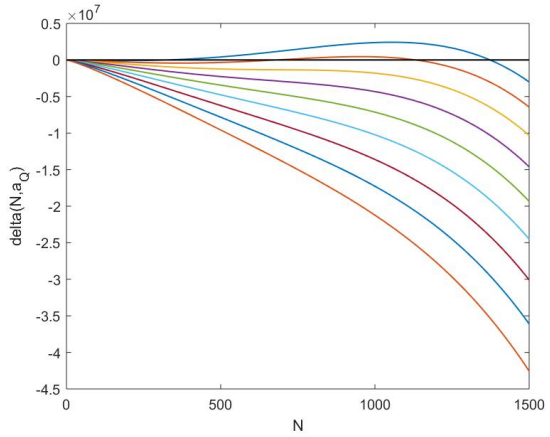

Figure 3: The figure shows the behavior of $\beta(N)$ as a function of $a_Q \in [0{,}1, 0{,}9]$, where all other parameters are given in (8).

where

$$\beta(N) = n_N N\left(1-\frac{N}{H_N}\right) - \frac{a_P\sqrt{N}H_P[n_P(1+b_PN)+e_Pa_P\sqrt{N}]}{n_P(1+b_PN)^2} - \frac{a_Q\sqrt{N}H_Q[n_Q(1+b_QN)+e_Qa_Q\sqrt{N}]}{n_Q(1+b_QN)^2}. \tag{7}$$

The function $\beta(N)$ is explored numerically for the assessment of its possible zeros. For this task we use the following set of parameters:

$$\begin{aligned} n_N = 0{,}3, \quad n_P = 0{,}4, \quad n_Q = 0{,}3, \quad H_P = 150, \\ H_Q = 1200, \quad H_N = 1500, \quad e_P = 0{,}8, \quad e_Q = 0{,}9, \\ a_P = 0{,}8, \quad a_Q = 0{,}2, \quad b_P = 0{,}4, \quad b_Q = 0{,}1. \end{aligned} \tag{8}$$

Figure 3 contains the plots of $\beta(N)$ for nine choices of the parameter a_Q, the predator Q hunting rate, in the interval $[0{,}1, 0{,}9]$, while all the remaining ones are taken from (8). Similarly in Figure 4 the varying parameter, in the same interval, is n_N, the prey N birth rate. Finally in Figure 5 we let n_Q, the predator Q birth rate, change. These three parameters have been selected because they appear to be the most important ones to influence the behavior of $\beta(N)$. Further, in all cases, it is seen that the number of the nontrivial roots changes, it may be zero, or up to two. Therefore the coexistence equilibrium is not guaranteed always to exist. Also, whenever it arises, it does it in pairs, through a saddle-node bifurcation.

Equilibria stability

To assess local stability, we need the Jacobian of (2):

$$J = \begin{bmatrix} J_{1,1} & 0 & J_{1,3} \\ 0 & J_{2,2} & J_{2,3} \\ J_{3,1} & J_{3,2} & J_{3,3} \end{bmatrix},$$

with

$$J_{1,1} = n_P\left(1-\frac{2P}{H_P}\right)+\frac{e_Pa_P\sqrt{N}}{1+b_PN}$$

$$J_{1,3} = \frac{e_Pa_PP}{2\sqrt{N}(1+b_PN)^2}$$

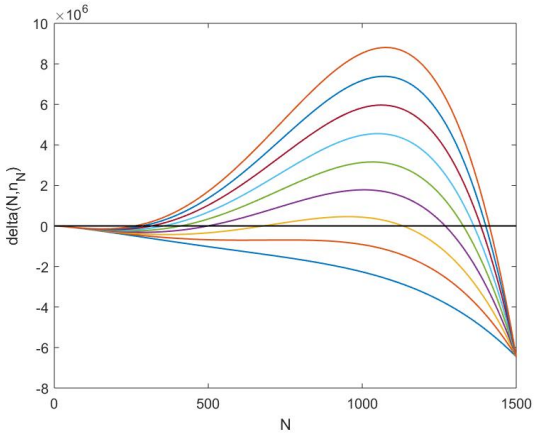

Figure 4: The figure shows the behavior of $\beta(N)$ as a function of $n_N \in [0{,}1, 0{,}9]$, where all other parameters are given in (8).

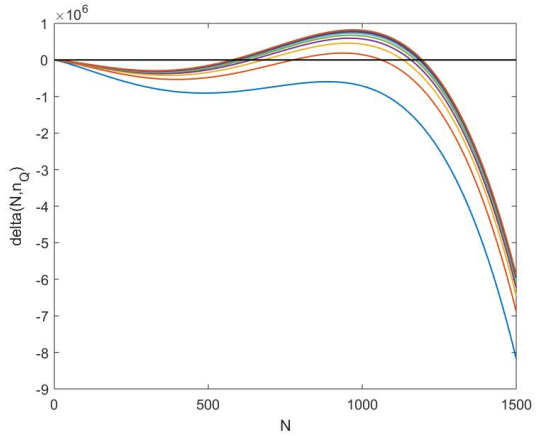

Figure 5: The figure shows the behavior of $\beta(N)$ as a function of $n_Q \in [0{,}1, 0{,}9]$, where all other parameters are given in (8).

$$J_{2,2} = n_Q\Big(1-\frac{2Q}{H_Q}\Big)+\frac{e_Q a_Q\sqrt{N}}{1+b_Q N}$$

$$J_{2,3} = \frac{e_Q a_Q Q}{2\sqrt{N}(1+b_Q N)^2}$$

$$J_{3,1} = -\frac{a_P\sqrt{N}}{1+b_P N}$$

$$J_{3,2} = -\frac{a_Q\sqrt{N}}{1+b_Q N}$$

$$J_{3,3} = n_N\Big(1-\frac{2N}{H_N}\Big)-\frac{a_P P}{2\sqrt{N}(1+b_P N)^2}-\frac{a_Q Q}{2\sqrt{N}(1+b_Q N)^2}$$

Because the equilibria with $N=0$ will have a singularity in the Jacobian, we will analyse them separately.

Equilibra with $N \neq 0$

At the point $E_N = (0,0,H_N)$ the Jacobian becomes a lower triangular matrix, with eigenvalues along the diagonal:

$$n_P+\frac{e_P a_P\sqrt{H_N}}{1+b_P H_N}>0, \quad n_Q+\frac{e_Q a_Q\sqrt{H_N}}{1+b_Q H_N}>0, \quad -n_N<0$$

and unconditional instability follows from the positivity of the first two.

For $E_{PN} = (\widehat{P}^*,0,\widehat{N}^*)$ one eigenvalue is immediately known, as the Jacobian factorizes:

$$J_{2,2} = n_Q+\frac{e_Q a_Q\sqrt{\widehat{N}^*}}{1+b_Q\widehat{N}^*}>0$$

and this is enough to ensure once again unconditional instability.

A similar result holds for $E_{QN} = (0,\widetilde{Q}^*,\widetilde{N}^*)$, for which

$$J_{1,1} = n_P+\frac{e_P a_P\sqrt{\widetilde{N}^*}}{1+b_P\widetilde{N}^*}>0$$

and also this point is always unstable.

For coexistence $E^* = E_{PQN} = (P^*,Q^*,N^*)$, note the simplifications:

$$J_{1,1}(E^*) = -n_P\frac{P^*}{H_P}, \quad J_{2,2}(E^*) = -n_Q\frac{Q^*}{H_Q},$$

$$J_{3,3}(E^*) = \frac{a_P P^*(1+2b_P N^*)}{2\sqrt{N^*}(1+b_P N^*)^2}+\frac{a_Q Q^*(1+2b_Q N^*)}{2\sqrt{N^*}(1+b_Q N^*)^2}-n_N\frac{N^*}{H_N}.$$

To assess stability we apply the Routh-Hurwitz conditions. The one on the trace gives

$$\frac{a_P P^*(1+2b_P N^*)}{2\sqrt{N^*}(1+b_P N^*)^2}+\frac{a_Q Q^*(1+2b_Q N^*)}{2\sqrt{N^*}(1+b_Q N^*)^2} < n_P\frac{P^*}{H_P}+n_Q\frac{Q^*}{H_Q}+n_N\frac{N^*}{H_N}. \tag{9}$$

The sum of the principal minors of order two is

$$M_2^* = n_P\frac{P^*}{H_P}n_Q\frac{Q^*}{H_Q}-n_P\frac{P^*}{H_P}J_{3,3}(E^*) \tag{10}$$
$$+\frac{a_P\sqrt{N^*}}{1+b_P N^*}\frac{e_P a_P P^*}{2\sqrt{N^*}(1+b_P N^*)^2}-n_Q\frac{Q^*}{H_Q}J_{3,3}(E^*)$$
$$+\frac{a_Q\sqrt{N^*}}{1+b_Q N^*}\frac{e_Q a_Q Q^*}{2\sqrt{N^*}(1+b_Q N^*)^2}$$

We now evaluate the determinant:

$$\det(J(E^*)) = n_P\frac{P^*}{H_P}n_Q\frac{Q^*}{H_Q}J_{3,3}(E^*) \tag{11}$$
$$-\frac{n_Q e_P a_P^2 P^* Q^*}{2H_Q(1+b_P N^*)^3}-\frac{n_P e_Q a_Q^2 P^* Q^*}{2H_P(1+b_Q N^*)^3}$$

to establish its positivity, giving the condition

$$\frac{n_P n_Q P^* Q^*}{H_P H_Q}J_{3,3}(E^*) > \frac{n_Q e_P a_P^2 P^* Q^*}{2H_Q(1+b_P N^*)^3} + \frac{n_P e_Q a_Q^2 P^* Q^*}{2H_P(1+b_Q N^*)^3} \tag{12}$$

The last requirement for stability, which we leave in a synthetic form, reads

$$\mathrm{tr}(J(E^*))M_2^* < \det(J(E^*)). \tag{13}$$

These conditions define a set in the parameter space that is nonempty. This statement arises from the numerical simulations, that indeed indicate that this point $E^* = E_{PQN}$ can be stably achieved, showing also that the feasibility conditions discussed formerly are satisfied for some parameter choices. Figures 6-9 show the various possibilities, in terms of the possible locations of the roots of the function $\beta(N)$. In particular note that whenever two such roots exist, one of them (the smaller one) leads to an unstable coexistence equilibrium, as it should be expected as the latter arises through a saddle-node bifurcation as remarked earlier. For the same reason we observe that in the top frame of Figure 9, when both roots coalesce, the equilibrium that is generated is also unstable.

Equilibria with $N = 0$

Observing the dominant behavior of the system near E_0, we have

$$\begin{aligned}
\frac{dP}{dt} &= n_P P\Big(1-\frac{P}{H_P}\Big)+\frac{e_P a_P\sqrt{N}P}{1+b_P N}\\
&\approx P[n_P+e_P a_P\sqrt{N}] \approx n_P P>0,\\
\frac{dQ}{dt} &= n_Q Q\Big(1-\frac{Q}{H_Q}\Big)+\frac{e_Q a_Q\sqrt{N}Q}{1+b_Q N},\\
&\approx Q[n_Q+e_Q a_Q\sqrt{N}] \approx n_Q Q>0,\\
\frac{dN}{dt} &= n_N N\Big(1-\frac{N}{H_N}\Big)-\frac{a_P\sqrt{N}P}{1+b_P N}-\frac{a_Q\sqrt{N}Q}{1+b_Q N}\\
&\approx \sqrt{N}[n_N\sqrt{N}-(a_P P+a_Q Q)],
\end{aligned}$$

and the consequence is unconditional instability due to the signs of the right hand sides of the first two equations.

For $E_P = (H_P,0,0)$, we find

$$\begin{aligned}
\frac{dN}{dt} = n_N N\Big(1-\frac{N}{H_N}\Big)-\frac{a_P\sqrt{N}P}{1+b_P N}-\frac{a_Q\sqrt{N}Q}{1+b_Q N} &\approx \sqrt{N}[n_N\sqrt{N}\\
-(a_P(P-H_P)+a_P H_P+a_Q(Q-H_Q)+a_Q H_Q)]&\\
\approx -\sqrt{N}(a_P H_P+a_Q H_Q)<0,&
\end{aligned}$$

so that along the N-axis the behavior is stable.

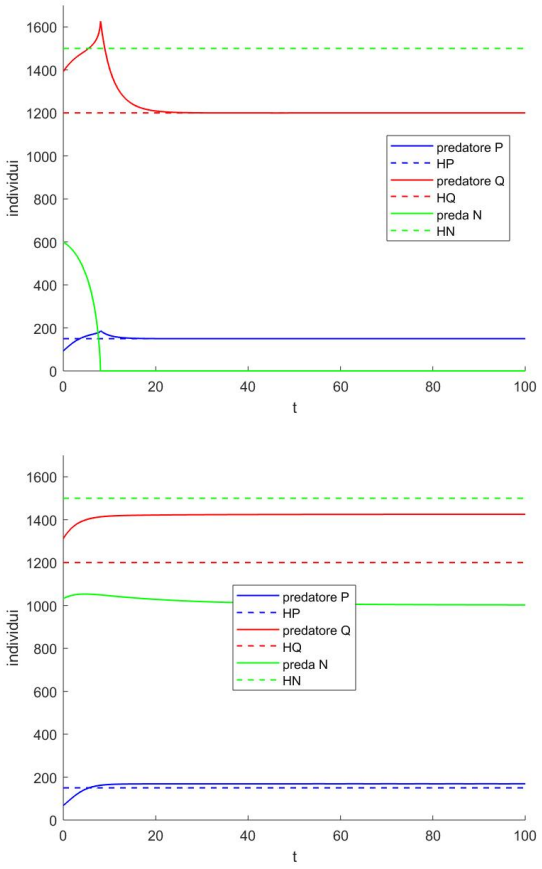

Figure 6: Coexistence obtained with the following parameter values: $n_N = 0{,}3$, $n_P = 0{,}4$, $n_Q = 0{,}3$, $H_P = 150$, $H_Q = 1200$, $H_N = 1500$, $e_P = 0{,}8$, $e_Q = 0{,}9$, $a_P = 0{,}8$, $a_Q = 0{,}2$, $b_P = 0{,}4$, $b_Q = 0{,}1$. The top frame corresponds to the initial condition near the zero $N_{1,\beta} = 678{,}6517$ of the function $\beta(N)$, which is seen to give an unstable equilibrium; the bottom one to the initial condition taken near the zero $N_{2,\beta} = 1132{,}4$, corresponding to a stable coexistence equilibrium.

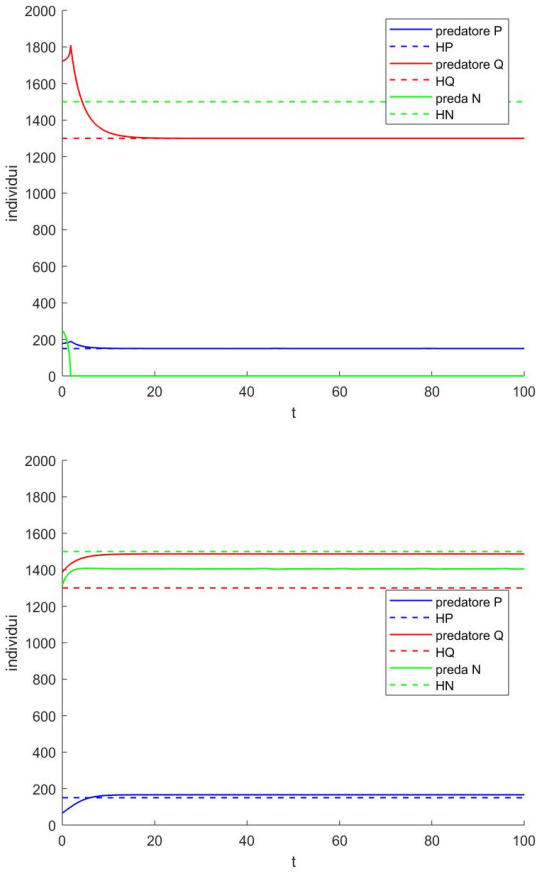

Figure 7: Coexistence obtained with the following parameter values: $n_N = 0{,}9$, $n_P = 0{,}4$, $n_Q = 0{,}3$, $H_P = 150$, $H_Q = 1300$, $H_N = 1500$, $e_P = 0{,}8$, $e_Q = 0{,}9$, $a_P = 0{,}8$, $a_Q = 0{,}9$, $b_P = 0{,}4$, $b_Q = 0{,}5$. The top frame corresponds to the initial condition near the zero $N_{1,\beta} = 258{,}6319$ of the function $\beta(N)$, which is seen to give an unstable equilibrium; the bottom one to the initial condition taken near the zero $N_{2,\beta} = 1416{,}4$, corresponding to a stable coexistence equilibrium.

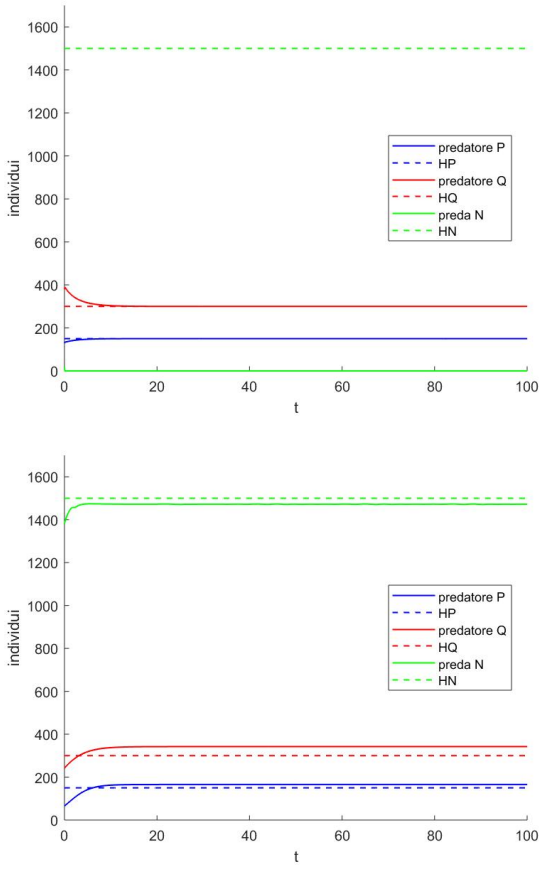

Figure 8: Coexistence obtained with the following parameter values: $n_N = 0{,}9$, $n_P = 0{,}4$, $n_Q = 0{,}3$, $H_P = 150$, $H_Q = 300$, $H_N = 1500$, $e_P = 0{,}8$, $e_Q = 0{,}9$, $a_P = 0{,}8$, $a_Q = 0{,}9$, $b_P = 0{,}4$, $b_Q = 0{,}5$. The top frame corresponds to the initial condition near the zero $N_{1,\beta} = 97{,}9228$ of the function $\beta(N)$, which is seen to give an unstable equilibrium; the bottom one to the initial condition taken near the zero $N_{2,\beta} = 1482{,}0$, corresponding to a stable coexistence equilibrium.

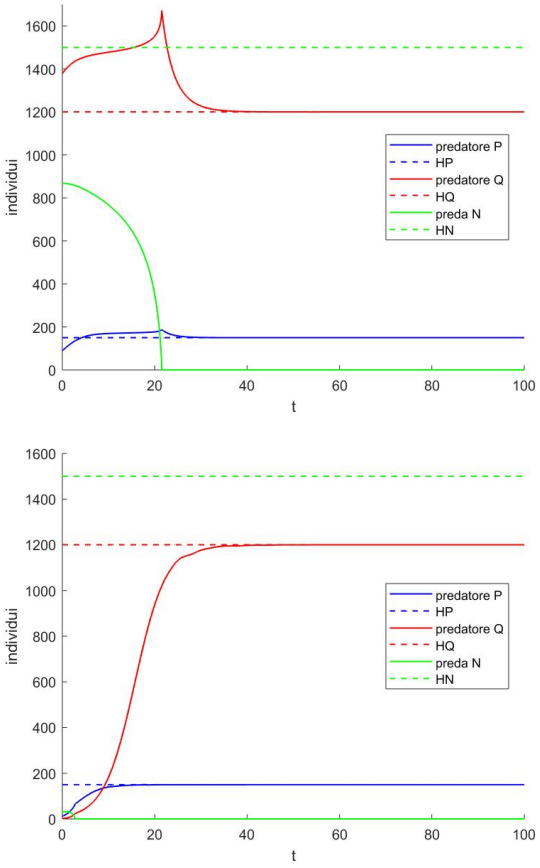

Figure 9: Top frame. Coexistence obtained with the following parameter values: $n_N = 0{,}3$, $n_P = 0{,}4$, $n_Q = 0{,}3$, $H_P = 150$, $H_Q = 1200$, $H_N = 1500$, $e_P = 0{,}8$, $e_Q = 0{,}9$, $a_P = 0{,}8$, $a_Q = 0{,}445$, $b_P = 0{,}4$, $b_Q = 0{,}2$. In this case the function $\beta(N)$ has just one zero, $N_{1,\beta} = 948{,}2506$, for which coexistence is unstable, the prey drifting to negative values and vanishing in a finite time. Bottom frame. Coexistence obtained with the following parameter values: $n_N = 0{,}3$, $n_P = 0{,}4$, $n_Q = 0{,}3$, $H_P = 150$, $H_Q = 1200$, $H_N = 1500$, $e_P = 0{,}8$, $e_Q = 0{,}9$, $a_P = 0{,}8$, $a_Q = 0{,}8$, $b_P = 0{,}4$, $b_Q = 0{,}2$. In this case the function $\beta(N)$ does not possess positive zeros. Again, the corresponding coexistence equilibrium is not attained.

TABLE 2: FEASIBILITY OF ALL THE EQUILIBRIA OF THE SYSTEM (2)

Equilibrium	Feasibility conditions
$E_0 = (0,0,0)$	–
$E_N = (0,0,H_N)$	–
$E_Q = (0,H_Q,0)$	–
$E_P = (H_P,0,0)$	–
$E_{QN} = (0,Q^*,N^*)$	$\Phi_Q(N) \cap \Psi_Q(N)$ sufficient: $\Phi_Q(N^+_{\Psi'}) \geq \Psi_Q(N^+_{\Psi'})$
$E_{PN} = (P^*,0,N^*)$	$\Phi_P(N) \cap \Psi_P(N)$ sufficient: $\Phi_P(N^+_{\Psi'}) \geq \Psi_P(N^+_{\Psi'})$
$E_{PQ} = (H_P,H_Q,0)$	–
$E^* = E_{PQN} = (P^*,Q^*,N^*)$	Arising through saddle-node bifurcation

The remaining minor of the Jacobian becomes a diagonal matrix, as no mutual interactions of the two predators are present:

$$\widehat{J} = \begin{bmatrix} n_P\left(1-\frac{2P}{H_P}\right) & 0 \\ 0 & n_Q\left(1-\frac{2Q}{H_Q}\right) \end{bmatrix}$$

giving the eigenvalues $-n_P$ and $n_Q > 0$, thereby implying unconditional instability.

For the point $E_Q = (0,H_Q,0)$ a similar result would hold as for E_P along the N axis. Again the submatrix of the Jacobian is diagonal, with eigenvalues $n_P > 0$ and $-n_Q$, showing once again instability.

However at the point $E_{PQ} = (H_P,H_Q,0)$, these eigenvalues are both negative, $-n_P$ and $-n_Q$, implying for this equilibrium unconditional stability. The fact that these eigenvalues are real prevents any possible occurrence of a Hopf bifurcation at this point.

DISCUSSION

In the Tables 2 and 3 we summarize all the equilibria behavior, giving their feasibility and stability conditions.

Ultimately, only two outcomes are possible. Either the prey disappear, and the two predators thrive at their carrying capacities, E_{PQ}, or the three populations coexist, E_{PQN}. In the former case the predators natural population levels H_P and H_Q are undisturbed since they are assumed not to interfere with each other. Furthermore, in this situation no persistent oscillations can arise. Thus the predators are always found at a stable level, as this point is unconditionally feasible and stable. Note also that this result implies that in the system the predator populations are always present, independently of what happens for the other possible equilibrium.

Coexistence is instead not guaranteed to arise. If it does, its onset occurs through a saddle-node bifurcation, which implies the simultaneous appearance of two such points, of which the one with the lower level of prey N is unstable. This saddle point partitions the phase space through a separating surface, so that two domains of attractions exist, one being the one of the prey-free equilibrium E_{PQ} and the other one of the coexistence point $E^* = E_{PQN}$. Thus the ultimate behavior of the system trajectories would in such case depend only on the present state of the system, i.e. the location of the initial condition.

The result that equilibrium E_{PQ} is unconditionally stable, coupled with the fact that two coexistence equilibria may arise in pairs, of which one unstable and one stable, as discussed above, indicates that in suitable circumstance bistability can be obtained.

Indeed, Figures 6-9 show graphically this behavior. In each case, for the same set of parameter values, the system trajectories tend to different equilibria, the prey-free point E_{PQ} in the top frame and coexistence E_{PQN} in the bottom one, just by changing the initial conditions, i.e. depending on the domain of attraction of which point the current state of the system is located. This result can suitably be exploited, so that at last bistability may result to be a very much important tool for addressing two relevant ecological problems, namely species eradication and preservation.

In case the prey is a nuisance, bistability could be exploited for its eradication, simply by trying to push the state of the system in the domain of attraction of the prey-free point E_{PQ}. To achieve this task, two imporant remarks should be made. First of all, such a "push" could be obtained by external, human driven means, such as insecticide spraying. Secondly, the external measure should be exerted in an amount small enough just to cross the separating surface, thereby also saving on costs.

If N is a species to be preserved instead, corresponding measures for its survival should be taken, so that the state of the system would be moved into the attraction domain of the coexistence equilibrium. Enhancing the chances of the species N to be preserved to survive could be achieved once more by external means, such as fostering its reproductivity or increasing its carrying capacity, or measures apt to reduce the predators hunting pressure. In the last case, for instance, a "measured" culling could be decided to be undertaken, sufficient enough to move the system trajectories into the coexistence equilibrium domain of attraction, thereby allowing the survival of the endangered species together with the two generalist predators.

Note that in the above discussion, the role of the separating surface is of paramount importance. However, where this manifold lies is unknown. This is an important remark, because knowing its location and the current state of the system would allow to adequately estimate the effort to be taken to move the system into the right attraction basin. Fortunately, to address and solve this problem, numerical schemes based on reliable and up-to-dated state of the art algorithms have been recently developed to numerically reconstruct in an efficient, reliable and fast way the separatrix, (Cavoretto et al., 2011, 2013, 2016a,b; De Rossi et al., 2018; Francomano et al., 2016, 2017, 2018; Hilker et al., 2017).

TABLE 3: STABILITY OF ALL THE EQUILIBRIA OF THE SYSTEM (2).

Equilibria	Stability conditions
$E_0 = (0,0,0)$	unstable
$E_N = (0,0,H_N)$	unstable
$E_Q = (0,H_Q,0)$	unstable
$E_P = (H_P,0,0)$	unstable
$E_{QN} = (0,Q^*,N^*)$	unstable
$E_{PN} = (P^*,0,N^*)$	unstable
$E_{PQ} = (H_P,H_Q,0)$	stable
$E_* = E_{PNH}$	(9), (13), (12)

Acknowledgments: Work partially supported by the project "Metodi numerici per l'approssimazione e le scienze della vita" of the Dipartimento di Matematica "Giuseppe Peano". Ezio Venturino is a member of the INdAM research group GNCS. The paper was written during a visit of Ezio Venturino to the Mathematics Department de la Universidad Tecnológica Metropolitana of Santiago,Chile, and the Universidad Católica de Talca, Chile; he thanks Prof. Ricardo Castro-Santis and and Prof. Fernando Córdova-Lepe, as well as their whole research groups for their kind invitation and support.

REFERENCES

[1] Acotto, F. and Venturino, E. (2022). "Modeling the herd prey response to individualistic predators attacks". *submitted*, 0.

[2] Ajraldi, V., Pittavino, M., and Venturino, E. (2011). "Modelling herd behavior in population systems". *Nonlinear Analysis Real World Applications*, 12:2319–2338.

[3] Baudrot, V., Fritsch, C., Perasso, A., Banerjee, M., and Raoul, F. (2018). "Effects of contaminants and trophic cascade regulation on food chain stability: Application to cadmium soil pollution on small mammals–raptor systems". *Ecological Modelling*, 383:33–42.

[4] Baudrot, V., Perasso, A., Fritsch, C., Giraudoux, P., and Raoul, F. (2016a). "The adaptation of generalist predators' diet in a multi-prey context: Insights from new functional responses". *Ecology*, 97(7):1832–1841.

[5] Baudrot, V., Perasso, A., Fritsch, C., and Raoul, F. (2016b). "Competence of hosts and complex foraging behavior are two cornerstones in the dynamics of trophically transmitted parasites." *Journal of Theoretical Biology*, 397:158–168.

[6] Belvisi, S. and Venturino, E. (2013). "An ecoepidemic model with diseased predators and prey group defense". *SIMPAT*, 34:144–155.

[7] Bondi, L., Ferri, J., Giordanengo, N., and Venturino, E. (2022). "Multiple predation on prey herding and counteracting the hunting". *submitted*.

[8] Bulai, I. M. and Venturino, E. (2017). "Shape effects on herd behavior in ecological interacting population models". *Mathematics and Computers in Simulation*, 141:40–55.

[9] Cagliero, E. and Venturino, E. (2016). "Ecoepidemics with infected prey in herd defense: the harmless and toxic cases". *IJCM*, 93(1):108–127.

[10] Cavoretto, R., Chaudhuri, S., Rossi, A. D., Menduni, E., Moretti, F., Rodi, M. C., and Venturino, E. (2011). "Approximation of dynamical system's separatrix curves, in: T. e. simos et al. (eds.)". *International Conference on Numerical Analysis and Applied Mathematics*, 1389:1220–1223.

[11] Cavoretto, R., Marchi, S. D., Rossi, A. D., Perracchione, E., and Santin, G. (2016a). "Approximating basins of attraction for dynamical systems via stable radial bases". *AIP Conf. Proc.*, 1738.

[12] Cavoretto, R., Rossi, A. D., and Perracchione, E. (2016b). "Fast and flexible interpolation via pum with applications in population dynamics". *AIP Conf. Proc.*, 1738.

[13] Cavoretto, R., Rossi, A. D., Perracchione, E., and Venturino, E. (2013). "Reconstruction of separatrix curves and surfaces in squirrels competition models with niche". *International Conference on Computational and Mathematical Methods in Science and Engineering*, pages 400–411.

[14] De Rossi, A., Perracchione, E., and Venturino, E. (2018). "Meshless partition of unity method for attraction basins of periodic orbits: Fast detection of separatrix points". *Dolomites Research Notes on Approximation*, 11(Special issue MATAA17):15–22.

[15] Djilali, S. (2019). "Impact of prey herd shape on the predator-prey interaction". *Chaos, Solitons & Fractals*, 120:139–148.

[16] Francomano, E., Hilker, F., Paliaga, M., and Venturino, E. (2016). "On basins of attraction for a predator-prey model via meshless approximation". *AIP NUMTA*, 1776:80–91.

[17] Francomano, E., Hilker, F., Paliaga, M., and Venturino, E. (2017). "An efficient method to reconstruct invariant manifolds of saddle points". *DRNA*, 10:25–30.

[18] Francomano, E., Hilker, F., Paliaga, M., and Venturino, E. (2018). "Separatrix reconstruction to identify tipping points in an eco-epidemiological model". *Applied Mathematics and Computation*, 318:80–91.

[19] González-Olivares, E., Rivera-Estay, V., Rojas-Palma, A., and Vilches-Ponce, K. (2022). "A leslie–gower type predator-prey model considering herd behavior". *Ricerche di Matematica*.

[20] Hilker, F. M., Paliaga, M., and Venturino, E. (2017). "Diseased social predators". *BMB*, 79(10):2175–2196.

[21] Jiang, H. and Tang, X. (2019). "Hopf bifurcation in a diffusive predator-prey model with herd behavior and prey harvesting". *Journal of Applied Analysis & Computation*, 9(2):671–690.

[22] Kooi, B. W. and Venturino, E. (2016). "Ecoepidemic predator-prey model with feeding satiation, prey herd behavior and abandoned infected prey". *Math. Biosc.*, 274:58–72.

[23] Melchionda, D., Pastacaldi, E., Perri, C., Banerjee, M., and Venturino, E. (2018). "Social behavior-induced multistability in minimal competitive ecosystems". *J. Theoretical Biology*, 439:24–38.

[24] Sieber, M., Malchow, H., and Hilker, F. (2014). "Disease-induced modification of prey competition in eco-epidemiological models". *Ecol. Complex.*, 18:74–82.

[25] Souna, F., Djilali, S., and Charif, F. (2020). "Mathematical analysis of a diffusive predator-prey model with herd behavior and prey escaping". *Math. Model. Nat. Phenom.*, 15.

[26] Vilches, K., González-Olivares, E., and Rojas-Palma, A. (2018). "Prey herd behavior modeled by a generic non-differentiable functional response". *Math. Model. Nat. Phenom.*, 13.

Normas de publicación

Envío de los manuscritos:

1. Revista Modelamiento Matemático de Sistemas Biológicos (MMSM) publica artículos originales e inéditos (en español o inglés), por lo que el manuscrito sometido no puede estar publicado, total o parcialmente en otro medio.

2. Los autores interesados en presentar un trabajo a MMSB **declaran que el manuscrito es original y no ha sido presentado simultáneamente a evaluación en otra publicación y que su evaluación y publicación es autorizada tácita y expresamente por todos los autores, posteriormente** enviar una copia de su trabajo en formato PDF, procesado en LaTeX2e, a través del **sistema de envío de la revista**. **La dirección es https://revistammsb.utem.cl/envio-de-articulos/**

3. El envío debe realizarlo el autor y, de tratarse de dos o más autores, debe designarse un autor correspondiente para ello, quien debe proporcionar correo electrónico y filiación institucional.

4. El autor correspondiente debe proporcionar el correo electrónico de todos los coautores con el fin de comprobar el consentimiento.

5. Los manuscritos deben contar con título, abstract y palabras claves en español e inglés.

6. Fuente financiamiento o patrocinador: todas las fuentes de financiamiento deben ser declaradas. (Nombre institución, código del proyecto o mención de beca).

7. Posibles conflictos de interés deben ser declarados al momento del envío.

Formato:

Formato: 1. Los trabajos a ser publicados en MMSB deben ser procesados en LaTeX2e, con uso del template proporcionado por la revista, el que incluye la bibliografía en BibTeX. Su uso es obligatorio, solo posterior a la aceptación del manuscrito. Véase template descargable en: https://revistammsb.utem.cl/normas-de-publicacion/

1. Los artículos deben ser redactados según las normas establecidas en el Manual de Estilo de Ediciones UTEM (https://editorial.utem.cl/tematica/manual-de-estilo/). Se excluye de esta consideración el capítulo 1 del mentado manual.

2. Asimismo, este manual se ve complementado por el documento de instrucción para los(as) autores(as). Véase formato instrucciones en inglés y español: https://revistammsb.utem.cl/normas-de-publicacion/

Evaluación:

1. Revisión por pares (peer review): el editor(es) evaluarán la pertinencia del trabajo en la línea editorial de la revista, una vez confirmado, los trabajos serán enviados a dos revisores independientes determinados por el editor **de la revista al que fue** asignado al manuscrito, en modalidad **doble ciego.**

2. Los **revisores evaluarán la** originalidad, corrección teórica y métodos utilizados.

3. Los trabajos pueden ser aceptados, aceptados con observaciones o rechazados. **El editor(es) es el responsable de comunicar la decisión final de aceptación o rechazo.**

4. En caso de manuscritos aceptados con observaciones, estas serán enviadas al autor correspondiente, quien tendrá el plazo de **30 días hábiles**. Si estas no son respondidas en el plazo establecido o las respuestas son insatisfactorias, el artículo se dará por rechazado.

Publicación:

1. Aceptado un trabajo, el autor deberá proporcionar los archivos fuentes del artículo, incluyendo el archivo .tex, los archivos gráficos en alta calidad necesarios para la compilación y el archivo .bib de las referencias bibliográficas. En el caso de incorporar elementos adicionales, estos podrán ser solicitados por la entidad editora de la revista, con la finalidad de que sean optimizados para su publicación.

2. Los trabajos aceptados serán incluidos en el volumen siguiente a la aceptación del artículo, **a menos que el editor informe lo contrario.**

3. Previo a la publicación, se realizará una corrección de estilo al manuscrito, cuyos comentarios quedarán registrados en la herramienta que Adobe Acrobat dispone para ello. El editor enviará al autor esta versión con comentarios, para aprobación final del autor. El editor será el encargado de gestionar eventuales correcciones y de comunicar el visto bueno final a la entidad editora. El artículo no será publicado sino se cuenta con esta autorización.

4. Copyright y tipo de licencia: Universidad Tecnológica Metropolitana bajo la licencia Creative Commons Atribución - CC BY.

5. Permisos a los autores: Permite el auto-archivo de la versión editorial (Post-print) en la web personal o institucional de los autores.

Aspectos éticos:

• Las responsabilidades éticas y legales por plagio, falsificación de datos, utilización indebida de material protegido por derecho de autor u otra infracción a la ética científica **en conformidad a las pautas del Commitée on Publication Ethics (COPE) https://publicationethics.org/core-practices,** es de absoluta responsabilidad de los autores. **Si se identifica un error u otra situación anómala, el autor deberá informar o responder a los editores por las acciones correctivas pertinentes.**

Actualizado 25/ 04 / 2022

UNIVERSIDAD TECNOLÓGICA METROPOLITANA
del Estado de Chile

UTEM

EDICIONES UNIVERSIDAD TECNOLÓGICA METROPOLITANA

VERSIÓN EN LÍNEA: ISSN 2735-6817

revistammsb.utem.cl